

This document is made available through the declassification efforts
and research of John Greenewald, Jr., creator of:

The Black Vault



The Black Vault is the largest online Freedom of Information Act (FOIA) document clearinghouse in the world. The research efforts here are responsible for the declassification of hundreds of thousands of pages released by the U.S. Government & Military.

Discover the Truth at: <http://www.theblackvault.com>

UNCLASSIFIED

AD NUMBER

AD357196

CLASSIFICATION CHANGES

TO:

UNCLASSIFIED

FROM:

~~CONFIDENTIAL~~

AUTHORITY

31 Jan 1977, DoDD 5200.10

THIS PAGE IS UNCLASSIFIED

CONFIDENTIAL

AD 357196

DEFENSE DOCUMENTATION CENTER

FOR

SCIENTIFIC AND TECHNICAL INFORMATION

CAMERON STATION, ALEXANDRIA, VIRGINIA



NOTICE: When government or other drawings, specifications or other data are used for any purpose other than in connection with a definitely related government procurement operation, the U. S. Government thereby incurs no responsibility, nor any obligation whatsoever; and the fact that the Government may have formulated, furnished, or in any way supplied the said drawings, specifications, or other data is not to be regarded by implication or otherwise as in any manner licensing the holder or any other person or corporation, or conveying any rights or permission to manufacture, use or sell any patented invention that may in any way be related thereto.

NOTICE:

THIS DOCUMENT CONTAINS INFORMATION AFFECTING THE NATIONAL DEFENSE OF THE UNITED STATES WITHIN THE MEANING OF THE ESPIONAGE LAWS, TITLE 18, U.S.C., SECTIONS 793 and 794. THE TRANSMISSION OR THE REVELATION OF ITS CONTENTS IN ANY MANNER TO AN UNAUTHORIZED PERSON IS PROHIBITED BY LAW.



357196

CATALOGUED BY DDC
AS AD No. _____

357196

WL TDR-64-93, Vol IV

~~CONFIDENTIAL~~

WL
TDR
64-93
Vol IV

(U) NUCLEAR PULSE PROPULSION PROJECT
(PROJECT ORION)

Volume IV

(U) Engineering Experimental Tests

Technical Summary Report

TECHNICAL DOCUMENTARY REPORT WL TDR-64-93, Vol IV



Research and Technology Division
AIR FORCE WEAPONS LABORATORY
Air Force Systems Command
Kirtland Air Force Base
New Mexico

January 1965

GROUP IV
Regraded at 3 year intervals
Declassified after 12 years

~~CONFIDENTIAL~~



FOR ERRATA

AD 357196

THE FOLLOWING PAGES ARE CHANGES

TO BASIC DOCUMENT

Research and Technology Division
AIR FORCE WEAPONS LABORATORY
Air Force Systems Command
Kirtland Air Force Base
New Mexico 87117

4 January 1967

ERRATUM

WL-TDR-64-93, Vol IV

(U, NUCLEAR PULSE PROPULSION PROJECT (PROJECT
ORION), Volume IV, (U) Engineering Experimental
Tests; Technical Summary Report, January 1965 (CONF)

Delete Restricted Data marking from back cover.

C. W. Haig
C. W. HAIG
Chief, Reports and Data Branch
Technical Information Division

AD-357196

357196

AD 357196

END CHANGE PAGES

Research and Technology Division
AIR FORCE WEAPONS LABORATORY
Air Force Systems Command
Kirtland Air Force Base
New Mexico

This report is classified Confidential, Group IV, because it reveals test information on the design and performance of nuclear devices of an advanced nuclear propulsion concept.

WARNINGS

This material contains information affecting the national defense of the United States within the meaning of the Espionage Laws, Title 18, USC, sections 793 and 794, the transmission or revelation of which in any manner to an unauthorized person is prohibited by law.

SPECIAL HANDLING REQUIRED--NOT RELEASABLE TO FOREIGN NATIONALS.

When U. S. Government drawings, specifications, or other data are used for any purpose other than a definitely related Government procurement operation, the Government thereby incurs no responsibility nor any obligation whatsoever, and the fact that the Government may have formulated, furnished, or in any way supplied the said drawings, specifications, or other data, is not to be regarded by implication or otherwise, as in any manner licensing the holder or any other person or corporation, or conveying any rights or permission to manufacture, use, or sell any patented invention that may in any way be related thereto.

This report is made available for study with the understanding that proprietary interests in and relating thereto will not be impaired. In case of apparent conflict or any other questions between the Government's rights and those of others, notify the Judge Advocate, Air Force Systems Command, Andrews Air Force Base, Washington, D. C. 20331.

Qualified users may obtain copies of this report from DDC.

~~CONFIDENTIAL~~

WL TDR-64-93, Vol IV

(U) NUCLEAR PULSE PROPULSION PROJECT
(PROJECT ORION)

Volume IV

(U) Engineering Experimental Tests

GROUP IV

Regraded at 3 year intervals
Declassified after 12 years

~~CONFIDENTIAL~~

~~CONFIDENTIAL~~

WL TDR-64-93, Vol IV

FOREWORD

The technical summary report on the Nuclear Pulse Propulsion Project (Project ORION) under Air Force Contract AF 29(601)-6214, Project 3775, Task 377501, is being published in four volumes. The volume titles are: Vol I--Summary Report; Vol II--Theoretical and Experimental Physics; Vol III--Engine Design, Analysis, and Development Techniques; and Vol IV--Engineering, Experimental Tests. This report was prepared by General Atomic Division, General Dynamics Corporation. The General Atomic report number is GA-5386. Inclusive dates of research were July 1963 through September 1964. The report was submitted for publication on 15 December 1964. The Air Force Program Monitor was Major John O. Berga, AFWL (WLDL-3).

The engineering experimental tests reported on in this volume were under the direction of J. C. Nance, Project Manager, C. V. David, head of engineering design, and E. A. Day, head of experimental engineering. Other General Atomic staff members contributing to this experimental work were G. O. Baker, E. R. Hager, L. O. Lavigne, W. H. Mandelco, R. D. Morton, W. O. Muhl, J. J. Novak, R. L. Rayman, C. H. Richards, R. R. Rumpf, K. J. Tom, and E. L. Wasser.

This report contains no classified information extracted from other classified documents.

This technical report has been reviewed and is approved.

John O. Berga
JOHN O. BERGA
Major USAF
Project Officer

John W. Talley
JOHN W. TALLEY
Lt Colonel USAF
Chief, Nuclear Applications
Branch

R. A. House
R. A. HOUSE
Colonel USAF
Chief, Development Division

(This page is Unclassified)

ii

~~CONFIDENTIAL~~

UNCLASSIFIED ABSTRACT

Segments of an ORION pusher plate and scaled primary shock absorbers with scaled pusher-shock-absorber attachments have been repeatedly shocked up to full stress conditions with high explosives (HE). The results of these response measurements and post-test inspections are presented along with the results of HE-pulse-generator development tests. In addition, a comparison of the results of a computer program and an experimental test of plate flexural stresses is presented. The primary importance of these results is the indication that ORION components can be developed to function in the manner prescribed by design studies and that nonnuclear pulse systems for the development and life-testing on the ground of full-size ORION vehicles are practical.

CONTENTS

1. INTRODUCTION (U)	1
1.1. Technical Background (U)	1
1.2. The Current Test Program (U)	2
1.3. Summary of Test Results (U)	2
2. IMPULSE GENERATION (U)	5
2.1. Spherical-HE-charge Pulse Generation (U)	5
2.2. Sheet-HE Pulse Generation (U)	12
3. PLATE RESPONSE TESTS (U)	19
3.1. Plates for Torus Tests (U)	19
3.2. The Dynamic Behavior of Plates Subjected to an Impulse Mismatch To Check BAMB Code Operation (U)	22
3.3. Structural Behavior of Steel Plates Subjected to Repeated Shock Loads (U)	29
4. PLATE-ATTACHMENT RESPONSE TESTS (U)	47
4.1. Test Objectives of the Current Program (U)	49
4.2. Test Results (U)	50
5. TORUS RESPONSE TESTS (U)	73
5.1. Test Objectives (U)	73
5.2. Torus-model Basic Design (U)	74
5.3. Single-torus Manufacturing and Quality Control (U)	81
5.4. Description of Experiment (U)	89
5.5. Experimental Results and Data (U)	91
5.6. Correlation of Test Results with Predicted Results (U)	123
5.7. Conclusions and Recommendations (U)	132
6. FUTURE EXPERIMENTAL ENGINEERING PROGRAM (U)	135
6.1. Pulse-generation Development (U)	135
6.2. Plate Response (U)	136
6.3. Three-torus System (U)	137
6.4. Torus-Plate Attachment (U)	137
6.5. Torus-stack-system Static Investigation (U)	138
7. CONCLUSIONS (U)	139
7.1. Pulse-generation Development (U)	139
7.2. Plate Response (U)	140
7.3. Plate-attachment Response (U)	140
7.4. Torus Response (U)	141
REFERENCES (U)	143

Figures

Fig. 2. 1--Schematic of test setup for measuring face-on time-resolved pressure pulses radially across plate (U)	7
Fig. 2. 2--The pressure-probe test setup (U)	7
Fig. 2. 3--High-speed framing-camera sequence of 2-lb C-4 spherical charge detonation (8 μ sec/frame) (U)	9
Fig. 2. 4--High-speed framing-camera sequence of TNT spherical-charge detonation (8 μ sec/frame) (U)	10
Fig. 2. 5--Reflected (face-on) pressure and impulse for spherical C-4 HE compared with other reported data (U)	11
Fig. 2. 6--Reflected impulse measured from 2. 1-lb C-4 HE charge fired in air (U)	11
Fig. 2. 7--Typical pressure pulses using different pulse-shaping materials and A-5 HE charges and 1-in. -thick plywood back-up material (U)	13
Fig. 2. 8--Pulse forms of interest to ORION (U)	14
Fig. 2. 9--Effect of foam (or fiberboard) density on peak pressure (all tests were made with 8-in. -thick foam or fiberboard) (U)	17
Fig. 2. 10--Effect of foam (or fiberboard) density on impulse (all tests were made with 8-in. -thick foam or fiberboard) (U)	17
Fig. 2. 11--HE pulse simulation test setup (U)	18
Fig. 3. 1--Failure of three aluminum plates (U)	21
Fig. 3. 2--Typical steel plate finished for torus testing (U)	22
Fig. 3. 3--Loading diagram for computer and HE tests for plate flexure (U)	23
Fig. 3. 4--Surface stress patterns for 24-in. -diam by 3/16-in. -thick steel plate with mismatch between impulse load and plate mass (U)	25
Fig. 3. 5--Strain signal at 3-in. radius (U)	27
Fig. 3. 6--Strain signal at 9-in. radius (U)	27
Fig. 3. 7--Measured impulse distribution compared with $\cos^4 \theta$ distribution (C)(Gp-4)	28
Fig. 3. 8--Welded test plate (U)	31
Fig. 3. 9--Typical loading pulse for welded test plate (U)	31
Fig. 3. 10--Polished and etched sections through weld of test plate (arrow indicates shock-loaded surface) (U)	32
Fig. 3. 11--Magnified crack end at weld of test plate (U)	34
Fig. 3. 12--Cracks from weld inclusion of welded test plate (U)	35
Fig. 3. 13--Sectioned welded test plate with internally cracked areas indicated (U)	36
Fig. 3. 14--Boss plate 1 with inspection strip (U)	36
Fig. 3. 15--Test setup for boss plate 3 (U)	38
Fig. 3. 16--Shock-loaded face of boss plate 1 (U)	38

Fig. 3. 17--Sketch indicating bulge caused by HE shock units of diameter equal to plate diameter (U)	39
Fig. 3. 18--Second test plate with integral full-scale shock-absorber attachment section showing inspection cuts (U)	40
Fig. 3. 19--Plane-plate-stress analysis and slow-decay pressure curve (U)	42
Fig. 3. 20--Plane-plate-stress analysis and rapid-decay pressure curve (U)	44
Fig. 4. 1--Typical plate test setups (U)	51
Fig. 4. 2--Four-boss aluminum test plate (U)	53
Fig. 4. 3--Aluminum boss plate after testing (U)	54
Fig. 4. 4--Aluminum plate with resin bead after testing (U)	56
Fig. 4. 5--Aluminum plate with torus attachment after testing (U)	57
Fig. 4. 6--First magnesium plate (no resin bead) after testing (U)	59
Fig. 4. 7--Second magnesium plate after testing (with resin bead installed) (U)	61
Fig. 4. 8--View of the short shield after testing (U)	63
Fig. 4. 9--Views of the tall shield before and after testing (U)	64
Fig. 4. 10--Plate with integral full-size shock-absorber attachment section (U)	66
Fig. 5. 1--Typical single-torus test setup (U)	75
Fig. 5. 2--Typical torus structural construction (U)	76
Fig. 5. 3--Typical resin-inflated torus bead attachment (U)	77
Fig. 5. 4--Typical three-torus (or multitorus) stack construction (U)	79
Fig. 5. 5--Typical knitted, reinforced structure construction (U)	80
Fig. 5. 6--Typical as connection between adjacent tori (U)	82
Fig. 5. 7--Typical filament-wound torus structure (U)	82
Fig. 5. 8--Inner-tube fabrication process (U)	84
Fig. 5. 9--Typical flat magnesium-bead-ring torus attachment (U)	86
Fig. 5. 10--Typical counterweight attachment to the single torus and inflation valve (U)	88
Fig. 5. 11--Typical setup of single-torus on test plate (U)	90
Fig. 5. 12--First torus (filament wound) failure (U)	93
Fig. 5. 13--First torus (filament wound) for checking on control rig (U)	94
Fig. 5. 14--Second torus (knitted structure) for checking on control rig (U)	95
Fig. 5. 15--Second torus after testing (U)	96
Fig. 5. 16--Third torus (knitted) failure (C)(Gp-4)	98
Fig. 5. 17--Fourth torus (filament wound) failure (U)	99
Fig. 5. 18--Typical single-torus-system cross section (clamped torus) (U)	100
Fig. 5. 19--Failure of first torus (filament wound) with counterweight (U)	102
Fig. 5. 20--Failure of second torus (knitted structure) with counterweight (U)	103

Fig. 5. 21a--Failure of third torus (knitted structure) showing the torus on the plate after testing, bead failure, over-all failure (U)	104
Fig. 5. 21b--Failure of third torus (knitted structure) showing inside and outside failures (U)	105
Fig. 5. 22--Typical torus failure at the attachment to the plate (plate side) (U)	106
Fig. 5. 23--Typical clamped torus attachment (U)	108
Fig. 5. 24--Plate-clamped single torus before test (U)	109
Fig. 5. 25--Clamped single torus after testing (U)	111
Fig. 5. 26--Single-torus instrumented test (U)	113
Fig. 5. 27--Accelerometer signals from second A-1 shot using different accelerometers (U)	114
Fig. 5. 28--Typical accelerometer signals from second A-1 shot (U)	115
Fig. 5. 29--2220 accelerometer signals (12, 000 g/cm) from first A-2 shot (U)	116
Fig. 5. 30--2220 accelerometer signals (6, 000 g/cm) from second A-2 shot (U)	117
Fig. 5. 31--Typical acceleration imposed on counterweight (U)	118
Fig. 5. 32--Counterweight acceleration, velocity, and displacement from A-2 shot (2 msec/cm) (U)	121
Fig. 5. 33--Counterweight acceleration and velocity from A-2 shot (1 msec/cm) (U)	122
Fig. 5. 34--Typical clamping ring screw damage (after 22 shots) (U)	125
Fig. 5. 35--Typical clamping boss shape for torus attachment (U)	128
Fig. 5. 36--Torus gas spring characteristics (U)	129

Tables

2. 1. Fiberboard test data (density = 13 lb/ft ³) (U)	15
2. 2. Fiberboard test data (density = 20 lb/ft ³) (U)	16
4. 1. Variations of groove dimensions in first boss-attachment plate (U)	67
4. 2. Variations of groove dimensions in second boss-attachment plate (U)	68
4. 3. Variations of groove dimensions in third boss-attachment test plate (U)	70
5. 1. Acceleration measurement test results (A-1) (U)	119
5. 2. Acceleration measurement test results (A-2) (U)	120
5. 3. Accelerometer signal delay (U)	124

UNCLASSIFIED

WL-TDR-64-93

1. INTRODUCTION (U)

(U) The ORION concept (propulsion of a space vehicle by a series of nuclear explosions) has been under study at General Atomic since November 1957. Briefly, the concept is described as follows: A large number of nuclear explosive devices (nuclear pulse systems), which are carried inside the vehicle, are delivered sequentially to an explosion point below the vehicle structure and then detonated. A large portion of the exploded nuclear pulse system is intercepted by a strong structural plate, the pusher, which forms the bottom of the vehicle. The momentum transferred from the high-velocity "plasma" to the pusher plate drives the pusher upward into two-stage shock absorbers which, in turn, transfer the momentum to the vehicle at acceleration levels within human tolerance.

1.1. TECHNICAL BACKGROUND (U)

(U) The over-all effectiveness of the ORION propulsion concept is determined to a large extent by the strength of the impulse received by the pusher plate. The design of the pusher and shock-absorber systems and the performance of the vehicle are closely related to the allowable peak pressure pulse delivered to the pusher by the pulse system. Theoretical studies of pusher designs to withstand high-intensity, high-velocity shock stresses have been made using high-speed digital computer programs. The flexure and membrane stresses of the pusher have also been calculated with the aid of the digital computer. However, allowable material stresses for repeated strong shock-loading are not well established, and computer programs are not available to aid in the analysis of the response of complex structures, such as the ORION plate with integrated structures for shock-absorber attachments. Thus, there has been a clear

requirement to study experimentally impulsively loaded scaled plates, plate segments, and plate and scaled shock-absorber assemblies. A system of pulse generation has been devised to produce pressure pulses in the range of interest to ORION.⁽¹⁾ This volume records the further development of such loading techniques and their application to ORION engineering design problems.

1. 2. THE CURRENT TEST PROGRAM (U)

(U) The test program discussed in this volume was undertaken

1. To investigate the response of scaled pusher test specimens to repeated impulse loads of interest to ORION, to study experimentally the effect of impulse-pusher-mass distribution mismatch, and to compare the experimental results with those predicted by the digital computer program Σ AMM.⁽²⁾ (U)
2. To initiate experimental studies of the response and performance of various portions of the first-stage shock absorber. These studies were undertaken to investigate the static and dynamic properties of shock-absorber materials, shock-absorber construction techniques, shock-absorber-pusher attachments, and scaled first-stage shock-absorber structures. (U)

1. 3. SUMMARY OF TEST RESULTS (U)

(U) The objective of this program was to produce experimental data pertinent to the engineering feasibility of the ORION concept. The status of proof-testing the unique ORION engineering problem areas is implicit in the results of this program. The results of these investigations are summarized as follows:

1. Chemical explosives (HE) have generated impulses similar in shape to and of approximately two-thirds the magnitude of the impulse expected from the nuclear impulse for the ORION 10-m vehicle. Although the actual ORION

UNCLASSIFIED

WL-TDR-64-93

pulse pressures may be simulated and, in fact, have been surpassed, some extension of the pulse duration is still required. However, there appears to be no practical obstacle to this goal. (U)

2. Tests on pusher-plate segments show that
 - (a) Specimens of a type of steel (USS T1) have withstood many (up to 41) strong shock loads with no detectable changes, whereas other specimens of this type of material have shown flaws after similar loading conditions. (U)
 - (b) A welded test sample exhibited internal cracking in the parent metal and essentially no cracking in the weld itself. The cracking was similar to flaws of an unwelded plate of the same material, and thus the origin of the flaws was not necessarily a result of the welding operation but probably resulted from flaws in the rolled plates from which the samples were made. (U)
 - (c) Shock-absorber attachment bosses (full-scale cross section) made as an integral part of the pusher plate withstood many strong shock loads of intensity similar to that required for OPTION nuclear operations. (U)
3. A good correlation was obtained between the BAMB computer program and HE experimental tests for plate flexural stresses due to impulse-pusher-mass mismatch. (U)
4. Two variations of a primary (toroidal) shock-absorber design using a urethane rubber bladder for gas containment and an organic filament structure were explored. Both types successfully withstood the required static-test pressures. The filament-reinforced knitted torus was tested to twenty-two full-velocity HE shock accelerations and remained intact. The measured response

UNCLASSIFIED

UNCLASSIFIED

WL-TDR-64-93

of this torus and a loading-ring attachment closely followed the calculated values. Attachment of the torus to the driving plate presented considerable difficulties. Development work remains to be done before this problem is satisfactorily answered. However, all the elements of such attachments have been successfully tested with the exception of the final operation of assembling the torus to the plate. Correction of design and fabrication shortcomings in this area should result in a successful attachment. (U)

UNCLASSIFIED

2. IMPULSE GENERATION (U)

(U) The ability to generate impulses of predictable characteristics was of paramount importance to the program for testing structural response to strong shock loading, including the response of plates, flexible shock absorbers, and the attachments between them.

(U) For dynamic response and structural integrity tests of full-size attachments and portions of full-size pusher plates, simulation of full-scale operational impulses over the areas of the test specimen was required. However, for certain response tests of scaled plates and scaled shock absorbers, considerably lower impulse intensities were required.

(U) In general, two high-explosive techniques for impulse generation were used for this program: a setup with the mass of HE separated from the target plate by air and a setup with the sheet HE separated from the target plate by a low-density material, such as foam plastic or fiberboard.

2.1. SPHERICAL-HE-CHARGE PULSE GENERATION (U)

(U) Tests were made with spherical HE charges to provide a reliable system for producing known, reproducible pulses on circular test plates. The results from the impulses of these charges were used to verify the results of a computer code for plate response. From previous extensive experience with the detonation of spherical HE charges in air, the HE sphere-air setup was expected to yield satisfactory pulse conditions. Although data for over-all face-on pressure and impulse for this geometry are practically nonexistent, some data of single-point face-on pressure and impulse are available. ⁽³⁾

UNCLASSIFIED

WL-TDR-64-93

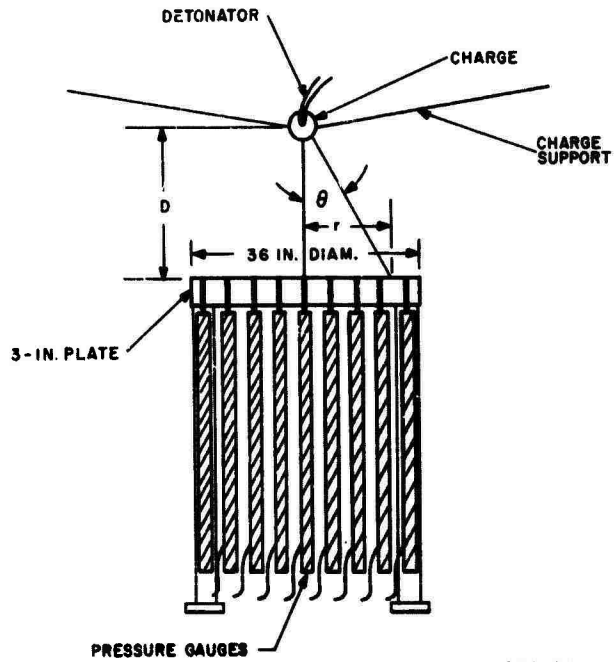
(U) The test setup consisted of a spherical HE charge placed above a heavy circular plate which was fitted with rapid-response piezo-electric pressure probes.⁽⁴⁾ Figure 2.1 is a schematic of the test setup to indicate the placement of the charge and pressure probes and Fig. 2.2 is a photograph of the actual setup.

(U) Composition C-4 was used as the explosive material for the charge. Matching hemispherical molds made of aluminum alloy were used for shaping the charges. The molds were sized for 2-lb, 5-lb, and 10-lb charges and were designed to fit into an existing press at the HE-charge fabrication facility. Each mold was fitted with a core to provide an opening for the insertion of an electric detonator. The detonator was positioned to initiate the charge from its center so that the impulse distribution would be as spherically symmetrical as possible.

(U) To avoid the recurrence of the low-order detonations that occurred during some of the earlier tests, a tetryl booster was used. A high-density (1.62 g/cm^3) tetryl pellet, 1/4-in. diam by 1/4-in. long, was located in the center of the HE sphere and the detonator was placed against a flat face of the pellet. This arrangement invariably produced high-order detonation.

(U) The measured pressure and impulse data appeared erratic for a true spherical detonation; this raised the question of whether the density of the composition C-4 charge was uniform. To check this, a few cast TNT spheres were used.

(U) In addition to the measurement of the pressure pulse generated by the detonation at various radial points on a plate situated face-on to the charge, high-speed framing-camera pictures of the explosion were taken to determine the sphericity of the expansion. Two such tests were made, one with a 2-lb molded C-4 spherical charge and the other with a 2-lb cast TNT spherical charge. The C-4 charge produced a good, uniform spherical fireball. The fireball of the TNT charge was not



(C) (Gp-4)

Fig. 2.1--Schematic of test setup for measuring face-on time-resolved pressure pulses radially across plate (U)



(C) (Gp-4)

Fig. 2.2--The pressure-probe test setup (U)

spherical and indications were that detonation difficulties occurred with the TNT. Figures 2.3 and 2.4 show sequential high-speed framing-camera photographs of these two tests. It was decided to proceed with the test program using the tetryl-boosted C-4 charge design.

(U) As the 2-lb C-4 sphere was considered to be the minimum-size charge that would reliably detonate with good spherical symmetry, no smaller sizes were used. Furthermore, the results from the tests with the 2-lb spheres indicated that larger charges would not be required for correlation with the BAMM Code results.

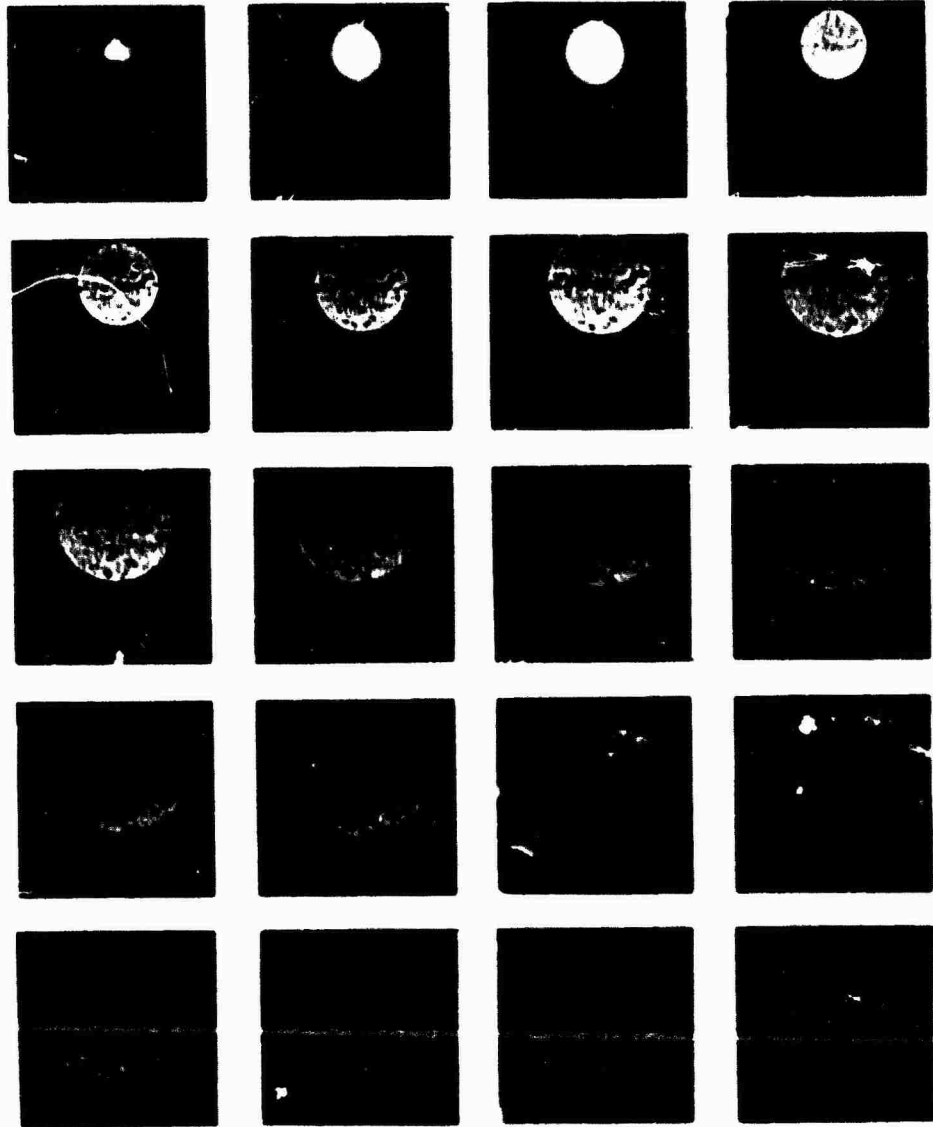
(C)(Gp-4) Time-dependent pressure was measured for 2-lb and 5-lb spherical charges at the plate centerline (face-on) and the results were checked with the data of Hoffman and Mills.⁽³⁾ A comparison of the data from these tests with those of Hoffman and Mills is given in Fig. 2.5. The impulse conditions needed for these tests required that relatively large charges be fired a short distance away from the reflection plate, or as plotted, $z = D/W^{1/3} \cong 1$, where D is the standoff distance, in feet, and W is the weight of the spherical charge, in pounds. The data of Hoffman and Mills started at $z \cong 1.5$. The relative agreement of these data provided confidence in the test setup and instrument calibration.

(C)(Gp-4) A series of tests were then made using 2-lb spheres fired at distances of 18 in., 24 in., 30 in., and 36 in. from the reflection plate so that the impulse as a function of radius of the plate could be measured. These data are shown in Fig. 2.6.

(U) The face-on impulse and peak pressure results agree reasonably well with the experimental data of others.⁽³⁾ Some of these data lie above the extrapolated data of Hoffman and Mills⁽³⁾ in the region of $D/W^{1/3} < 1.5$. This is to be expected because the mass of the HE compared with the mass of the air in the solid angle increases as $D/W^{1/3}$ decreases until the HE mass becomes an appreciable factor in the momentum-transfer process. The radial distribution of impulse as measured was quite similar to that expected. There were conditions in many tests

UNCLASSIFIED

WL-TDR 64-93



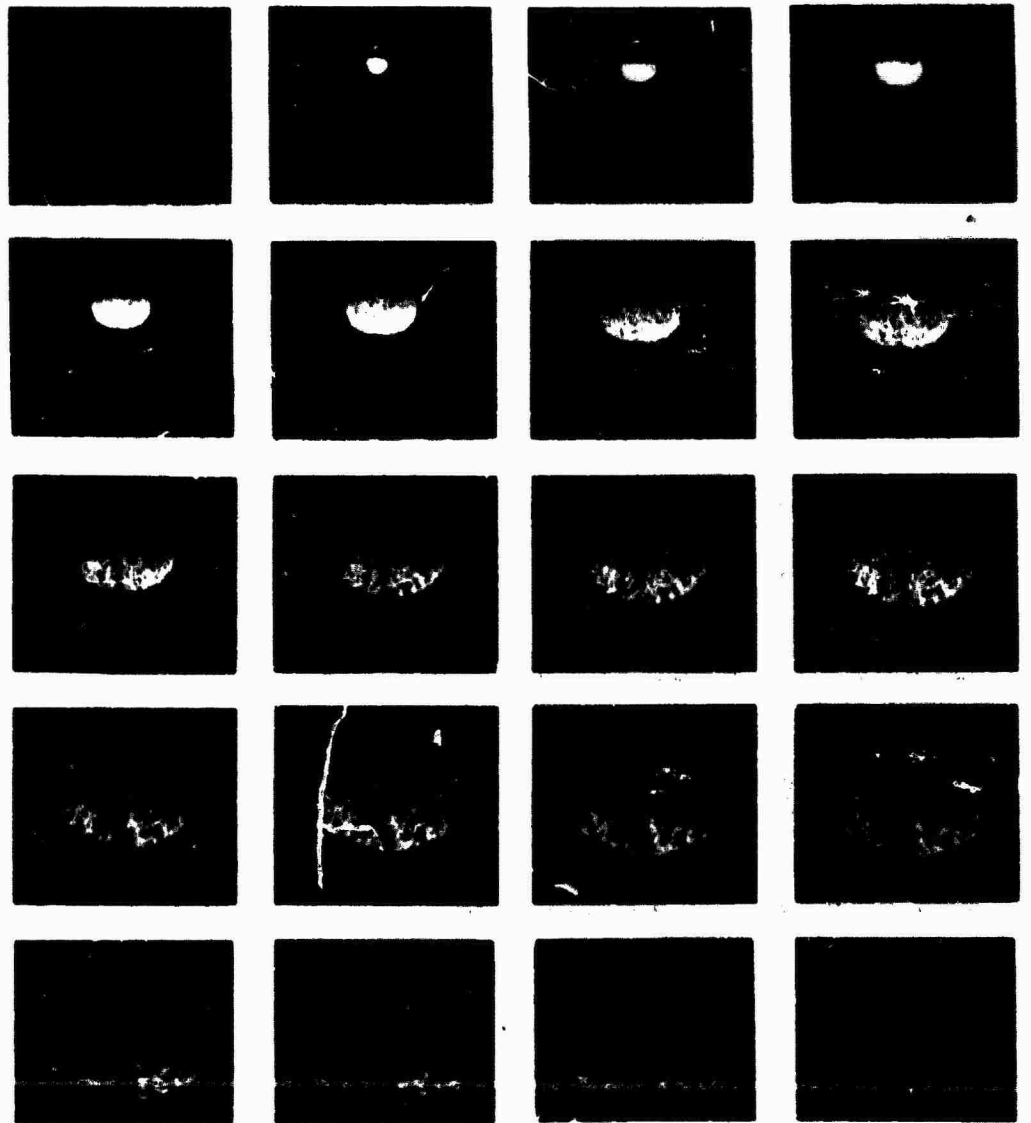
(U)

Fig. 2.3--High-speed framing-camera sequence of 2-lb C-4 spherical charge detonation (8 μ sec/frame) (U)

UNCLASSIFIED

UNCLASSIFIED

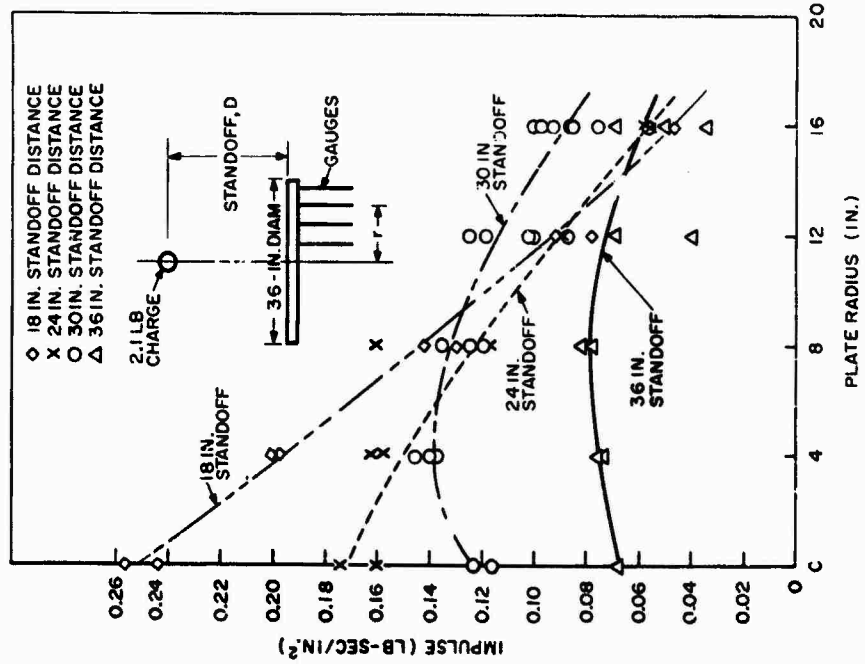
WL-TDR-64-93



(U)

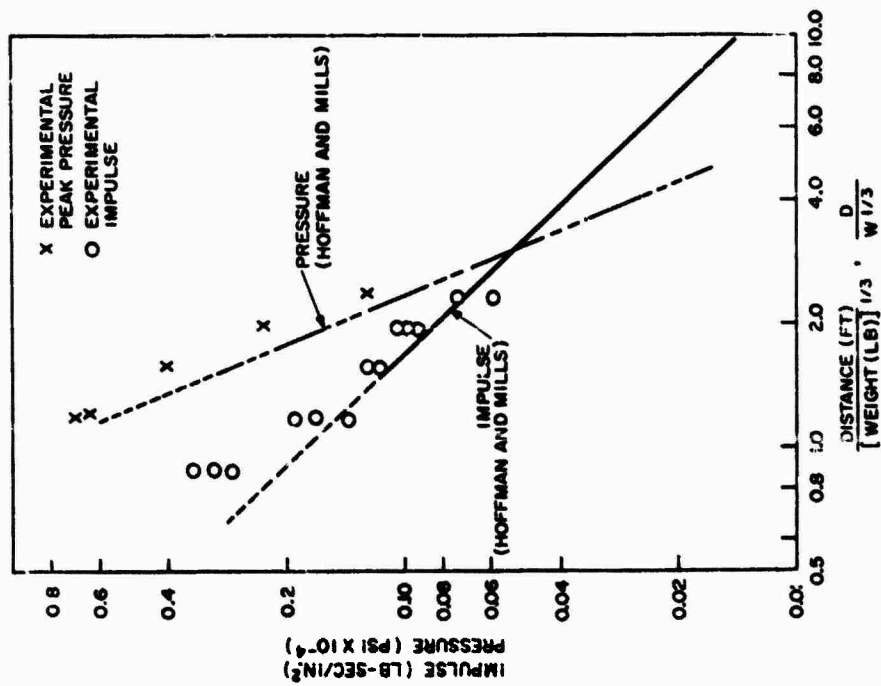
Fig. 2.4--High-speed framing-camera sequence of TNT spherical-charge detonation (8 μ sec/frame) (U)

UNCLASSIFIED



(C) (Gp-4)

Fig. 2.6--Reflected impulse measured from 2.1-lb C-4 HE charge fired in air (U)



(U)

Fig. 2.5--Reflected (face-on) pressure and impulse for spherical C-4 HE compared with other reported data (U)

which indicated lower impulse at the center than at some of the radial locations. When this occurred, tests were rerun with pressure gauges interchanged. Invariably, the same radial pressure patterns on the plate resulted. The significance of these unexpected results as they apply to a specific test is discussed in Section 3. 2. 3.

2. 2. SHEET-HE PULSE GENERATION (U)

(U) The work on pulse generation using sheet HE was directed toward the development of pulse generators which would deliver specified forcing functions for specific tests and pulse loads as close to the requirements of a full-size ORION engine as possible. The test setup for pulse generation is described in detail in Ref. 1.

(C)(Gp-4) Some test-plate segments with shock-absorber attachments (see Sections 3 and 4) were developed. The arrangements used in the plate-segment test were of two designs, each of which gave approximately the same pulse characteristics. One consisted of A-5 HE* with 4 in. of 4-lb/ft³ plastic foam† and 1 in. of plywood backup; the other consisted of A-5 HE with 8 in. of 13-lb/ft³ fiberboard with 1 in. of plywood backup. Typical impulses from these two pulse units are shown in Fig. 2. 7.

(C)(Gp-4) Other types of HE pulse generators used included A-1 and A-2 with 4 in. of 2-lb/ft³ foam with no backup to shock-load the plate in the single shock-absorber test (see Section 4).

(C)(Gp-4) A pulse with peak pressures in the range of interest to ORION but of shorter duration has been producible for sometime. Extending the time without increasing the peak pressure was one of the objectives in simulating pressures for a full-size ORION plate.

(U) *The sheet high explosive used was DuPont 506A series, which is approximately 85% PETN mixed with rubber binder. In this report reference is made to this material as follows: A-1 is 506A-1, A-2 is 506A-2, etc., A-1 is 1 g/in.², A-2 is 2 g/in.², etc.

(U) †Styrofoam, a polystyrene foam made by the Dow Chemical Company.

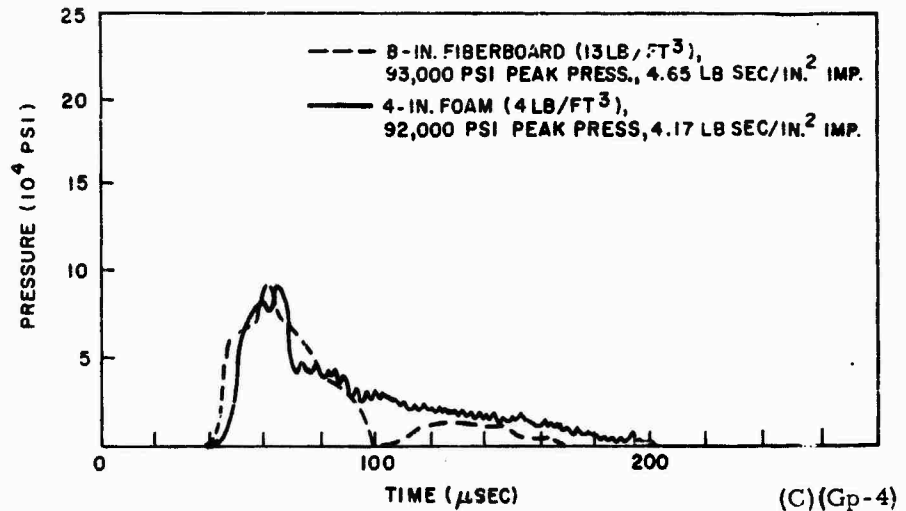


Fig. 2.7--Typical pressure pulses using different pulse-shaping materials and A-5 HE charges and 1-in. -thick plywood back-up material (U)

(U) Some exploratory shots with fiberboard indicated that this inexpensive material might be a good substitute for the more expensive dense foam. A series of tests with 13-lb/ft³ and 20-lb/ft³ fiberboard produced promising results. Typical pulse forms are given in Fig. 2.8, where the test data are compared with the calculated pressure pulse at the center of the pusher for the 10-m ORION engine. Tables 2.1 and 2.2 give the results of this series of tests.

(U) A comparison of the fiberboard test data with those of dense foam⁽¹⁾ indicates good correlation when the scatter in the data distribution is taken into consideration. Data scatter, as observed for foam and discussed in Re. 1, also exists with fiberboard, although the surface-damaging effects are less pronounced than with foam. The comparison for peak pressure is given in Fig. 2.9 and that for impulse is given in Fig. 2.10.

(U) From the experience gained during this test program and from previous experimental work,⁽¹⁾ the experimenter can approximate the structure of an HE pulse unit to deliver a selected impulse at a plate surface.

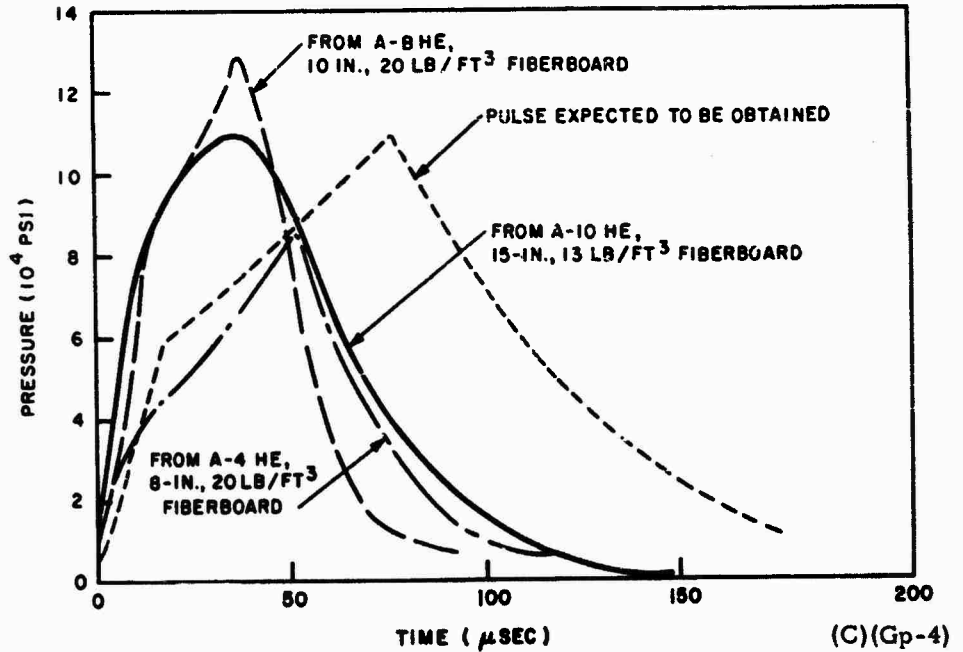


Fig. 2.8--Pulse forms of interest to ORION (U)

This current program, however, did not include the orderly, parametric study of the effects on impulse resulting from changes in HE pulse-generator components that would be necessary to define the design of sheet HE pulse generators. The data collected from these tests were obtained for specific purposes and were consistent with those reported in Ref. 1. However, much additional information concerning the general character of the sheet HE pulse-generator design was obtained during the course of this program. First, it was confirmed that detonating the generators other than at the edge produced a nonuniform circular-shaped pressure that was centered under the point of detonation. The diameter of the highest pressure ring is approximately 0.5 times the foam thickness. All tests using fiberboard were edge detonated. Second, the edge effects resulting in plate damage (peening) within 3/4 in. of the plate edge can be eliminated by extending the HE generators and the plate surface. The

Table 2. 1
FIBERBOARD TEST DATA (U)
(Density = 13 lb/ft³)

HE	Fiberboard Thickness (in.)	Plywood Backup (in.)	P _{max} (psi)	T (μsec)	$\left(\frac{I}{\text{in.}^2}\right)$	Test Plate Diam. (in.)
A-4	8	1	108,500	95	3.63	36
A-4	8	1	93,500	90	3.84	36
A-6	12	1	71,700	120	5.00	36
A-6	12	1	116,000	120	7.10	36
A-8	12	1	100,000	140	4.05	36
A-8	12	1	110,000	100	4.50	--
A-8	12	1	118,000	100	4.70	--
A-2	4	1	89,000	60	2.06	12
A-3	8	1	31,000	150	3.42	12
A-2	4	1	37,200	40	0.84	12
A-2	4	1	57,000	70	1.50	12
A-3	4	1	130,000	40	1.97	12
A-2	4	3	70,000	80	2.24	12
A-2	4	3	39,000	40	0.94	12
A-2	4	3	70,000	50	2.36	12
A-2	4	3	66,000	80	2.17	24
A-2	4	3	66,000	60	1.97	24
A-3	6	3	~70,000	---	----	12
A-4	8	1	82,500	100	5.15	24
A-4	8	1	-----	---	----	12
A-10	15	1	105,000	160	7.10	36
A-5	8	1	91,000	120	6.80	24
A-5	8	1	93,000	100	6.27	12
A-5	8	1	93,000	110	5.10	24
A-5	8	1	97,000	100	4.80	24
A-5	8	1	108,000	100	5.70	24
A-5	8	1	93,000	80	4.65	12
A-5	8	1	81,000	110	6.25	12
A-5	8	1	62,000	150	5.87	12

(C)(Gp-4)

Table 2.2
FIBERBOARD TEST DATA (U)
(Density = 20 lb/ft³)

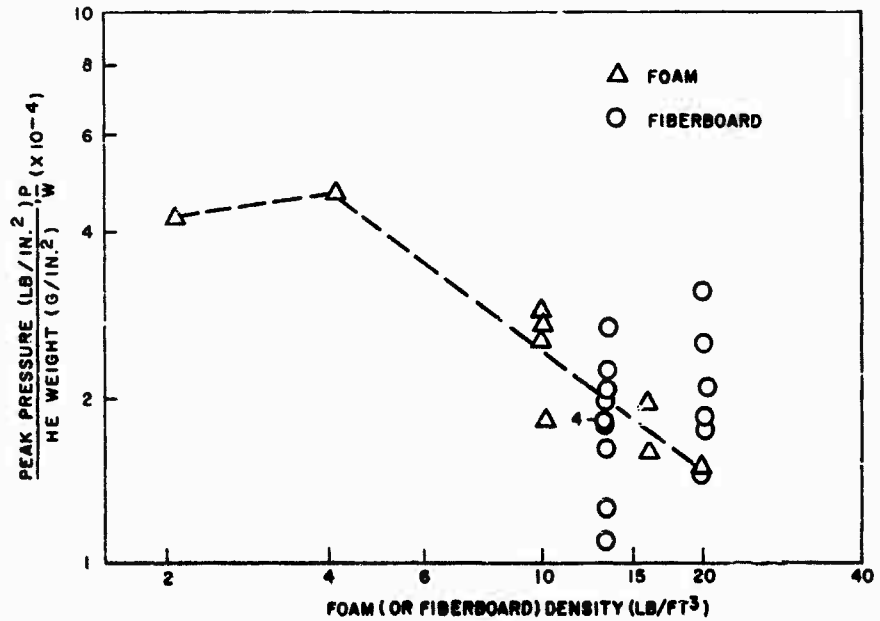
HE	Fiberboard Thickness (in.)	Plywood Backup (in.)	P _{max} (psi)	T (μsec)	I (lb-sec / in. ²)	Test Plate Diam. (in.)
A-9	8	1	138,000	~ 150	5.63	36
A-4	8	1	82,500	~ 140	4.70	36
A-4	8	1	73,500	125	4.60	36
A-4	8	1	70,000	155	4.53	36
A-8	10	1	128,000	140	5.65	36
A-8	12	1	71,500	90	2.90	36
A-4	8	1	150,000	140	9.75	24
A-4	8	1	100,000	120	5.80	24
A-4	4	1	200,000	50	3.10	12
A-2	4	1	100,000	80	2.98	12

(C)(Gp-4)

plate surface can be effectively extended by accelerating the target plate from a heavy metal ring. Figure 2.11 shows a sketch of the setup employing this technique. Third, inexpensive fiberboard will function in a manner equivalent to that of similar-density plastic foam. No surface damage on T1 steel plate surfaces was observed when fiberboard was used.

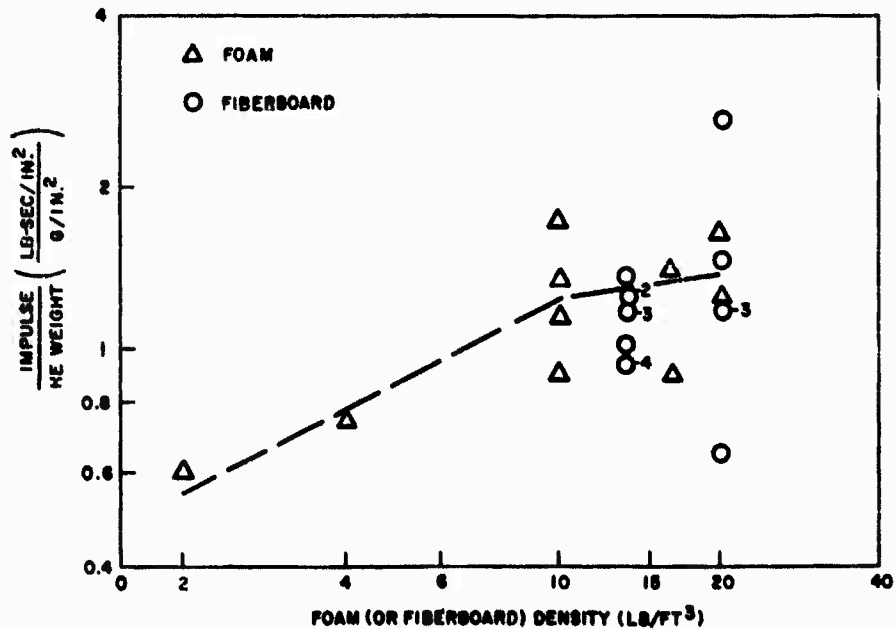
(U) For testing plates as thick as the 10-m ORION pusher with the impulse required for the center of the pusher, additional experience is required to extend the observed data. This is no evidence from the current experimental work that this should not be a readily obtainable goal.

(U) Following additional experience in pulse-generator design and testing to provide the desired pressure-time history corresponding to a discrete radial location on the pusher plate, techniques should be developed to provide a smooth variation of loading in the radial direction. There is no evidence to indicate that this will be overly difficult.



(U)

Fig. 2.9--Effect of foam (or fiberboard) density on peak pressure (all tests were made with 8-in. -thick foam or fiberboard) (U)



(U)

Fig. 2.10--Effect of foam (or fiberboard) density on impulse (all tests were made with 8-in. -thick foam or fiberboard) (U)

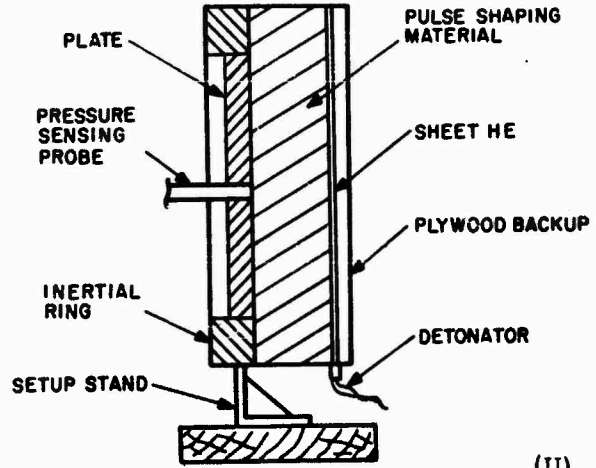


Fig. 2.11--HE pulse simulation test setup (U)

3. PLATE RESPONSE TESTS (U)

(U) Three main types of plate-response tests were conducted with well-defined goals in mind. These goals were to

1. Qualify the plates to be used with the single-torus and multitorus systems,
2. Obtain information on the dynamic behavior of plates subjected to an impulse mismatch for comparison with the BMM Code results, and
3. Obtain information on the structural behavior of steel plates to multi-exposures to establish a relationship between their engineering properties and their fatigue life.

3.1. PLATES FOR TORUS TESTS (U)

(U) The dynamic testing of torus structures using HE requires a pusher plate of satisfactory stiffness to prevent bending and of sufficient toughness to prevent cracking during the anticipated duration of the tests. Different materials were tested for the torus testing phase. The method of selecting the different plate materials is given Section 4.2.

3.1.1. Aluminum-plate Response (U)

(C)(Gp-4) Three 7075-T6 aluminum alloy plates, 2.0 in. thick and 26 in. in diameter, were exposed to impulses with peak pressures between 70,000 and 80,000 psi. The yield strength of this material is comparable to these pressures. It was hoped, in spite of the poor shock and notch properties of this material, that these plates could withstand several such impulses without failure. The mismatch of impulse to plate mass was expected to be small, so little bending was anticipated.

(U) In all tests, a small crack about 2 in. long appeared near the center of the plate after the first or second exposure. This crack was on the plate face opposite the face exposed to the explosion. After additional exposures, the crack extended several inches in length until finally the plate split in two. Photographs of these three plates are shown in Fig. 3.1. The fracture was of a brittle nature and occurred because of the very low elongation characteristics of this alloy. Further discussion of these tests is presented in Section 4.2.

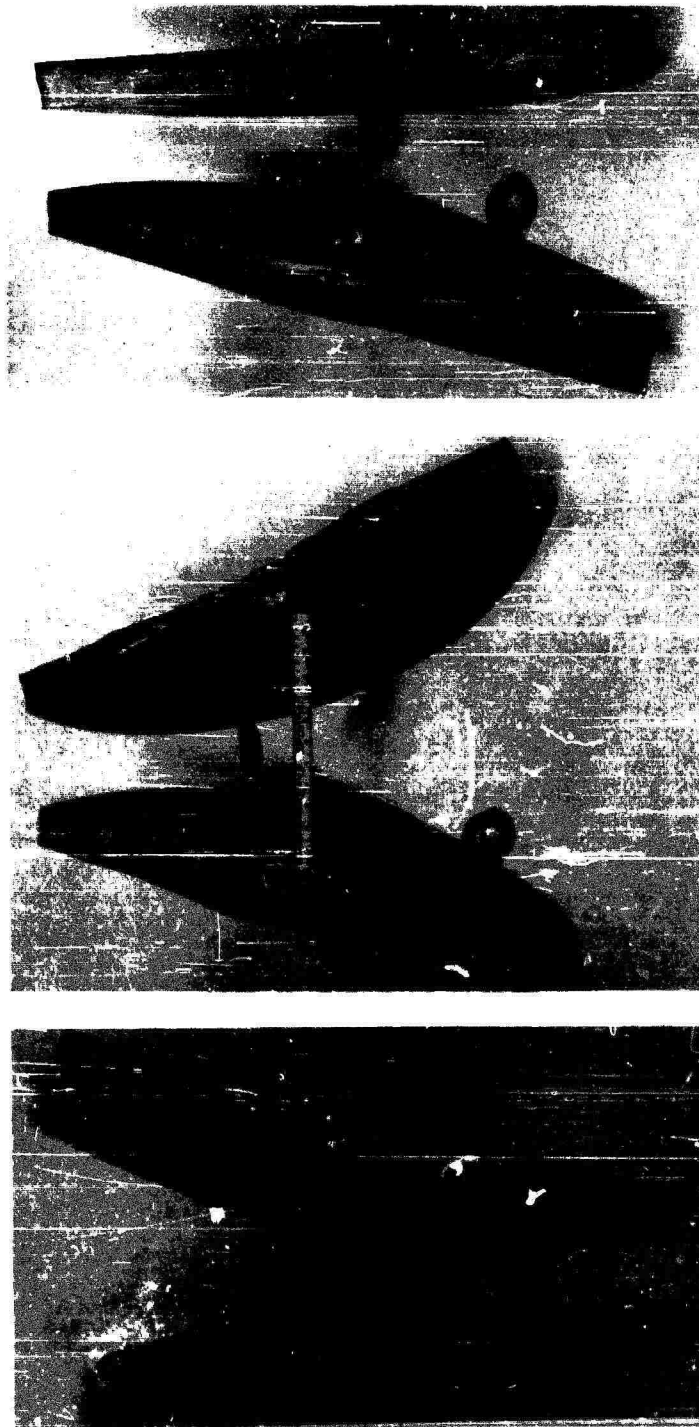
3.1.2. Steel-plate Response (U)

(U) A relatively high-strength steel (USS T1 Type 321B, 140,000-psi yield strength) was used in the fabrication of two identical test plates for the shock-absorber program. Each had a shock-absorber-attachment groove machined into one surface. The opposite surface was flat. Figure 3.2 is a photograph of a finished plate (see Fig. 5.10 for plate dimensions and the shock-absorber test setup). Each plate was machined from a section of a forged plate.

(C)(Gp-4) These plates were shock-loaded with sheet HE and pressure-attenuated with foam plastic to produce maximum peak pressures of 70,000 to 80,000 psi. Normal shock-absorber tests were done at lower peak pressures. There was no damage to the plates from the shock-loading. A discussion of the response of the plate and groove is given in Section 4.3.3.

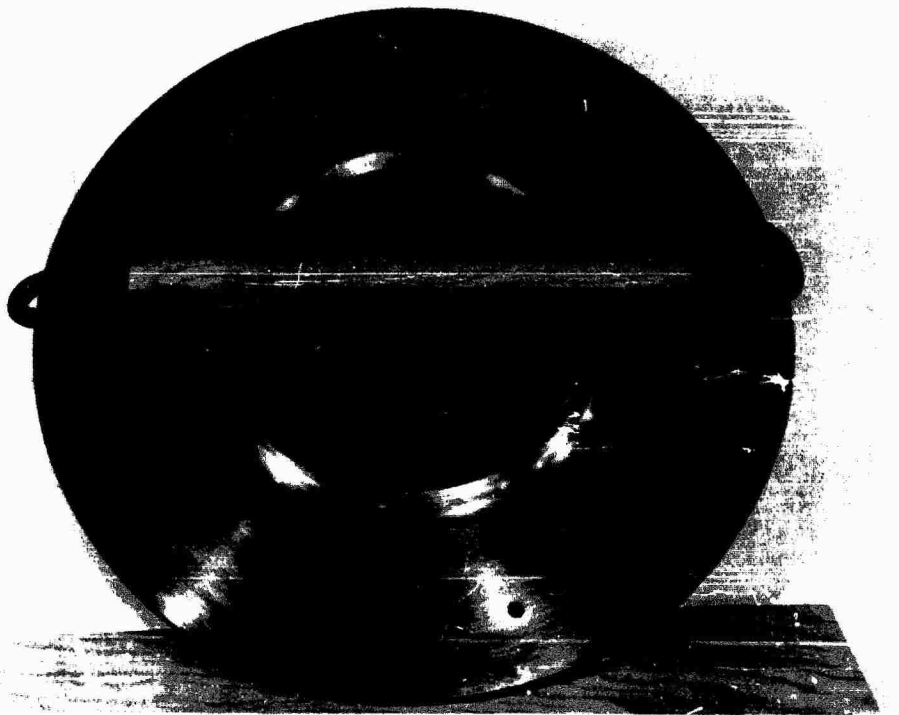
3.1.3. Results of Plate-response Testing (U)

(U) These tests confirmed previous experience that materials under strong shock-loading should be tough, particularly if the peak pressure is near the rated yield strength of the material. The 7075-T6 aluminum alloy was not ductile enough to withstand one shock without damage when the pulse pressure peak approached the rated yield stress. The T1 steel, on the other hand, can withstand many pulses when the peak pulse pressure is slightly below the rated yield stress. Whenever material of steel density is satisfactory for plates in the shock-absorber tests, the T1 321B steel is used.



(E)

Fig. 3.1--Failure of three aluminum plates (U



(U)

Fig. 3. 2--Typical steel plate finished for torus testing (U)

(U) Tests on some small magnesium alloy plates with attachment grooves indicated that ZK-60-T5 alloys might be satisfactory when low-density plate material is required (see Section 4. 3. 2). Preliminary tests on 6061-T6 aluminum-alloy plates indicated that this alloy can withstand shock-loading far better than the 7075-T6 alloy. However, the yield strength of any material should not be exceeded if it is to be subjected to repeated strong shock loads, even if the material is quite ductile.

3. 2. THE DYNAMIC BEHAVIOR OF PLATES SUBJECTED TO AN IMPULSE MISMATCH TO CHECK BAMB CODE OPERATION (U)

(U) One of the functions of the BAMB Code⁽²⁾ is to analyze the response of a circular plate to a time-step velocity which varies with plate radius, corresponding to a mismatch between the plate-mass distribution and an incident impulse distribution. The impulse and plate mass must

be symmetrical about the centerline of the plate. Experimental confirmation of the accuracy of the BAMB Code was considered to be important as this code has been the basic tool for pusher design and loading mismatch tolerance calculations.

3.2.1. The Computer Experiment (U)

(C)(Gp-4) A program was set up using a 24-in. -diam plate of uniform thickness (3/16 in.) and uniform density (steel) and an initial velocity that would simulate the loading of a spherical-HE-charge detonation in air. Twenty velocity increments across the plate radius were programmed to follow the relation $u_r = u_0 \cos^4 \theta$. A velocity distribution was selected so that u_0 , the center velocity, was 50 ft/sec and u_e , the velocity of the edge, was 25 ft/sec. The values of velocity, u , angle, θ , and stand-off distance, D , are shown schematically in Fig. 3.3.

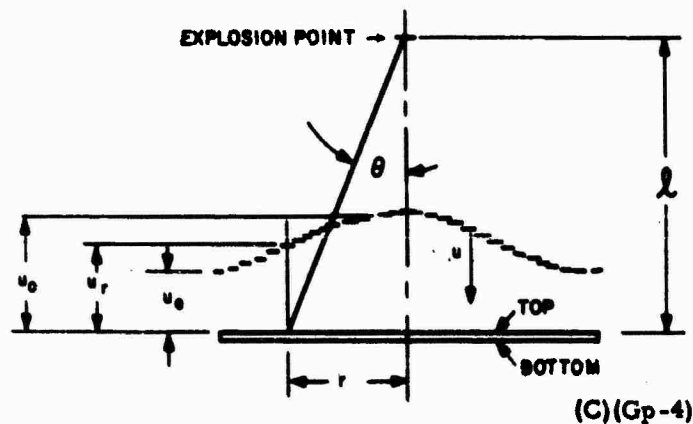


Fig. 3.3--Loading diagram for computer and HE tests
for plate flexure (U)

(C)(Gp-4) The computer data for the plate response to these initial conditions showed that a peak stress occurred as alternate tensile and compression stresses due to radial bending at a radius of approximately 3 in. The tangential, or hoop, stress at no time exceeded the radial stress. The calculation of the real pulse duration ran for 6 msec with data readout at each 100 μ sec. The natural period of ringing of the plate was

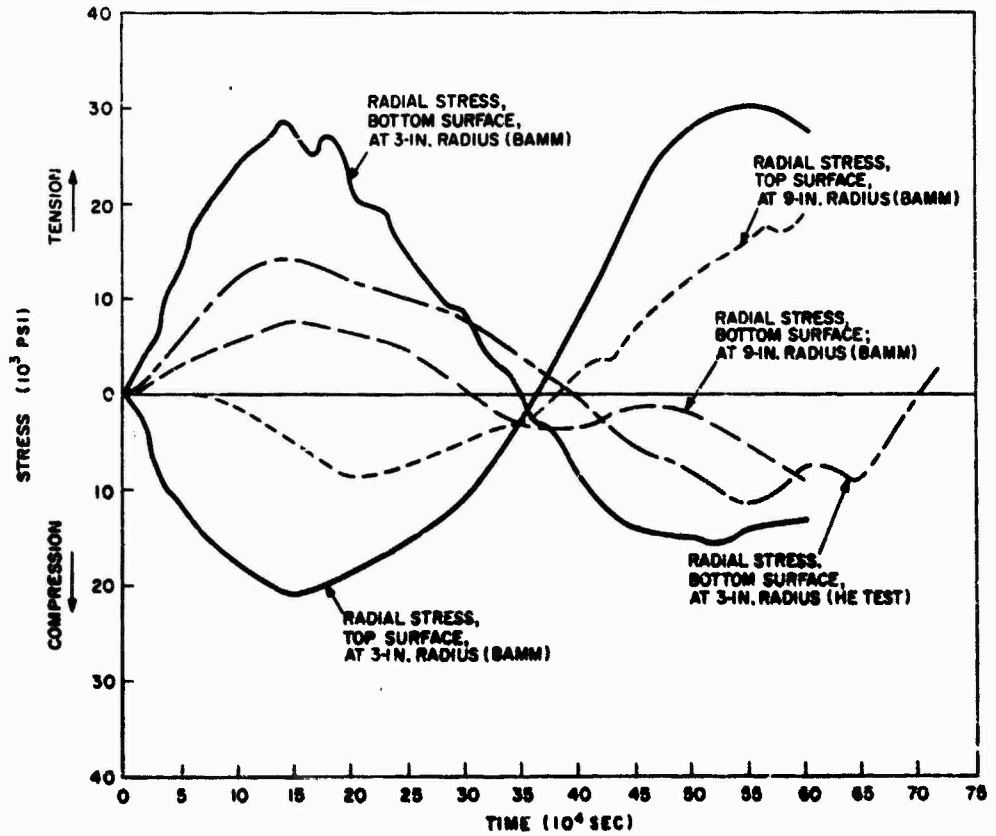
approximately 140 cps (7 msec per cycle). The radial-stress history of the top and bottom surface of the plate at 3-in. and 9-in. radii are shown in Fig. 3.4. For comparison, a curve for an HE test at 3-in. radius is also shown.

3.2.2. The HE Experiments (U)

(C)(Gp-4) The radial distribution of impulse produced when a spherical mass of HE (Composition C-4) is detonated on axis but at a distance from a circular plate was discussed in Section 2.1. It should be noted that there was scatter in the impulse at the measured points about the $I_r = I_0 \cos^4 \theta$ distribution. There was considerably more scatter in impulse per unit area when the charge was placed closer to the plate. To duplicate the conditions of the computer experiment, a spherical charge of less than 2 lb would have to be placed less than 24 in. from the plate. But as discussed in Section 2.1, 2 lb was a practical minimum-size spherical charge, and the minimum stand-off distance for this size charge was approximately 30 in. With these limitations, the velocity range of a 24-in.-diam. steel plate 3/16-in. thick would be 85 fps at the center and 63 fps at the edge if a $\cos^4 \theta$ impulse distribution were delivered by the charge. Although the velocity range of 22 fps for the HE experiment is slightly less than the 25 fps for the computer experiment and the radial distribution is slightly different because the values of D are different in the two cases, it is obvious that the differential radial velocity distribution of the computer problem is within the expected tolerance of velocities induced by the HE impulse.

(U) Strain gauges cemented to the protected surface of the plate were used to indicate the strain history of that surface at radial positions of 3 in. and 9 in. A dynamic strain-gauge potentiometer circuit with cathode-ray oscilloscope readout of the signal was used. This circuit is similar to that described in Ref. 5.

(C)(Gp-4) Results of these HE tests indicated a plate "dishing" mode of vibration with a fundamental frequency closely matching that predicted



(C)(Gp-4)

Fig. 3.4--Surface stress patterns for 24-in.-diam by 3/16-in.-thick steel plate with mismatch between impulsive load and plate mass (U)

by the BMM Code, e. g. , 140 cps (7 msec per cycle). Figure 3.5 shows the oscilloscope trace of a typical strain pattern. As might be expected from the irregularities in the HE detonation and in the higher modes of vibration in the test plate, appreciable energy at frequencies higher than the fundamental mode is indicated at the 3-in. -radius test point. A curve showing the approximate average of the fundamental frequency is compared with the results of the computer experiment in Fig. 3.4. The strain-gauge data taken at the 9-in. radius are shown in Fig. 3.6. Here, the higher-frequency components dominate the signal. A 7-msec duration fundamental cycle may be present, but if so, its amplitude is small. This is not inconsistent with the computer results, which show considerably lower amplitudes for stress at the 9-in. radius than that at the 3-in. radius.

3.2.3. Comparison of Results of Calculations and HE Experiments (U)

(C)(Gp-4) From a comparison of the results of the computer problem and the HE experiment, the following conclusions were drawn:

1. Correlation of the fundamental ringing frequency of the plate was excellent.
2. Correlation of the differential velocity-induced stresses as determined by the two approaches was good. At the 3-in. radius, the ratio of the calculated stress to the experimental stress was approximately 2:1. Since stress is proportional to the energy and consequently to the velocity squared, the ratio of calculated velocity to the experimental velocity is 1:0.7, which is within the uncertainty of the HE tests. The uncertainty of impulse (and velocity) distribution is indicated in Fig. 3.7.

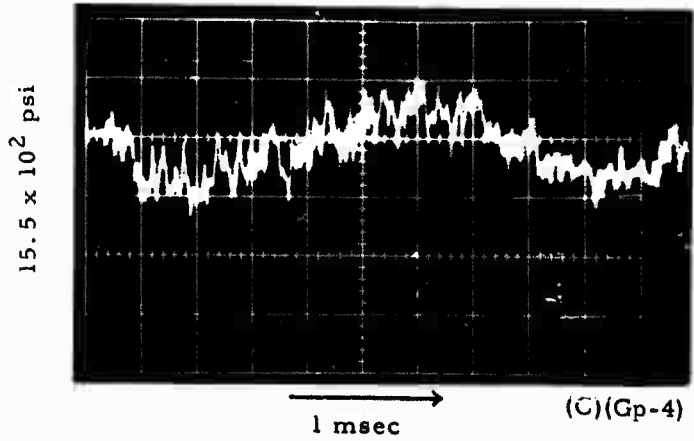


Fig. 3.5--Strain signal at 3-in. radius (U)

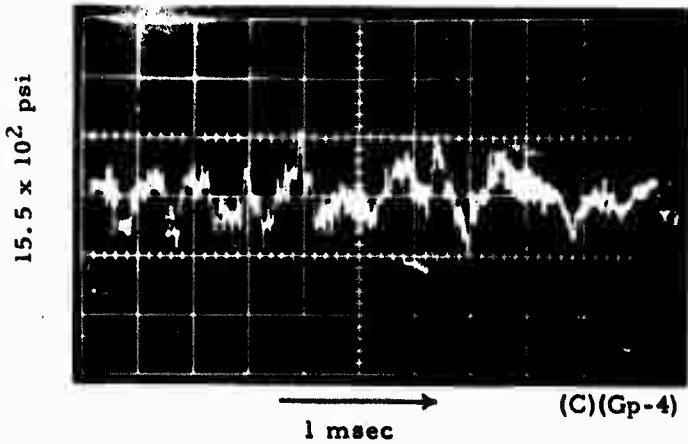


Fig. 3.6--Strain signal at 9-in. radius (U)

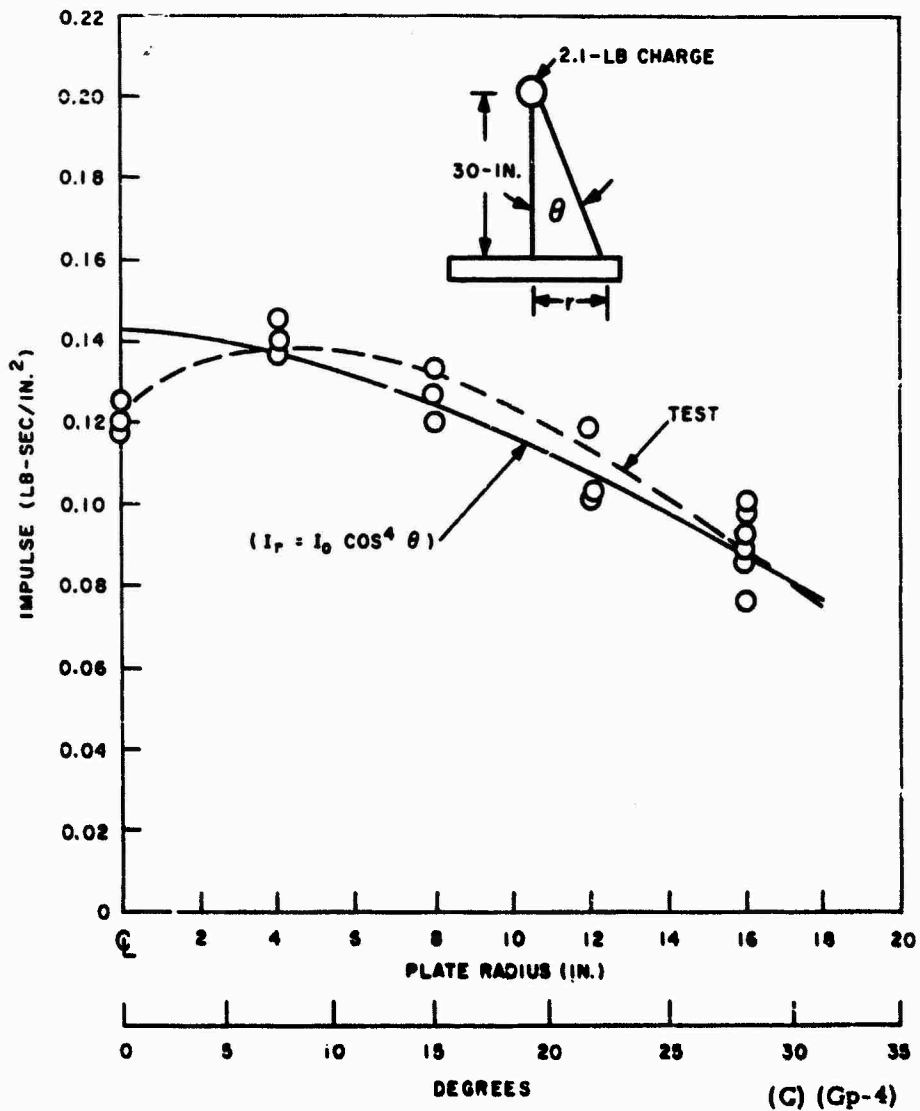


Fig. 3.7--Measured impulse distribution compared with $\cos^4 \theta$ distribution (C)(Gp-4)

More extensively instrumented plates for the HE tests, in which plate velocity distribution is accurately measured, would improve this correlation.

3. Relative stress levels in the fundamental mode are properly predicted by the BMM Code. The code indicated, and the HE test verified, the existence of considerably higher stresses at the 3-in. -radius point than at the 9-in. -radius point for a 12-in. -radius plate.

(U) Although the correlation of the results of the two methods is somewhat less than desirable in all respects, it appears that there are no gross discrepancies in the Code; wherever applicable, it can be used with confidence in calculating the structural response of the pusher.

3.3. STRUCTURAL BEHAVIOR OF STEEL PLATES SUBJECTED TO REPEATED SHOCK LOADS (U)

(U) In the consideration of candidate materials for the 10-m-diam ORION pusher plate, certain requisite properties become apparent. These include compressive yield strength higher than the expected peak pressure pulse; tough, ductile, crystalline structure; density high enough to minimize residual strain energy per pulse; amenability to current construction techniques, such as welding, heat-treating, etc.; and machinability.

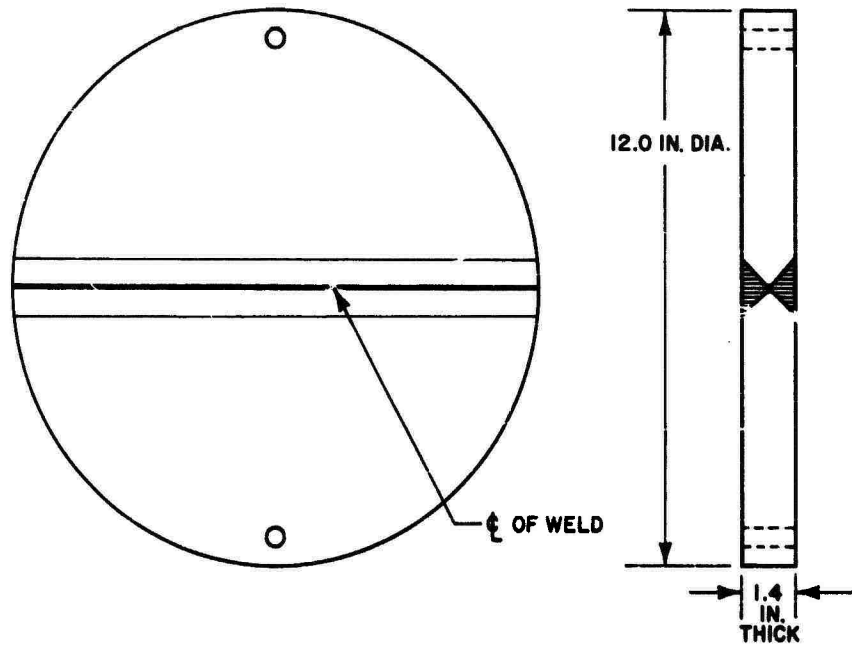
(U) Although the 10-m-diam pusher plate can be machined in its finished size on existing machines (40-ft boring mills), current practices appear to preclude the possibility of forging a plate that size from a single billet and thus welding may be required. The manufacturer's data indicate that USS T1 constructional alloy steel is compatible with essentially all of the above requirements, except that specific data on the effect of strong shock-loading on this material or its welds were not available. Previous experience with shock-loading of T1 steel was reported in Ref. 1.

3. 3. 1. Welded Test Specimen (U)

(U) To investigate the quality of welds in T1 steel of the thickness required for the ORION pusher-plate construction, a 12-in. -diam welded test specimen was made from a 1-1/2-in. -thick plate. The details of construction are shown in Fig. 3. 8. The welding was manual metal arc in accordance with the manufacturer's recommended procedure. After welding, the plate was ground flat on both surfaces.

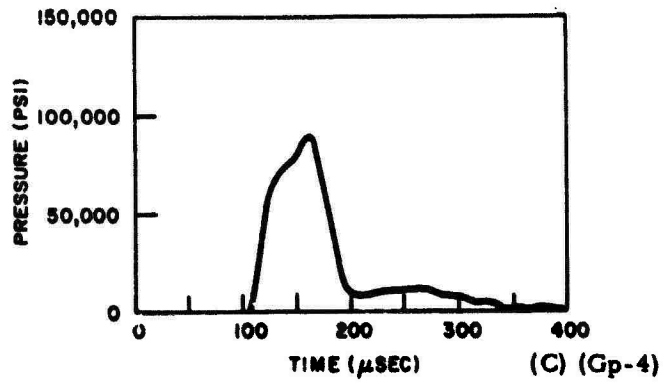
(C)(Gp-4) 3. 3. 1. 1. Tests on Welded Specimen. No special laboratory test of the plate was made prior to the HE shock-loading since it was believed that any weld failure could be traced to flaws after the fact. The test plate was exposed to fifty strong shock loads from edge-detonated sheet HE. Each pulse had a peak pressure of approximately 85,000 psi; the pulse shape is shown in Fig. 3. 9. After the sixth test, slight surface irregularities appeared in the center of the weld and along the heat-affected zones, all of which were on the surface opposite the shock-loaded surface. Similar irregularities may possibly have developed on the pulsed surface, but these would have been masked by minor surface irregularities resulting from the HE pulse load. At a later time in the test sequence, the heat-affected zones on the pulsed surface became optically prominent. After approximately ten shock tests, no progression of these irregularities on the surfaces was apparent.

(U) 3. 3. 1. 2. Post-test Inspection of the Welded Specimen. A rectangular sample (1 in. by 2 in.) was cut from the test plate. The faces of the sample were polished and etched and then photographed. The two faces of the section through the weld are shown in Fig. 3. 10. It is interesting to note that the T1 steel had sustained a serious crack on each side of the weld. There appeared to be a slight crack in the weld, but when magnified, the weld was intact. In fact, the weld appeared to be holding this small section of the plate together. On one face of the segment the crack in the steel had penetrated the weld by approximately a millimeter.



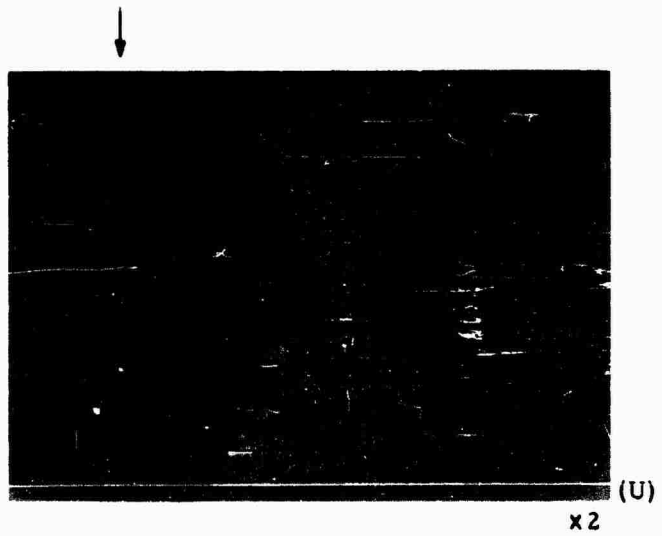
(U)

Fig. 3. 8--Welded test plate (U)

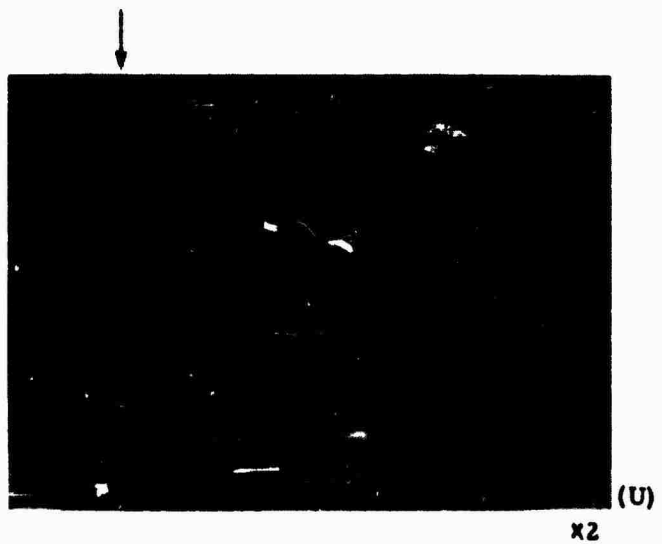


(C) (Gp-4)

Fig. 3. 9--Typical loading pulse for welded test plate (U)



(a)



(b)

Fig. 3.10--Polished and etched sections through weld of test plate (arrow indicates shock-loaded surface) (U)

The end of the crack that terminates at the weld is shown magnified in Fig. 3.11, where (b) is a further magnification of a portion of (a) and (c) is a greater magnification of the indicated area in (b).

(U) An inspection of the weld inclusions revealed the start of minor cracks in some locations. The root inclusion of face (a) in Fig. 3.10 has a crack propagating from each end; apparently there are none in the vicinity of a small inclusion. The root inclusion of face (b) in Fig. 3.10 has no cracks, but the large inclusion has three very small cracks. The photographs in Fig. 3.12 show the cracks which originated in the root inclusion of face (a) in Fig. 3.10. Note that crack b, which extends through the heat-affected zone, is approximately ten times longer than crack c, which extends into the weld metal.

(U) After examination of the rectangular sector taken from the welded test plate, it was decided to determine the extent of internal cracking. Radial (approximately) strips about 3/8 in. in width were sawed from the plate. The strips were ground on both faces, treated with a fluorescent die (Magnaflux-Zygo process), and inspected under infrared light. The general extent of the internal cracking, as well as the pattern of the inspection strips, is shown in Fig. 3.13. Inspection showed that approximately half of the total plate area contained cracks which were located within 1/4 in. of the center plane of the 1.4-in.-thick plate. There was no evidence of cracks extending through the weld nor of any cracks extending into the external surfaces of the plate.

3.3.2. Boss-plate Specimens (U)

(U) Three boss plates were made of USS T1, but no effort was made to ensure that any two of the plates were made from the same melt. The material for each plate was purchased separately. The boss plates were essentially the same size as the welded test plate (i. e., 12 in. in diameter by 1-1/2 in. thick) but they had a section of a full-size attachment boss on one surface. This design is described in more detail in Section 4. One of these plates with a saw-cut inspection strip in place is shown in Fig. 3.14.



(a)

x2

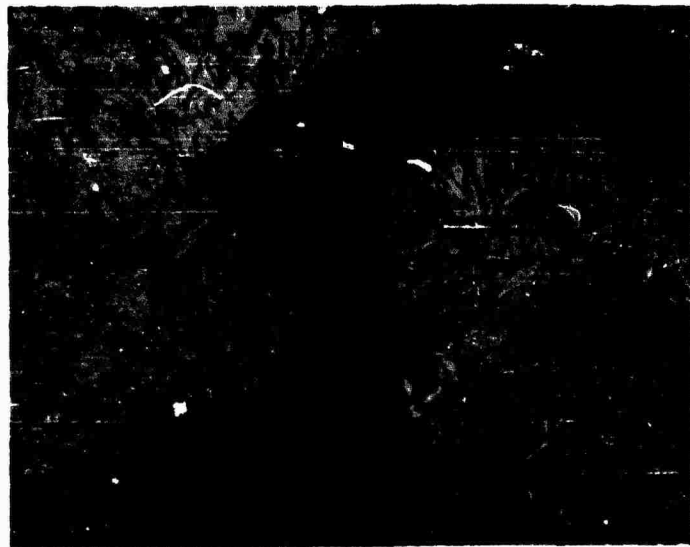
(U)



(b)

x50

(U)

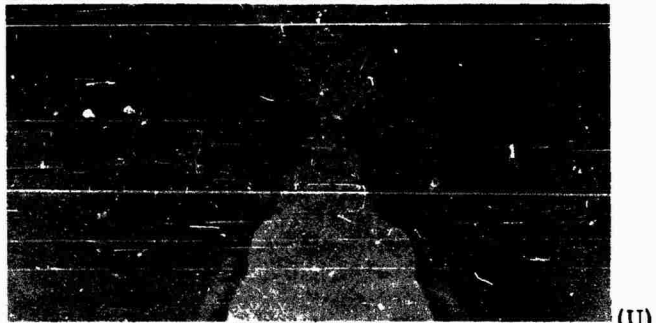


(c)

x500

(U)

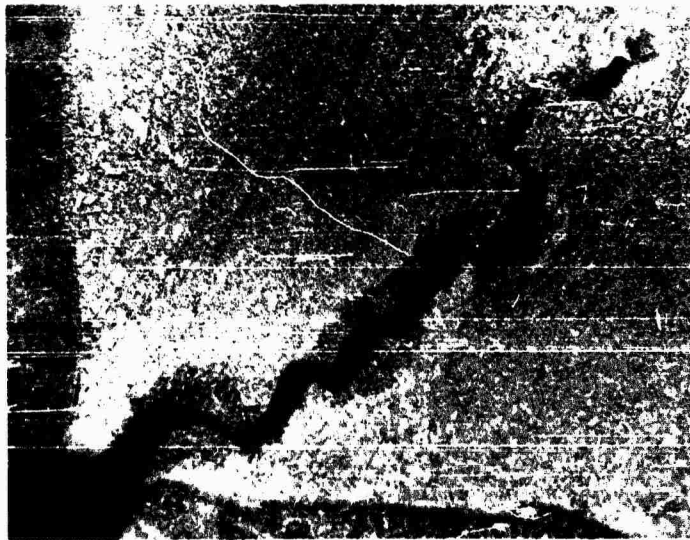
Fig. 3.11--Magnified crack end at weld of test plate (U)



(U)

x2

(a)



(U)

x50

(b)

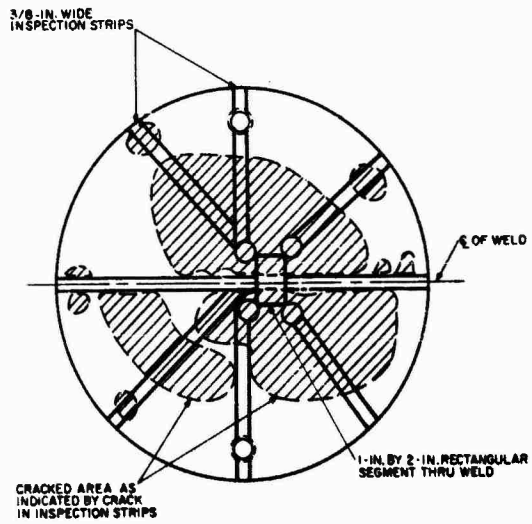


(U)

x200

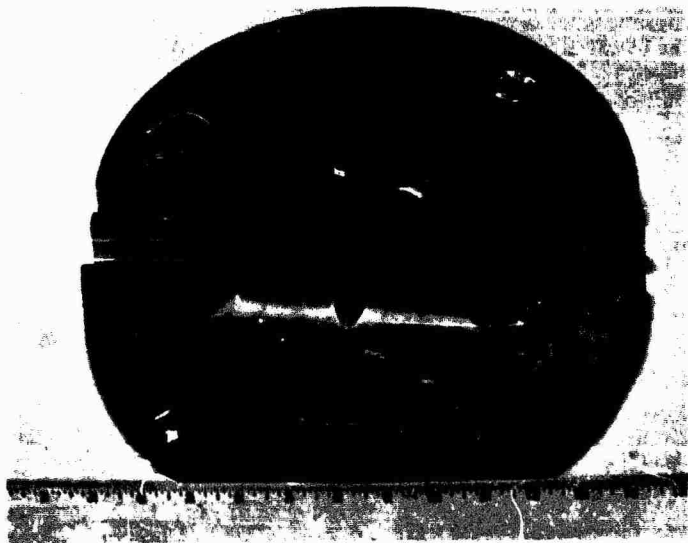
(c)

Fig. 3. 12--Cracks from weld inclusion of welded test plate (U)



(U)

Fig. 3. 13--Sectioned welded test plate with internally cracked areas indicated (U)



(U)

Fig. 3. 14--Boss plate 1 with inspection strip (U)

(U) 3. 3. 2. 1. Boss-plate Loading. Plate 1 was shock-loaded thirty times. Each pulse was essentially equal to the shock-loading of the welded test plate, but each of the HE pulse units were center-detonated. Plate 2 was shocked forty-one times; each time the HE unit was edge-detonated. The pulse units were the same as those used in the welded-test-plate series. Plate 3 was shock-loaded thirty times. However, for this test series the HE pulse unit and test setup were modified from those used with the welded test plate and the first two boss plates. Test plate 3 was fitted into a heavy steel ring and then both were accelerated with edge-detonated sheet HE separated from the plate by 8 in. of 13-lb/ft³ fiberboard. This setup is shown in Fig. 3. 15.

(U) 3. 3. 2. 2. Results of Shock-loading Boss Plates. Plate 1, which was shocked with center-detonated HE units, developed a characteristic circular indentation on the shocked surface. This indented area was approximately 2 in. in diameter and 1/16 in. deep, as shown in Fig. 3. 16. The plate edge bulged, as indicated in the sketch in Fig. 3. 17. This edge bulging resulted from the HE-pulse-unit edge effects. It was also present in the welded test plate and in boss plate 2. No change in diameter occurred in boss plate 3 with the steel-ring extension when the HE unit was edge-detonated.

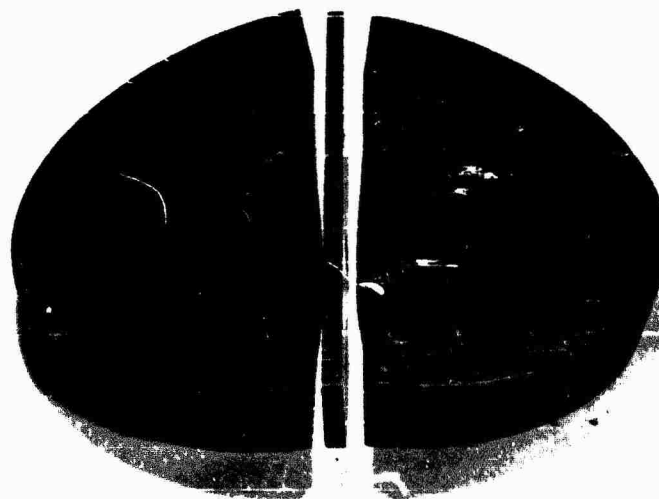
(U) A crack 1-1/2 in. long appeared at the bottom of the groove in plate 1. Except for this major crack and two small surface checks, no other cracks were observable on the surface. The inspection strip, when ground and treated with fluorescent dye and observed under infrared light, showed a small surface crack under the tip of each boss and major cracks within the body of the plate. These larger cracks were similar in size and appearance to those in the welded test plate. Fig. 3. 17 also shows the extent of the cracks in the inspection strip.

(U) Plate 2 showed blast surface damage similar to plate 1, except that no center circular indentation was present. Three inspection



(U)

Fig. 3.15--Test setup for boss plate 3 (U)



(U)

Fig. 3.16--Shock-loaded face of boss plate 1 (U)

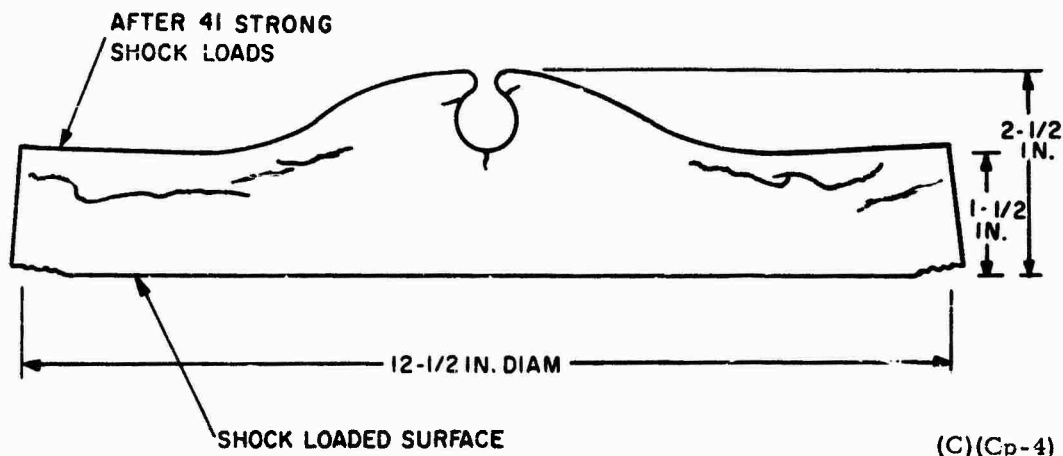
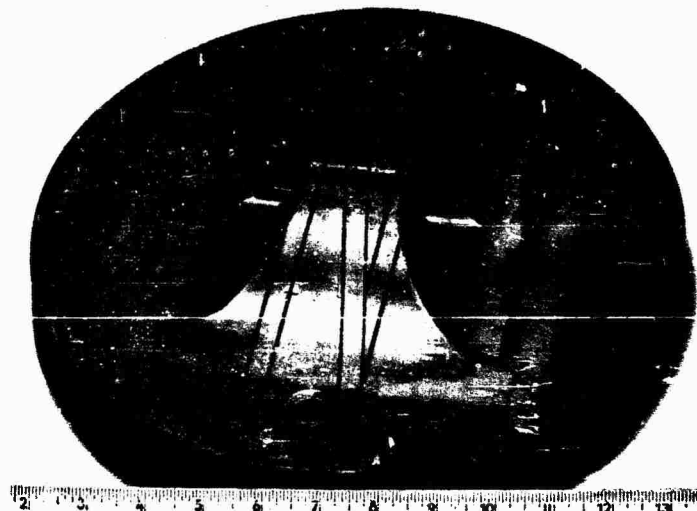


Fig. 3. 17--Sketch indicating bulge caused by HE shock units of diameter equal to plate diameter (U)

strips were cut from the boss section and cuts were also made through the holes, as shown in Fig. 3. 18. Inspection with the Magnaflux-Zygro process revealed no cracks in any of the cut surfaces.

(U) Plate 3 indicated little dimensional change (see Table 4. 3). Because of the good external appearance of this plate, additional shock-loading seemed advisable; therefore, no inspection strips were cut from this plate.

(U) It can be concluded from the repeated strong shock tests on these three boss plates and the welded test plate that under certain conditions, T1 steel can withstand many shock loads but under similar loading conditions cracks sometimes develop. The further pursuit of candidate materials for the ORION pusher should include careful quality control of test materials and a systematic study of the growth of flaws. Also, several other higher-strength metals should be considered. As indicated later, the decay rate of the forcing function can affect the internal stress patterns of the shocked



(C)(Gp-4)

Fig. 3.18--Second test plate with integral full-scale shock-absorber attachment section showing inspection cuts (U)

sample; however, for practical test and operational pulses and irregularly shaped plate sections (e. g., plates with bosses), this is not expected to be of major importance.

3.3.3. Internal Cracking of Shock-loaded Plates (U)

(U) The welded test plate and the boss plate 1 showed internal cracks when post-test inspections were made. Postulations of the origin and growth of these cracks are presented in the following paragraphs.

(U) Some plates showed cracks, whereas others with essentially identical loading conditions did not; it is therefore assumed that the cracked plates contained small cracks or flaws which may have been present in the plate stock from which the test specimen was cut. Minor gas or slag inclusion in the rolling process could result in plane flaws parallel to the rolled surfaces. In the welded test plate, thermal-stress cracks may have resulted from the welding operation even though very small rates of heat were used; forty-three weld passes were used in the butt joint of the 1 1/2-in. -thick plate.

(U) Crack growth due to shock-loading can be expected under certain conditions that result from the time distribution of pressure of the pulse and the behavior of shock transmission through or across any existing flaw. For example, tensile stresses can develop in the plate in the direction of the applied pressure pulse provided the rate of rise or decay of the pulse is fast compared to the characteristic strain transit time through the plate. Furthermore, when tensile stress is present, strong stress concentrations can develop at the crack edge to cause the crack to propagate.

(U) The characteristic strain-wave transit time, τ , through a plate of thickness, t , and made of a material with an acoustical velocity c , is

$$\tau = \frac{t}{c} .$$

For the steel used in these tests, c is 200,000 in./sec, or 0.2 in./ μ sec., and the plates were all approximately 1-1/2 in. thick. Therefore,

$$\tau = \frac{1.5}{0.2} = 7.5 \mu\text{sec} .$$

(C)(Gp-4) If the rise and decay rates of the pulse are gradual, as expected for nuclear-pulse operation (see Fig. 2.8), or like the smoothed, measured pressure pulse curve shown in Fig. 3.19, it can be shown that a plate with $\tau = 7.5 \mu\text{sec}$ will not undergo appreciable plane tensile stresses as a result of the pressure pulse. By geometrically inducing the pressure pulse into the target plate and using time as the common coordinate, one finds that at time equal to τ the stress pattern in the plate is coincident with the first 7.5 μsec of the pressure pulse as shown in the stress plot in Fig. 3.19. Also, at time equal to τ , the compressive strain wave has just reached the free surface of the plate and at the next instant will start being transmitted or reflected, depending on the characteristic impedance match between the plate and the material adjacent to it. In the tests, the plates were in contact with air and the impedance match was extremely poor, and thus the internal reflection of the compression wave was made

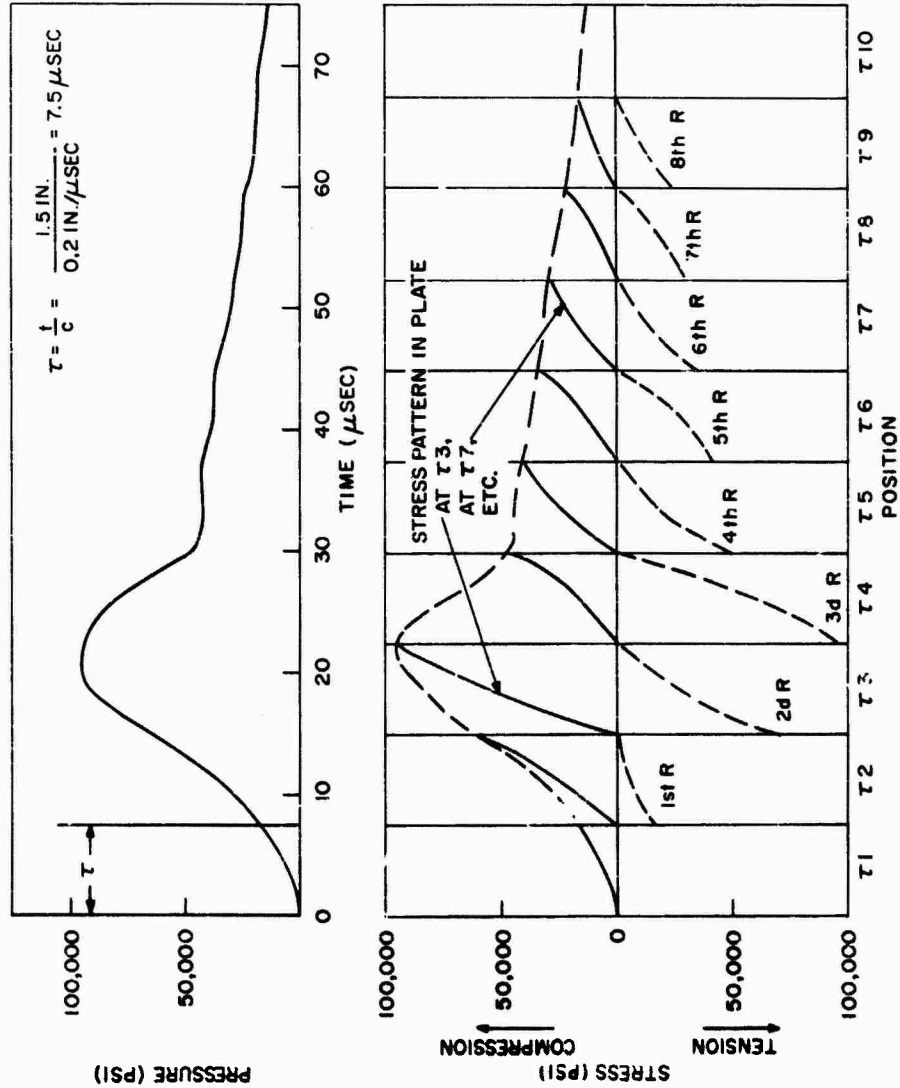


Fig. 3.19--Plane-plate-stress analysis and slow-decay pressure curve (U) (C)(Gp-4)

into an equal tension wave that traveled in the opposite direction. The amount of reflected tension wave subtracts from the value of the incoming compression wave. As shown in Fig. 3.19, at time 2τ , the test plate occupies a time-oriented position in the pressure pulse, as indicated by position $\tau 2$. At that position, the compressive stress of $\tau 1$ has been reflected as a tensile stress; the distribution is indicated as the first reflection, 1st R. When this reflected tensile stress is algebraically added to the new incident compressive pulse, the stress distribution for the plate at the instant 2τ (15 μ sec after 0) is shown as the solid line. By repeating this process, one can determine the plane-wave stress distribution in the plate throughout and after the duration of the pulse. As indicated in Fig. 3.18, no significant tensile stress is developed.

(C)(Gp-4) When a plate encounters a pressure pulse with a rapid rise or decay rate, significant tensile stresses can result. A pressure pulse with a rapid decay rate, such as that shown in Fig. 3.20, when used in a stress analysis similar to that of Fig. 3.19, illustrates how this tensile-stress condition develops. Such a stress is indicated in position $\tau 4$ of the stress plot in Fig. 3.20. This analysis indicates the possibility of appreciable tensile stresses, which, in this example, is ~25 percent of the maximum pulse pressure.

(U) The effect of a crack of zero thickness in the path of a compressive strain wave is negligible; i e., the compressive force can pass across the crack with little effect at the crack periphery. On the other hand, if a tensile strain wave encounters such a crack, it cannot be transmitted and thus is reflected internally as a compression wave. Under these conditions the periphery of the crack is subjected to a strong shear force as the tensile wave passes through the solid material adjacent to the crack and is reflected from the crack. This condition can cause the crack to propagate.

(U) In complicated cross sections of material, such as those required in the attachment bosses, very complex stress reflections and

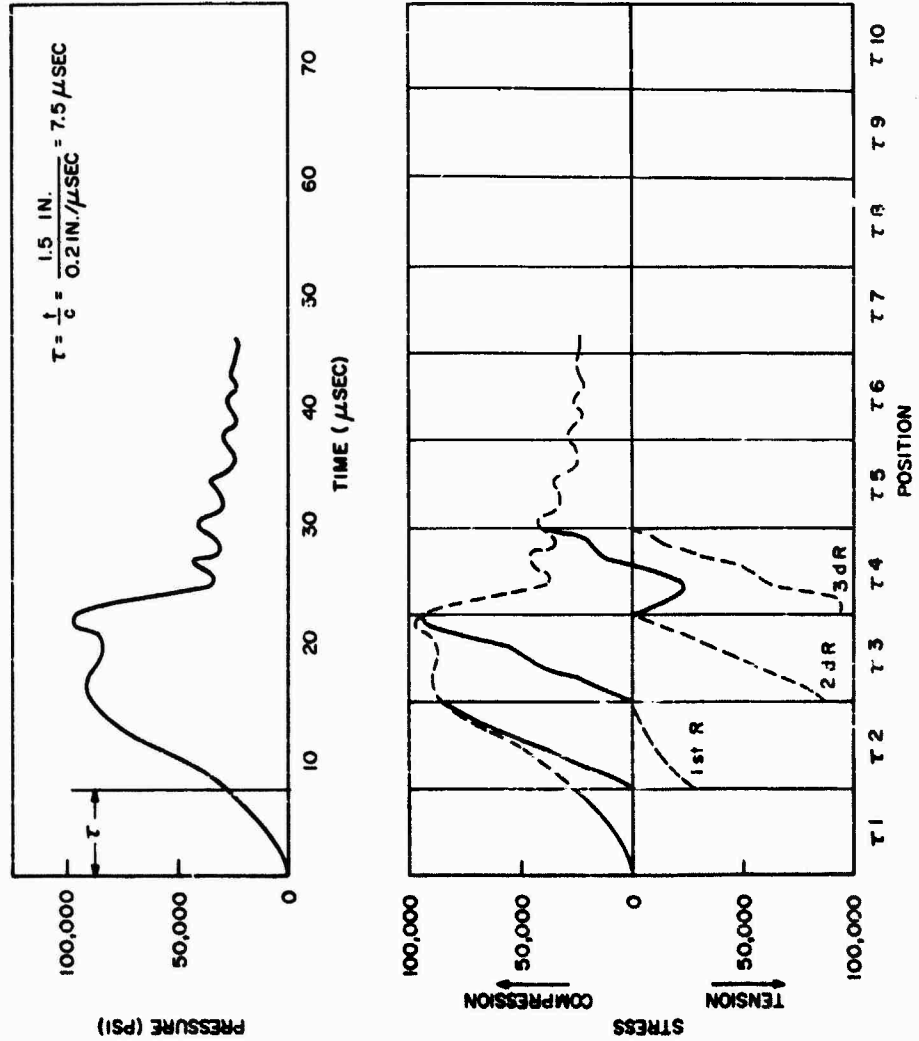


Fig. 3. 20--Plane-plate-stress analysis and rapid-decay pressure curve (U) (C)(Gp-4)

concentrations can develop. Any flaws which enhance stress concentrations are almost certain to propagate and grow into major flaws. Because of this complex stress condition in the boss area, it is believed that excellent quality control of pusher material will be required even if the pressure-pulse conditions are such that tensile stress would not be induced in a plane pusher plate.

3.3.4. Large-diameter Thin Plate (U)

(C)(Gp-4) The effect of radial strain waves converging into a small volume of the pusher plate material, as with a cylindrical implosion, has been studied theoretically. This effect has been of some concern to the designer. A test to give a general indication of the seriousness of this problem was devised. A plate, 45 in. in diameter, was cut from 1/4-in.-thick USS T1 steel stock for testing. This plate was exposed to several HE shock loadings of short duration ($\sim 20 \mu\text{sec}$) and peak pressures ranging from 50,000 to 100,000 psi. The tests resulted in plate velocities of 200 to 450 ft/sec, as derived from Fastax camera pictures. After the first three shots, from which no obvious damage resulted, three strain gauges were cemented to the back surface of the plate. One was located at the center, one radially situated near the edge, and the third tangentially situated approximately 1 in. in from the edge. The plate was subjected to three more tests and no apparent damage resulted from the shock loading; the strain gauges indicated a surface stress of less than 100,000 psi.

(U) The only conclusion that can be drawn from this short series of tests is that no obvious evidence of stress concentration of damaging magnitude was detected.

4. PLATE-ATTACHMENT RESPONSE TESTS (U)

(C)(Gp-4) Previous experimental investigations⁽¹⁾ of the response of structures bolted to plates which were subjected to severe impulses demonstrated that the bolting of any rigid structure, even a very small one, to a plate was not satisfactory because the bolts or screws would loosen after each impulse exposure. This loosening resulted from the screws not having the property to store elastically the kinetic energy delivered to the bolted structures by the plate at their interface. The prospect of bolting, bonding, or welding attachments to the plate was thus abandoned. The concept of integral clamping bosses on the pusher plate evolved as a consequence of these earlier investigations, which are described in Ref. 6 and in Volume III of this report.

(C)(Gp-4) A major problem with the boss-type attachment concerns the solid locking of the torus attachment bead inside a clamping-boss groove. Various design ideas have been investigated, such as the insertion of a metal cable inside the torus bead after its installation in the groove, but these more elaborate ideas did not appear practicable during the current study because of the limited program scope. A simpler and less expensive concept was adopted for study: a liquid resin is injected inside the torus bead after installation of the bead into the plate groove and the resin is then cured under pressure to provide the positive lock required.

(C)(Gp-4) As discussed in Section 1, the present program envisioned, under optimum circumstances, the testing of a single torus assembly, a three-torus assembly at the cable-stand facility, and, finally, a full torus system consisting of four stacks of seven torus layers (a 4 by 7 torus system) on a fixed test stand. As the single-torus system and the three-torus

system are not attached to the test stand and are free to move with the plate, very small masses are required on the free end of the system, and thus the energy storage capacity of these torus systems is adequate. When the torus system is attached to a fixed test stand, the plate mounted on the opposite end of the torus stack must weigh considerably less than the scaled-down equivalent pusher plate if the correct velocity increment of the plate is to be obtained. In either case, the plate simulating the pusher plate must be rigid and must not deform appreciably after many exposures. In the single-torus and three-torus systems, a heavy plate is acceptable and desirable to provide strength. These considerations led to the following choices of test configuration:

1. The single-torus and three-torus systems were to be mounted on 1.5-in. -thick 7075-T6 aluminum plates and accelerated with sheet HE (as described in Section 2).
2. The 4 by 7 torus system was to be attached to a light magnesium-alloy plate and accelerated with spherical or shaped HE charges in air.

(U) The choice of 7075-T6 aluminum was predicted on the fact that high pressure peaks would result (see Section 2 and therefore a high yield stress was required, even though the brittle characteristics of this alloy were known. Steel alloys were at first rejected because of the difficulties anticipated in the machining of the clamping groove and because, for the same diameter and weight, the aluminum plate would deform less for the same impulse mismatch.

(U) A ZK-60-T5 magnesium alloy was chosen since it had the highest yield strength available for the plate size under consideration (3 ft diam and 1.5 in. thick). The yield strength of this alloy is much higher than the pressure peaks expected from HE charges in air. Furthermore, this alloy has good ductility after forging and for the same weight results in more rigid plates than an aluminum alloy.

(C)(Gp-4) It was subsequently found that 7075-T6 aluminum was much too brittle (see Section 2), so USS T1 Type 321B steel (140,000-psi stress

yield) was considered. Thus, these three basic metals were investigated for the response testing of the 1/3-scale torus-model clamping boss. However, since USS T1 321B steel in thicknesses of several inches is not presently available, this alloy cannot be considered for the pusher-plate fabrication. USS T1 Type A firebox-quality steel is the only type that is currently available in thicknesses up to 6 in. Therefore, a full-size clamping-boss plate sample was made with this alloy. The yield strength of this steel is between 90,000 and 100,000 psi at room temperature, which corresponds to the pressure peak developed by the propellant stagnating against the pusher plate (see Volume III of this report).

(U) At the beginning of the current test program several types of resins were considered as a possible torus locking material, but a quick survey of their characteristics and a few static tests eliminated most of them. The requirements are severe: the cured resin must not be brittle, it must be hard and not too ductile, it should have a low viscosity at temperatures of 150°F or lower, and it should cure at that temperature or below. The pot time must be at least 15 min, and preferably much longer. Of all the resins investigated, NARMCO 3135-7111 formulation was the type that satisfied all these requirements. Other resins might be suitable, but no further investigation was made when a satisfactory resin was found. Therefore, only the selected resin was submitted to shock tests. It was molded inside Tygon tubes having the same wall thickness as that expected for the torus clamping bead.

4.1. TEST OBJECTIVES OF THE CURRENT PROGRAM (U)

(U) The tests carried out on plate attachments were intended to provide information on the material strength to (1) qualify the plate torus attachments for the torus test program reported in Section 5, (2) qualify the torus-attachment locking devices, and (3) study the response of full-size clamping-boss sections to full impulse loads.

(U) Only a small number of exposures to shock-loading were required for (1) and (2), and these corresponded to the number of

exposures that was expected for the subsequent torus test program, namely, between twenty and thirty exposures.

(U) For (3), testing was to be continued until a major failure or dimension change of the test sample occurred; the larger the number of exposures, the better.

(U) In addition to these three major objectives, incidental information, such as the response of short rigid structures bolted to plates and used to protect the torus system, was obtained.

4.2. TEST RESULTS (U)

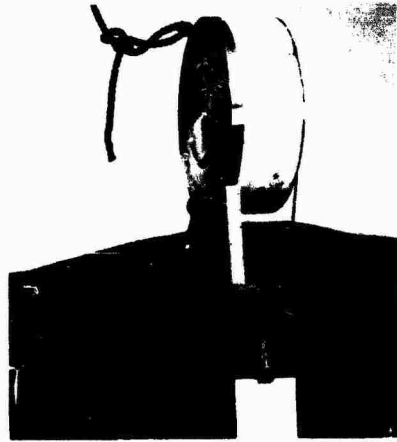
(U) The number and variety of plate-attachment response tests were so extensive that a classification of the tests was necessary for the presentation of the results. The tests were classified according to the nature of the test article and the type of test. As explained in Section 4.1, the choice of plate material for the testing of the torus system was initially 7075-T6 aluminum alloy and subsequently USS-T1 321B steel, which explains why so much testing was done with aluminum plates. This series of tests was finally divided into the following groups:

1. Aluminum plates with simulated torus clamping bosses and groove (qualification for single-torus testing).
2. Magnesium plates with simulated torus clamping bosses and groove (qualification for multitorus testing).
3. USS T1 steel plates with simulated torus clamping bosses and groove (qualification for single-torus testing).
4. Shields for the torus systems (qualification for single-torus and three-torus testing).
5. Full-size torus-clamping-boss test plates (for response testing).

Figure 4.1 shows typical test setups for such plate tests.

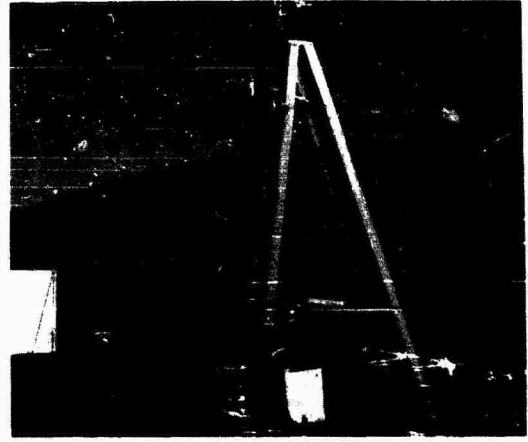
4.2.1. Aluminum Plates (U)

(C)(Gp-4) Two 7075-T6 aluminum plates, 12 in. in diameter and 1 in. thick, were tested. The first plate had bosses machined on one side and the bosses were grooved to simulate the geometry of the clamping boss



(C)(Gp-4)

(a) Aluminum plate setup for torus testing (U)



(C)(Gp-4)

(b) Magnesium plate and 2-lb spherical-shaped HE charge (U)



(C)(Gp 4)

(c) Magnesium plate and 10-lb conical-shaped HE charge (U)

Fig. 4.1--Typical plate test setups (U)

designed for the torus-model tests. A sketch of this test plate is given in Fig. 4.2. Although this plate was to have been exposed to full-impulse multishots to study the response of the clamping-boss lips, it was only exposed to three shots (one A-2 and two A-3 HE charges). The velocity increment was between 140 and 160 ft/sec.

(U) Cracks starting from the sharp angle made by the boss walls and the flat plate face were noticed after the first exposure. The cracks increased in size after each exposure until two bosses spalled off the plate after the third exposure. Various resin samples had been tightly inserted inside the boss grooves before the tests. After the third exposure, one resin sample (NARMCO 3135-7111) was still intact, whereas the other samples had cracked and were considered to be too brittle.

(U) The clamping boss lip opening and the groove diameters were gauged before the first test and after each test; their dimensions changed only slightly (less than 0.002 in.).

(U) From the nature of the cracks and the boss failure, the brittle characteristics of the 7075-T6 aluminum apparently caused the cracks to start at the point where stress concentration occurred, namely, at the sharp angle indicated by the arrow in Fig. 4.2. Various views of the plate at the end of the test series are shown in Fig. 4.3.

(U) Since the clamping-boss dimensions had remained relatively constant and the resin (NARMCO 3135-7111) sample had performed satisfactorily, a second plate of the same material was made with a circular groove and a clamping boss without sharp angles. Resin was injected into a Tygon tube located inside the groove to simulate the torus clamping bead.

(C)(Gp-4) This second plate was subjected to seventeen exposures (A-3) with a velocity increment of about 200 ft/sec or more. The clamping-boss lips closed ~0.005 in. during these tests. A small crack developed in the resin after five exposures. At the end of the test series, five cracks were apparent in the test plate. Cracks in the clamping-boss lip above the resin injection holes started after the fifth exposure. After the ninth

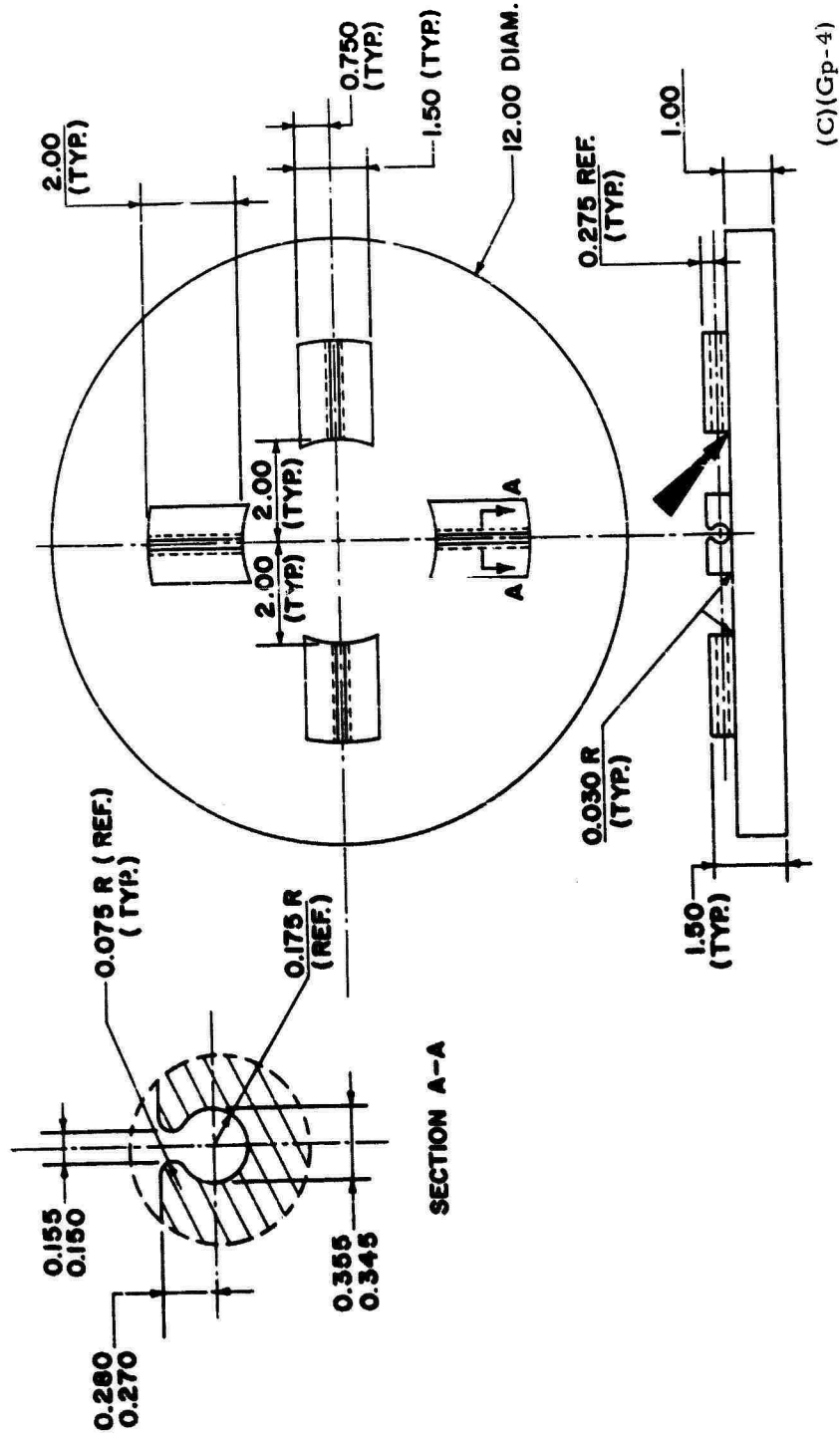


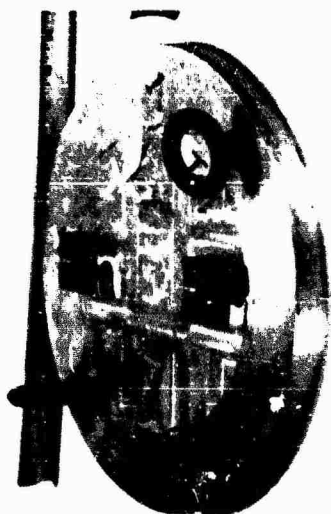
Fig. 4.2--Four-boss aluminum test plate (U)



(b) Spalled-off boss
(C)(Gp-4)



(d) Plate surface exposed to HE
(C)(Gp-4)



(a) Over-all aspect
(C)(Gp-4)



(c) Boss spalling
(C)(Gp-4)

Fig. 4.3--Aluminum boss plate after testing (U)

exposure, the lips above both resin injection holes were cracked through. At the end of the test series, a crack had propagated from one resin injection hole almost to the other, but this part of the boss lip was still holding to the plate. Several views of the plate after the completion of the tests are shown in Fig. 4.4.

(U) A third 7075-T6 aluminum plate was made to accommodate the attachment for the single-torus system. It was subjected to two A-3 exposures. After the first exposure, a 2-in.-long crack appeared at the plate center and after the second shot, the crack extended several inches. The clamping-boss lip between the two adjacent resin injection holes spalled off and a small crack appeared at the bottom of the groove parallel to its centerline. No further tests were made with this plate. Views of this plate after the tests are shown in Fig. 4.5.

(U) As a result of these tests, several conclusions were reached:

1. The NARMCO 3135-7111 resin would be adequate for torus assembly to the plate,
2. The aluminum alloy 7075-T6 was not satisfactory (this conclusion was reached independently from that given in Section 3), and
3. The clamping-boss design was satisfactory.

4.2.2. Magnesium Plates (U)

(C)(Gp-4) The magnesium alloy ZK-60-T5 had been chosen as the best material for the plate mounted on the 4 by 7 torus assembly (as explained in Section 4.1). Since only a small impulse was required for the multitorus test (because of the limited energy storage capacity of the torus system), the impulse desired could not be obtained with the sheet-HE-attenuator combination. Therefore, spherical or conical HE charges in air were chosen as the energy source. These charges yield a peak pressure that is not only lower than the sheet HE, but also well below the yield strength of the magnesium alloy. Two magnesium plates, ~10 in. in diameter and



(b) Resin injection holes (C) (Gp-4)



(d) Plate surface exposed to HE (C) (Gp-4)



(a) Plate after testing (C) (Gp-4)



(c) Simulated injection hole (C) (Gp-4)

Fig. 4. 4--Aluminum plate with resin bead after testing (U)



(a) Over-all plate aspect

(C) (Gp-4)



(b) Typical crack near plate center

(C) (Gp-4)



(c) Clamping-boss lip spalling and crack at the groove bottom

(C) (Gp-4)

Fig. 4.5--Aluminum plate with torus attachment after testing (U)

5/8 in. thick, were used. A bead clamping boss with a groove was machined on each plate. The groove in the first plate was left empty, but the groove in the second plate was equipped with a resin bead similar to that used with the second aluminum plate.

(C)(Gp-4) 4.2.2.1. Magnesium Plate with Empty Groove. The first eight exposures of this plate were made with 10-lb spherical charges, each of which give a velocity increment of ~ 180 ft/sec. There was no noticeable change in the plate except a very small crack that developed at the top of a resin injection hole; there was no dimensional change of the groove. To accelerate the test program, A-1 sheet HE was tried for the ninth test. With the velocity increment obtained, the plate face exposed to HE was badly pitted by attenuator debris, so this technique was abandoned.

(C)(Gp-4) To obtain a higher impulse but still keep the peak pressure below the magnesium yield point and avoid debris damage, it was decided to use 10-lb conically shaped HE charges. These charges yielded a velocity increment of 350 to 500 ft/sec. After two such exposures, the clamping boss lips closed ~ 0.005 in. and the plate bent $\sim 1/4$ in. Since slight signs of ablation were visible after the 10-lb spherical-charge shots, it was decided to apply heavy grease on the face exposed to the blast to protect the plate adequately. This scheme worked satisfactorily. The photographs in Fig. 4.6 show this plate after the testing.

(C)(Gp-4) 4.2.2.2 Magnesium Plate with Resin Bead Installed. The second plate was exposed to nine 10-lb spherically shaped charges and then to fifteen 10-lb conically shaped charges. There was no noticeable change in the plate dimensions after the spherical-charge test series. One crack started at a resin injection hole after the third conical-charge shot. After the fourth exposure, a crack appeared in the resin. Finally, after the ninth exposure, another crack started at one of the eyebolt holes. After the twelfth shot (with the 10-lb conical charge), the clamping-boss lip opened from 0.002 to 0.005 in. After the final tests, the lips above five



(C) (Gp-4)
(b) Detail of boss holes



(C) (Gp-4)
(d) Ablated surface and debris impact damage



(C) (Gp-4)
(a) Over-all aspect of the plate



(C) (Gp-4)
(c) Plate surface exposed to HE

Fig. 4.6--First magnesium plate (no resin bead) after testing (U)

of the seven resin injection holes had cracks and the resin had cracked in six spots. Views of this plate are shown in Fig. 4.7.

(U) The results obtained during this test series indicated that the magnesium alloy chosen would probably be adequate for at least fifteen shots with a 4 by 7 torus system on the test stand.

4.2.3. Steel Plate (U)

(U) A USS T1 steel plate was machined like the third aluminum plate, except the diameter was reduced to 24 in. and the thickness was reduced to about 5/8 in. to obtain the required velocity increment. The plate was first exposed to six A-3 HE shots with no attachment and then to six additional A-3 shots with a dummy torus shield bolted to the back face to simulate an uneven mass distribution.

(C)(Gp-4) The plate velocity increment obtained was between 180 and 190 ft/sec, which corresponds to about 150 percent of the full nominal impulse considered for the torus system. After a total of twelve shots, the clamping-boss dimensions were practically unchanged and the plate remained essentially flat.

(U) After the third shot, small cracks appeared on the plate face exposed to the HE. After the plate was cleaned and was given a small amount of local grinding, it was found that the cracks were caused by forging scales and were very shallow. They did not grow after additional testing and no other cracking appeared later.

(U) These test results were deemed satisfactory, and this plate design was adopted for all subsequent tests of single-torus and three-torus systems. All plates built from this steel alloy and according to this design performed well without a single failure in all subsequent tests.

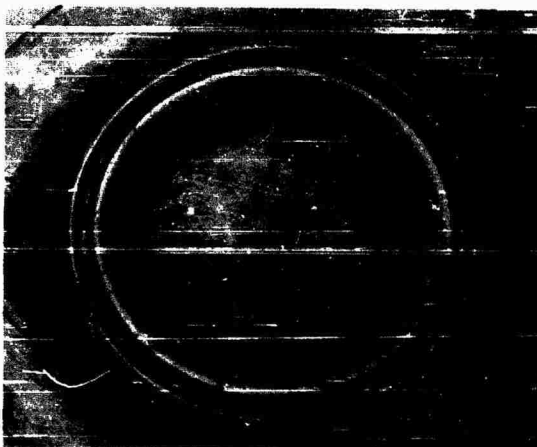
4.2.4. Torus-system-shield Qualifying Tests (U)

(U) The torus shield was designed to protect the torus system from flying solid debris and the shock wave in the air around the plate and to prevent damage to the torus in the event the plate broke loose from the cable stand before it was completely stopped. The shields were made of 6061-T6 aluminum alloy.



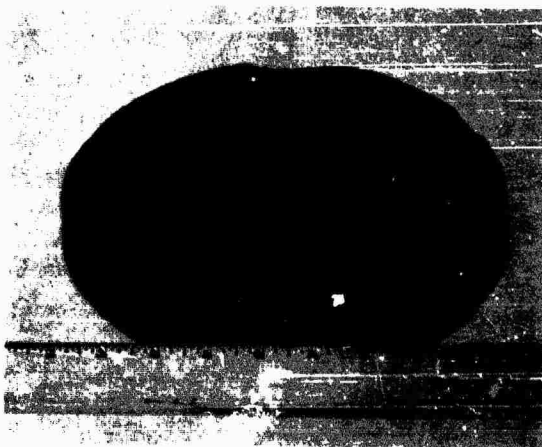
(a) Over-all plate aspect

(C)
(Gp-4)



(b) Boss-hole cracks

(C)
(Gp-4)



(c) Plate surface exposed
to HE

(C)
(Gp-4)

Fig. 4.7--Second magnesium plate after testing (with resin bead installed)(U)

(U) The shields were of two sizes, one for the single-torus system and a taller one for the three-torus system. Qualification tests were conducted to ensure that the shields could withstand several blast exposures without major damage and that their failure, if any, would not damage the torus system. As explained in Section 5, the screws bolting the shields to the steel plate had to be retorqued after each exposure.

(U) The "short" shield was exposed to one A-2 HE shot and then to four A-3 HE shots. After the third shot, a crack appeared along the longitudinal weld of the shield, which started bulging near the flange. Two small cracks also appeared at the flange weld.

(U) Since it was determined that these welds did not have the quality specified, the shield was rewelded for continued testing. Good welds properly heat treated were found to be capable of withstanding several such exposures.

(U) As the upper cone rim of the shield was badly buckled after the last shot, it was decided to shorten the rim. This modification proved satisfactory. The damage to the test item is shown in the photographs of Fig. 4.8.

(U) The taller shield was exposed to a total of eight shots. After the first exposure of A-2 HE, a 3-in. -long crack developed, but it was obviously the result of a defective weld. After the second exposure (A-3 HE), three cracks were observed at the flange weld, and after the third exposure, the entire length of the longitudinal weld was cracked. The lower part of the shield started showing a pronounced amount of bulging, so the shield was rewelded and tested again. The bulging at the shield base increased to the point where a complete convolution (bellows effect) was formed. Also, several screws were stripped from the support plate (aluminum alloy). This shield is shown before and after testing in Fig. 4.9.

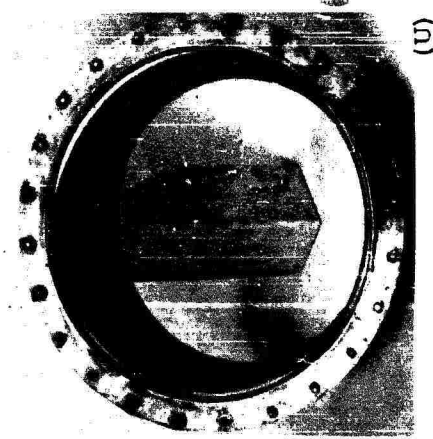


(U)

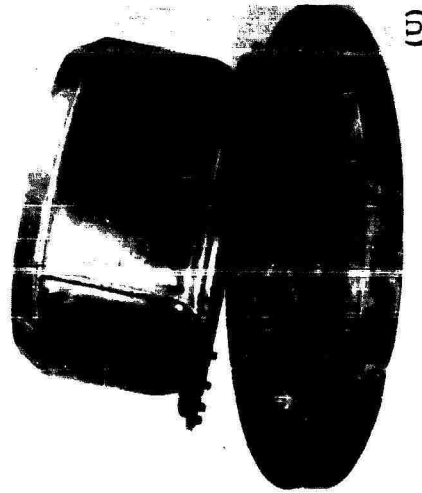


(U)

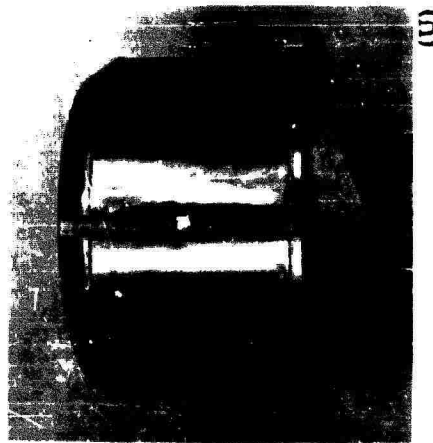
Fig. 4.8-- View of the short shield after testing (U)



(c) After testing



(b) After testing (still attached to the plate)



(a) Before testing

Fig. 4.9--Views of the tall shield before and after testing (U)

(U) The results of these tests demonstrated that this type of shield could be used reliably for torus protection and that even when cracks, pronounced deformations, etc., were present before the test, no catastrophic failure occurred. This shield design was adopted for all torus tests.

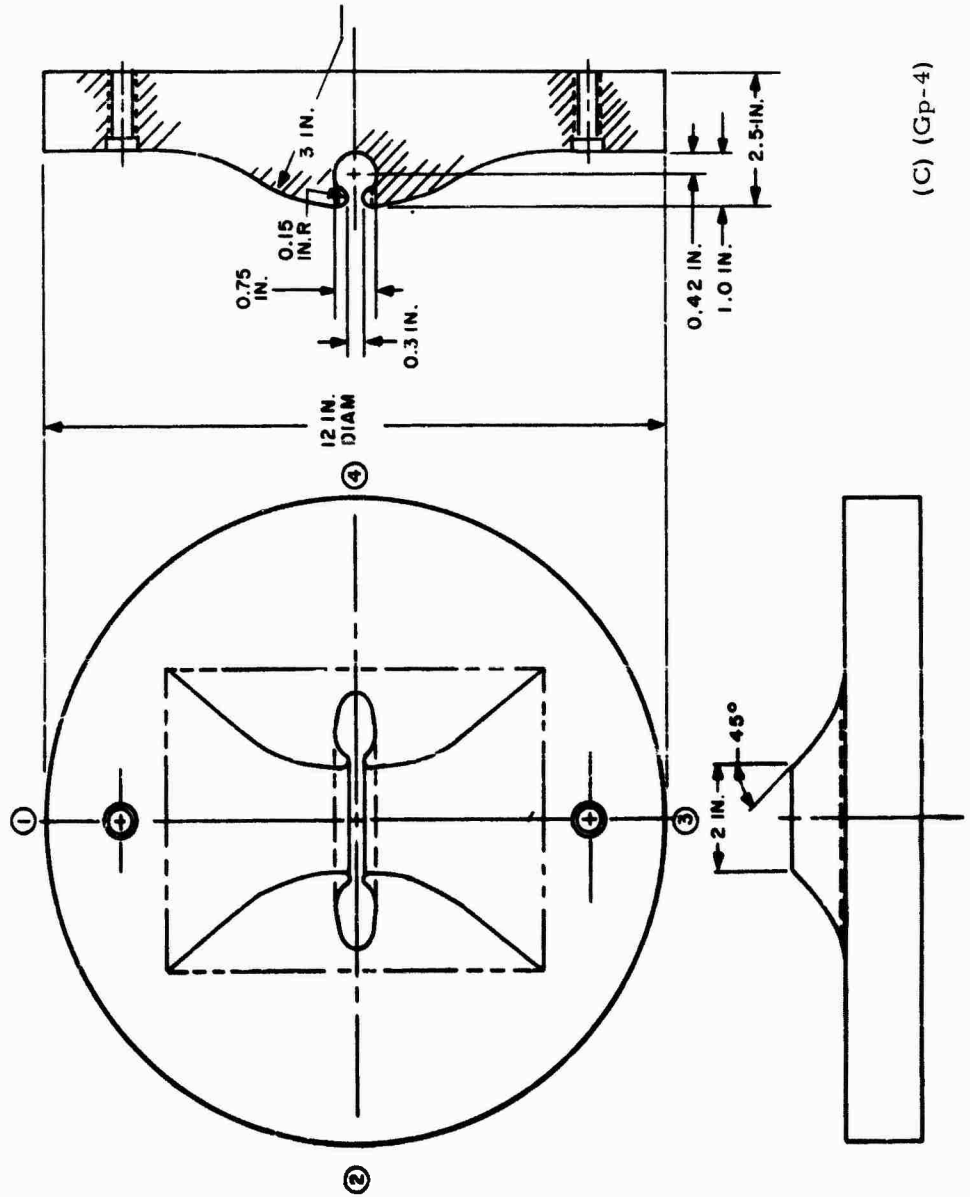
4.2.5. Full-size Clamping-boss-section Plate (U)

(U) Three sample plates were made of USS T1 Type A firebox-quality steel and were about 1-1/2 in. thick. A small section of a full-size torus clamping boss was machined on the solid plate to simulate the exact boss cross-section shape and dimensions of a typical full-size section of a 10-m engine pusher plate. The machining was done accurately so that changes in shape and dimensions after a given number of exposures could be measured to within 0.001 to 0.002 in. A drawing of these test plates is given in Fig. 4.10.

(C)(Gp-4) The first sample plate was subjected to thirty exposures with a corresponding velocity increment of 120 to 140 ft/sec. A small crack 1/4 in. long appeared about 4 in. from the plate center after the fifteenth exposure, but it did not spread from the subsequent exposures. A second crack similar to the first appeared after the twenty-seventh exposure. After the last exposure, a 1-1/2-in.-long crack appeared at the bottom of the groove about 1 in. from the center of the plate. This last crack was serious, and no further testing was performed.

(U) The plate surface exposed to HE was damaged considerably. A groove, 1/16 in. deep and 1/2 in. wide, had been "peened" on the plate, forming a circular groove about 2 in. in diameter. Also, a small groove was visible about 1/4 in. from the plate edge and the plate edge was bulged about 1/8 in. These conditions may be seen in Figs. 3.16 and 3.17.

(U) Since it was suspected that the surface damage resulted from center-detonating the sheet HE, it was decided to edge-detonate the



(C) (Gp-4)

Fig. 4.10--Plate with integral full-size shock-absorber attachment section (U)

HE in subsequent tests. The variation in the dimensions of the clamping-boss groove as the result of these tests is presented in Table 4.1. The locations where measurements were made are indicated on Fig. 4.10.

(U) The results of post-test sectioning and inspection of the plate were discussed in Section 3.

Table 4.1
VARIATIONS OF GROOVE DIMENSIONS IN
FIRST BOSS-ATTACHMENT PLATE (U)
(in inches)

Exposure	Boss Hole ID			Boss Slot		
	Right	Center	Left	Right	Center	Left
0	0.748	0.748	0.748	0.299	0.299	0.299
7	0.749	0.749	0.749	0.302	0.302	0.302
13	0.764	0.763	0.764	0.317	0.316	0.315
16	0.765	0.764	0.766	0.317	0.318	0.321
19	0.768	0.766	0.765	0.319	0.319	0.320
22	0.770	0.768	0.767	0.321	0.317	0.319
25	0.773	0.771	0.767	0.323	0.320	0.322
30	0.774	0.775	0.777	0.328	0.326	0.321

(C)(Gp-4)

(U) The second test plate was exposed to forty-one impulses from edge-detonated sheet HE. No external cracks were visible at the end of this test series and there was no surface damage. However, the plate was bowed approximately 1/8 in. and the edge had bulged 1/8 in. in a fashion similar to that of the first plate. There were no other external signs of damage.

(U) After testing, this second plate was sectioned as described in Section 3. No flaws or cracks were revealed from the Zyglo inspection. Table 4.2 gives the results of the variations of groove dimensional changes in the second plate.

Table 4.2

VARIATIONS OF GROOVE DIMENSIONS IN
SECOND BOSS-ATTACHMENT PLATE(U)
(in inches)

Exposure	Boss Hole ID			Boss Slot		
	Right	Center	Left	Right	Center	Left
0	0.748	0.748	0.748	0.298	0.298	0.298
1	0.749	0.749	0.749	0.300	0.300	0.300
2	0.749	0.749	0.749	0.301	0.301	0.301
3	0.747	0.747	0.747	0.300	0.300	0.300
4	0.746	0.746	0.746	0.299	0.299	0.299
5	0.745	0.745	0.745	0.301	0.301	0.299
6	0.745	0.745	0.745	0.301	0.301	0.301
7	0.745	0.745	0.745	0.300	0.300	0.300
8	0.745	0.745	0.745	0.301	0.300	0.300
9	0.745	0.745	0.745	0.302	0.301	0.300
10	0.735	0.752	0.755	0.302	0.302	0.301
11	0.755	0.753	0.754	0.301	0.301	0.301
12	0.754	0.752	0.754	0.302	0.302	0.302
13	0.755	0.754	0.754	0.304	0.304	0.304
14	0.756	0.753	0.756	0.304	0.304	0.305
15	0.755	0.747	0.747	0.306	0.305	0.305
16	0.749	0.744	0.756	0.304	0.305	0.304
17	0.756	0.753	0.756	0.304	0.307	0.304
18	0.756	0.753	0.758	0.305	0.306	0.305
19	0.756	0.754	0.754	0.305	0.305	0.304
20	0.758	0.754	0.755	0.305	0.306	0.305
21	0.754	0.755	0.757	0.304	0.303	0.303
22	0.759	0.755	0.755	0.305	0.306	0.307
23	0.761	0.756	0.757	0.308	0.310	0.309

(C)(Gp-4)

Table 4.2--Continued

Exposure	Boss Hole ID			Boss Slot		
	Right	Center	Left	Right	Center	Left
24	0.758	0.755	0.755	0.309	0.310	0.310
25	0.758	0.756	0.756	0.309	0.308	0.307
29	0.761	0.756	0.759	0.310	0.310	0.309
33	0.759	0.758	0.762	0.310	0.312	0.311
37	0.763	0.758	0.762	0.316	0.316	0.315
41	0.763	0.757	0.761	0.313	0.314	0.314

(C)(Gp-4)

(U) The third plate was identical to the two previous test plates except that its outer surface was machined to give a close-tolerance diameter and an outer ring was fitted to the plate with a few thousandths of an inch clearance. The surfaces of the plate and ring were flush on the HE-exposure side. This arrangement effectively extended the plate surface and radial dimension of the incident impulse and eliminated plate-surface damage, i. e., bulging of shocked surface, which caused a flare on the outer edge, and the typical peened groove near the periphery.

(U) This plate-ring arrangement was exposed to thirty impulses from edge-detonated sheet HE. Careful measurements taken between tests are recorded in Table 4.3. These measurements show that almost imperceptible physical distortion resulted from the thirty shock loads. No surface flaws or surface cracks were observed after any of these tests. Because of the excellent condition of this plate, additional life-testing is desirable; therefore, no destructive inspection was made.

(U) Measurements of dimensional changes on the test plates were made with a series of plug gauges of varying diameters. These gauges gave a good indication of gross changes. After several shots, however, it became apparent that the deformation that occurred in the boss hole and slot was not uniform, and it was necessary to use

Table 4.3

VARIATIONS OF GROOVE DIMENSIONS IN
THIRD BOSS-ATTACHMENT TEST PLATE (U)
(in inches)

Exposure	Boss Hole ID			Boss Slot			Plate Diameter	
	Right	Center	Left	Right	Center	Left	Pts. 1-3	Pts. 2-4
0	0.750	0.750	0.750	0.300	0.300	0.300	11.968	11.968
1	0.750	0.749	0.749	0.300	0.300	0.300	11.969	11.969
2	0.749	0.749	0.749	0.300	0.300	0.300	11.969	11.968
3	0.749	0.749	0.749	0.300	0.300	0.300	11.969	11.969
4	0.749	0.749	0.749	0.300	0.300	0.300	11.969	11.969
5	0.749	0.749	0.749	0.300	0.300	0.300	11.969	11.969
6	0.749	0.749	0.749	0.300	0.300	0.300	11.969	11.969
7	0.749	0.749	0.749	0.300	0.300	0.300	11.969	11.969
8	0.749	0.749	0.749	0.300	0.300	0.300	11.969	11.969
9	0.749	0.749	0.749	0.300	0.300	0.300	11.969	11.969
10	0.749	0.749	0.749	0.300	0.300	0.300	11.969	11.969
15	0.749	0.749	0.749	0.300	0.300	0.300	11.969	11.969
20	0.749	0.749	0.749	0.300	0.300	0.300	11.969	11.969
25	0.749	0.749	0.749	0.300	0.300	0.300	11.969	11.969
30	0.749	0.749	0.749	0.300	0.300	0.300	11.969	11.969

Exposure	Plate Thickness				Plate Flatness	
	Pt. 1	Pt. 2	Pt. 3	Pt. 4	Pts. 1 - 3	Pts. 2 - 4
0	1.534	1.533	1.526	1.524	0.000 to -0.012	0.001 to -0.001
1	1.535	1.533	1.526	1.524	0.000 to -0.012	0.000 to -0.001
2	1.535	1.534	1.526	1.524	0.002 to -0.010	-0.004 to -0.004
3	1.535	1.534	1.526	1.524	0.002 to -0.010	-0.004 to -0.004
4	1.535	1.534	1.526	1.524	-0.003 to -0.006	+0.003 to -0.008
5	1.535	1.534	1.526	1.524	0.000 to -0.007	0.002 to -0.008
6	1.535	1.534	1.526	1.524	0.005 to -0.013	0.001 to -0.008
7	1.535	1.534	1.526	1.524	0.006 to -0.013	0.001 to -0.008
8	1.535	1.534	1.526	1.524	0.000 to -0.005	0.004 to -0.002
9	1.535	1.534	1.526	1.524	0.000 to -0.006	0.004 to -0.002
10	1.535	1.534	1.526	1.524	0.000 to -0.006	0.004 to -0.002
15	1.535	1.534	1.526	1.524	0.001 to -0.005	0.003 to -0.004
20	1.535	1.534	1.526	1.524	0.002 to -0.000	0.003 to -0.005
25	1.535	1.534	1.526	1.524	0.001 to -0.002	0.004 to -0.015
30	1.535	1.534	1.526	1.524	0.002 to -0.002	0.004 to -0.015

micrometers to measure both ends and the center of the machined boss. The measurements taken after the last exposures are reflected in the data compiled in Tables 4.1 and 4.2. Reference measurement points on the test plates are shown in Fig. 4.10.

(U) The diameter measurements made on the third test plate were obtained from four reference points that were 90° apart and located adjacent to the outer circumference of the plate. These points were scribed on the plate prior to the test series to assure consistency in measurements. The plate flatness was measured using a reference plate surface and a dial indicator. Measurements were made from the plate center (zero reference) by moving the dial indicator radially to each of the four reference points located on the plate circumference.

(C)(Gp-4) Conclusions drawn from the tests of these three USS T1 steel plates with integral full-size clamping boss are the following:

1. The design of the attachment, which is an integral part of the pusher material when the material has strong, tough properties, can be expected to successfully withstand many loads of a magnitude of direct interest to ORION. However, if the pulse distribution has areas of high intensity, as indicated by the surface damage on the first plate, or if the material has processing flaws, serious cracking and ultimate failure may be expected.
2. Close simulation of the operational impulse is most important for realistic testing of pusher plates or pusher-plate segments. Edge effects of the pulse unit for segment loading and HE detonation location are conditions which can cause impulse concentrations.

~~CONFIDENTIAL~~

WL-TDR-64-93

3. Fatigue testing of larger pusher segments with half-scale or larger attachment bosses should be carried out to qualify candidate pusher materials. A 1-1/2-in. - thick, 24-in. -diam test plate with a 16-in. -diam integral attachment fired from a steel ring should give good results.

~~CONFIDENTIAL~~

5. TORUS RESPONSE TESTS (U)

(C)(Gp-4) The design of the ORION first-stage shock-absorber system as it is now envisioned originated three years ago and is discussed extensively in Ref. 6. The system design is based on a flexible toroidal shock absorber attached to the pusher plate. The use of a toroidal gas spring system was proposed five years ago and a small model of such a system was built and tested three years ago. This work is reported in Ref. 7. The results obtained with this crudely constructed model were very encouraging and warranted further consideration. It was concluded that such a system could be attached to a plate and subjected to impulses up to 70 ft/sec without failure. After eight full-impulse exposures, the system still operated satisfactorily and did not fail structurally when exposed to a 50 percent increase in impulse over the nominal design value. Furthermore, it was demonstrated that this system was also quite satisfactory for impulses that were off-centered beyond any practical tolerance limits.

(C)(Gp-4) This earlier model was heavier than required for satisfactory operation of the full-size system and therefore could not be exposed to the contemplated full plate-velocity increment of 140 to 150 ft/sec (see Vol. III of this report).

(U) The first-stage shock-absorber system attached to the pusher plate is considered to be one of the most critical engineering items of the nuclear-pulse propulsion engine. Thus, it was selected as a priority item to be investigated experimentally.

5.1. TEST OBJECTIVES (U)

(U) The primary objective of this test program was to demonstrate a satisfactory design for the first torus of a toroidal shock absorber,

scaled down from the full-size system (10-m engine), that could withstand a full impulse (up to 140 to 150 ft/sec velocity increment) while employing realistic system weights. This involved studies of the torus attachment to the plate, the torus structural integrity, and the ability of the torus to hold pressure after repeated exposures.

(U) A secondary test objective was to demonstrate that several tori could be stacked and connected together to form an integrated gas spring that would operate in tension and compression under repeated full-impulse loading conditions.

(U) Finally, it was hoped that the dynamic response of a four-stack, seven-layer torus system could be investigated. Each one of these objectives or steps were to be sequenced so that the hardware for each step would be qualified during the preceding step.

5.2. TORUS-MODEL BASIC DESIGN (U)

(C)(Gp-4) A 1/3-scale torus was deemed to be the most convenient for manufacturing and testing. Figure 5.1 shows a scaled single-torus system ready for testing. The first torus model consisted essentially of nylon cloth sewed around bicycle inner tubes.⁽⁷⁾ This type of construction is structurally inefficient and heavy because the cloth fibers are not ideally oriented and the inner-tube wall is too thick. The only way to lighten the system is to use high strength-to-weight ratio materials for the structure and thin-wall sealant to prevent gas leakage. The separate inner-tube type of sealant was chosen because it requires less material than the impregnation of the structural filaments and the filling of the voids between to attain the same scaling quality. Since no such inner tubes were available commercially, they had to be specially designed and manufactured, as discussed in Section 5.3.

(C)(Gp-4) The use of filaments to build the torus structure was selected over cloth (either bidirectional or unidirectional) because better materials are available in filament form and also because it is easier to make use of their full strength, if properly oriented.⁽⁸⁾ At least two basic

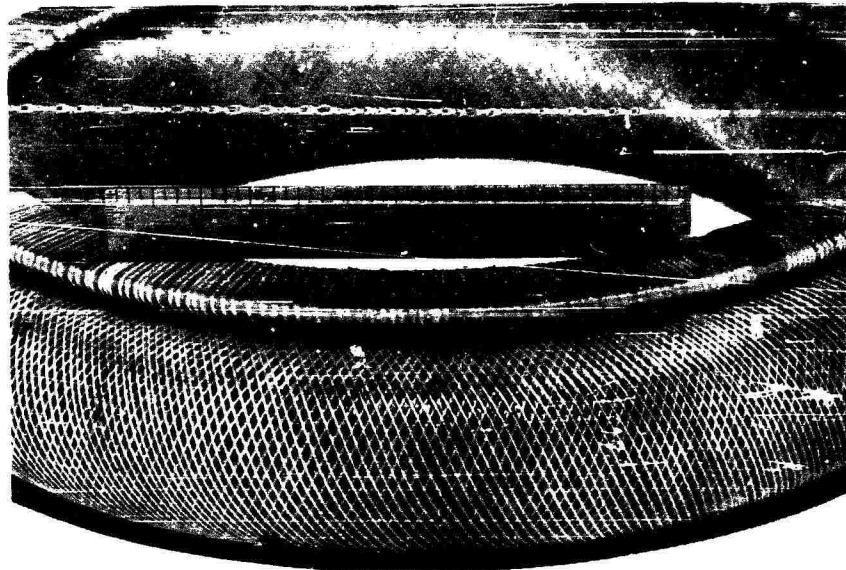


(U)

Fig. 5.1--Typical single-torus test setup (U)

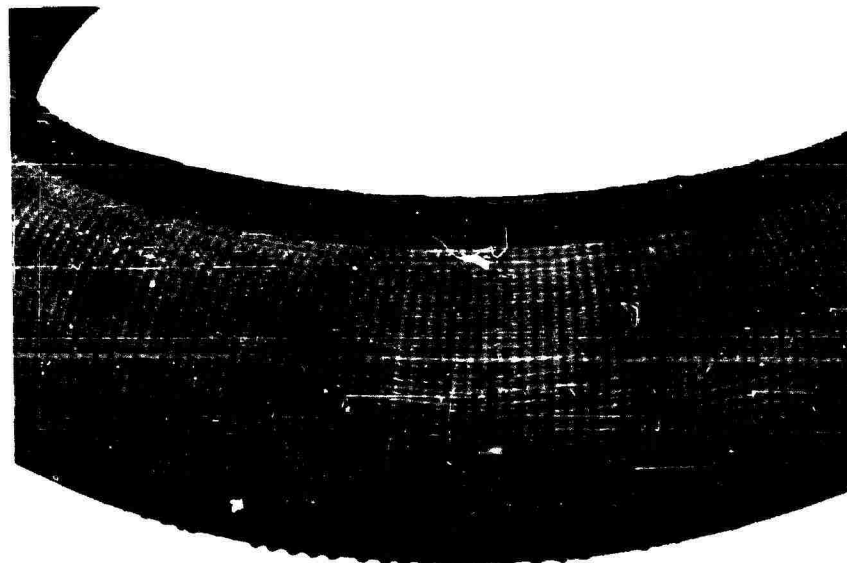
methods for filament arrangement were possible in the construction of a deformable toroidal pressure vessel, namely, double helix winding and knitting. These methods can, of course, be combined if desired. Photographs of tori built with these techniques are shown in Fig. 5.2.

(U) The design of the attachment of the first torus to the plate has been investigated⁽⁶⁾ and, as explained in Section 4, a resin-inflated locking bead was adapted as the solution of this problem. This scheme is shown schematically in Fig. 5.3. A small cross-section, thin-wall inner tube was laced to the torus structure and inflated with liquid resin after it was installed inside the locking groove. When the resin is cured, the torus is locked solidly to the plate. Although this solution did not prove to be satisfactory (see Section 5.5), the basic idea was retained



(C) (Gp-4)

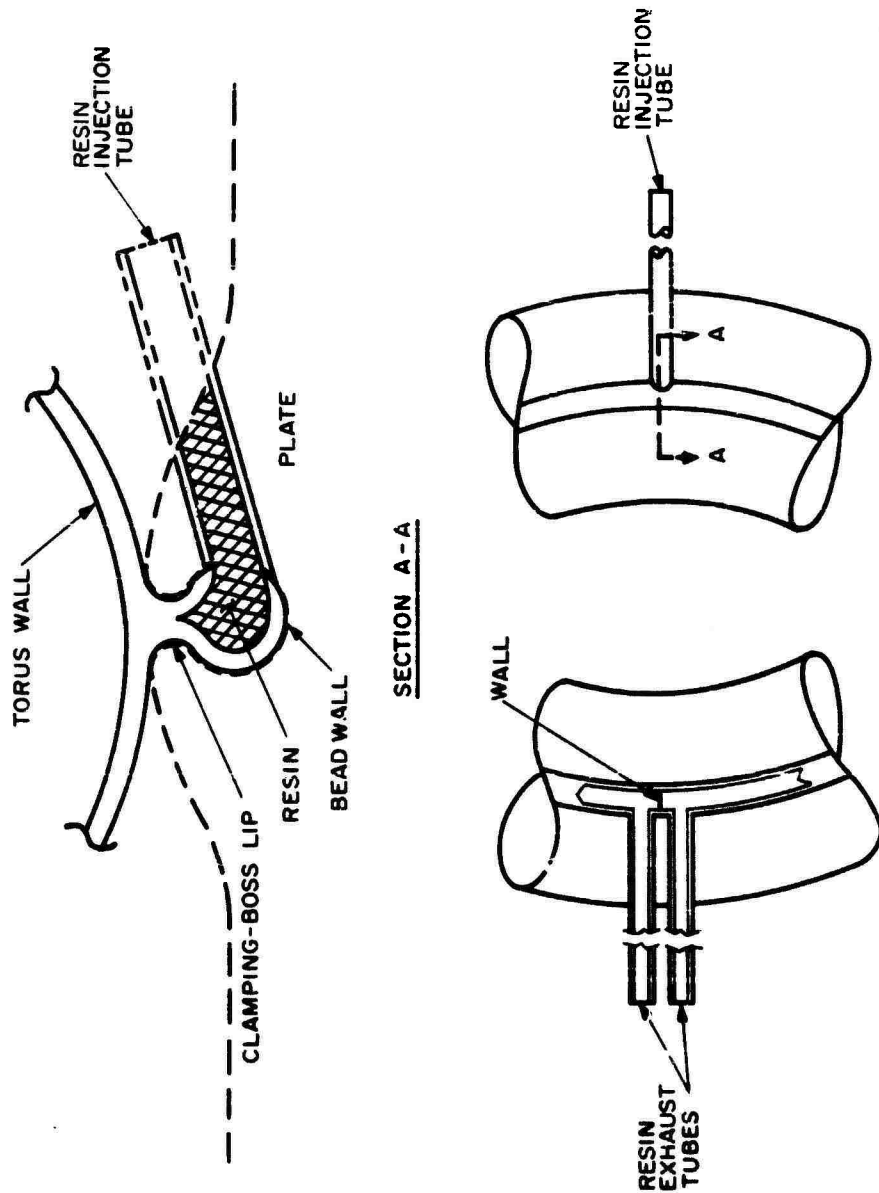
(a) Filament wound



(C) (Gp-4)

(b) Knitted structure and meridional reinforcement

Fig. 5.2--Typical torus structural construction (U)



(C) (Gp-4)

Fig. 5.3--Typical resin-inflated torus bead attachment (U)

for the attachment of a solid-core bead to the torus. Essentially, this design ensured that when in tension, the torus reaction on the plate would be transmitted through structural filaments, and thus the use of bonds and additional dead weights would be avoided. Variations of this basic idea were tried for various reasons, as explained in Section 5.5, but all the tori tested during this program were constructed according to this basic design.

(C)(Gp-4) Only single-torus systems were tested during this program, but the multitorus stack has been designed. An experimental three-torus stack model incorporating most of the design features of the multitorus stack has been built. This was done to check the manufacturing process and to ensure that the system could be assembled and pressurized and would hold the pressure. For convenience, bicycle inner tubes were used in this system. However, because of the large mass of the inner tube, dynamic testing was impractical, although the basic design appears to be sound. A combination of the filament-winding and filament-knitting techniques was used for the three-stack torus system since it seemed to provide the most promising solution. The filament structure was knitted flat and the filaments used in lieu of the wound filaments (see Section 5.5) were interwoven with the knitted structure during the knitting process. The structure area was made large enough to cover the entire torus wall assembly. This structure was then wrapped around the torus inner tube. The two walls (inside and outside the torus stack) were then stitched together between each inner tube. The last inner tube was installed later since the last torus was clamped with two bead rings, one for each wall. This is illustrated in Fig. 5.4. The knitting meshes were prearranged by hand so that the tori would assume the correct shape and dimensions when they were inflated. The loops of the wound filaments were made to provide for the insertions of the clamping bead and the clamping rings. These rings were split and inserted before inflation of the tori. In Fig. 5.5 the detailed filament structure is shown laid out before assembly around the inner tube (for a single-torus system).

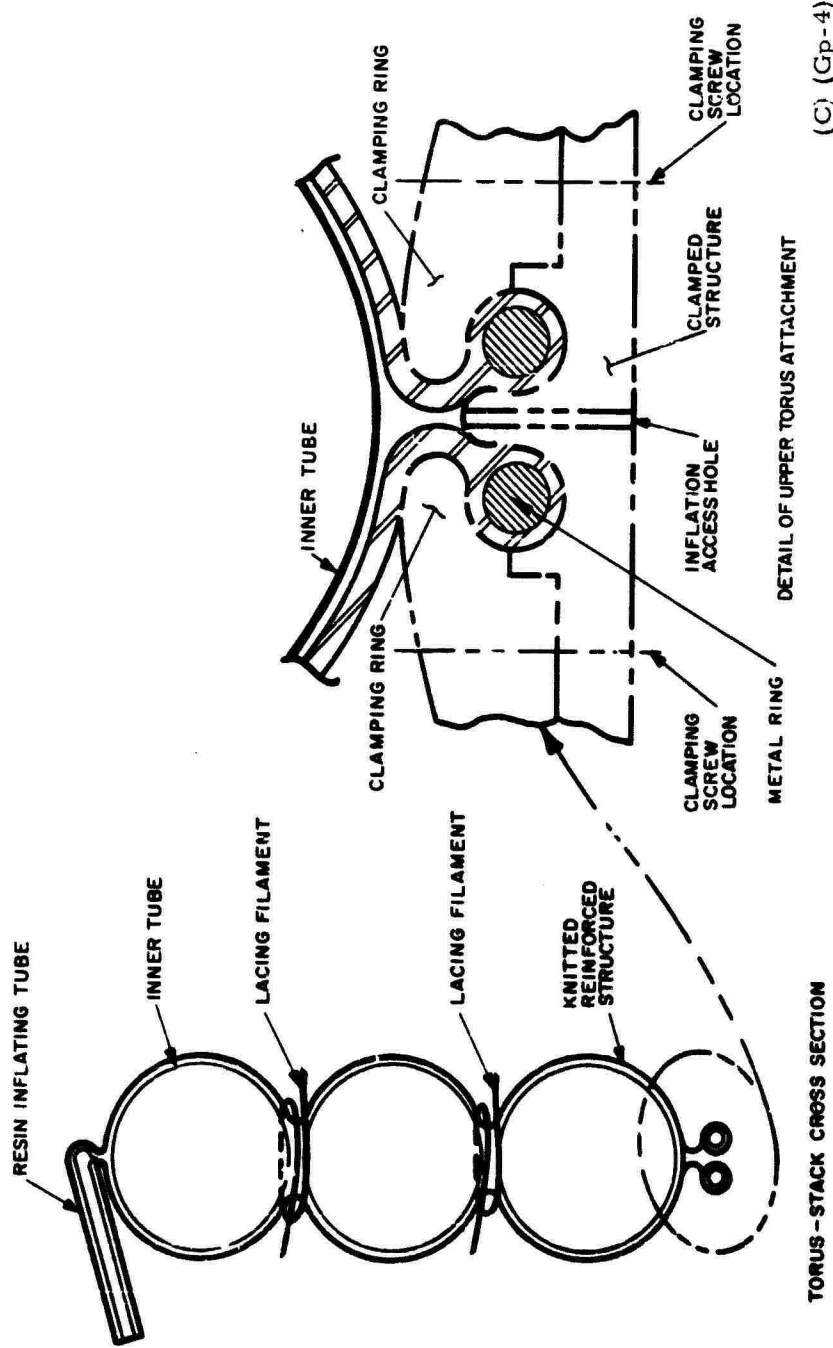
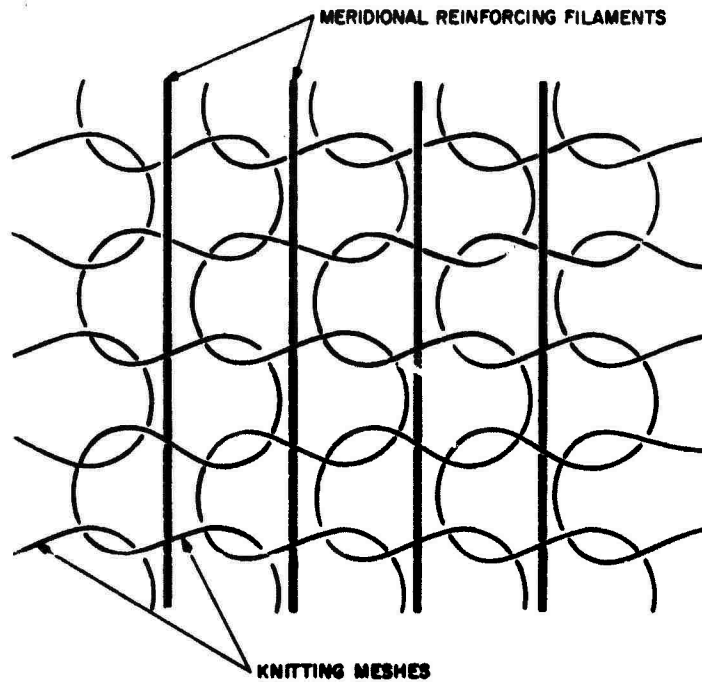
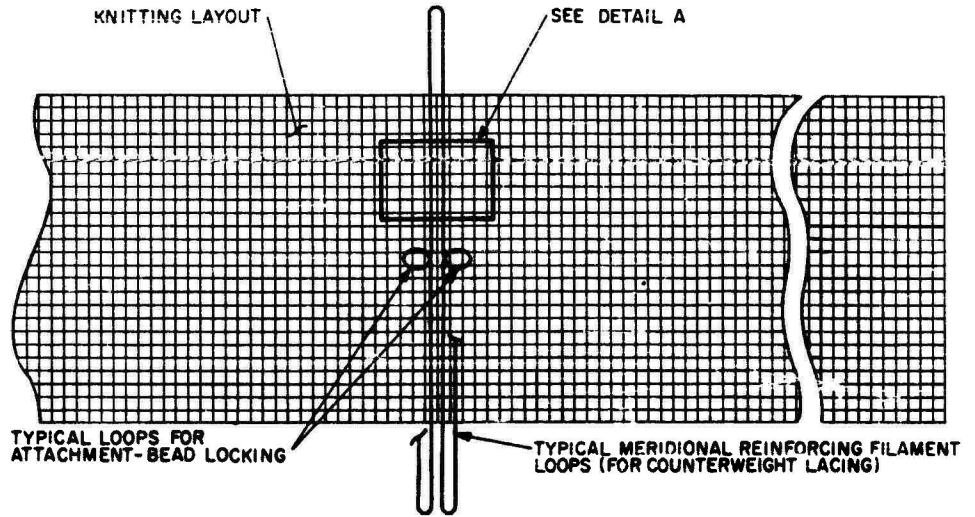


Fig. 5.4-- Typical three-torus (or multitorus) stack construction (U)

(C) (Cp-4)



DETAIL A

(U)

Fig. 5.5--Typical knitted, reinforced structure construction (U)

(U) The gas connection between tori was designed as shown in Fig. 5.6. A light magnesium hollow spool was inserted inside a nipple bonded to the inner-tube wall. The nipple hole had grooves, which operate like O-rings in series, pressed against the spool walls. This arrangement allowed a slight misalignment and a small relative motion between adjacent tori and still minimized the gas leakage. The same type of nipple was used on the single-torus system for inflation with an hypodermic needle.

5.3. SINGLE-TORUS MANUFACTURING AND QUALITY CONTROL (U)

(U) As explained in Section 5.2, two basic filament arrangements are possible. The ideal one emphasized the filament winding since, at least in the neutral position, the filaments can be wound along a variable-pitch-angle helix and under the correct tension so that all filaments are equally stressed without shear or bending. Such a filament-wound single torus is presented in Fig. 5.7. A special filament-winding machine was modified by the subcontractor* so that such tori could be wound automatically. The other major components are the inner tube, the inflation valve, and the plate clamping bead.

5.3.1. Inner Tube (U)

(U) The weight of the inner tube must be the minimum necessary to prevent leakage. Furthermore, the wall thickness must be as uniform as possible. These requirements eliminated several possible fabrication techniques, such as dipping and molding, because of the high cost of reliable and satisfactory tooling. It was decided to use an urethane rubber tape (Seilon) wrapped around a mandrel and cured under pressure. The pressure on the Seilon during the process was obtained by wrapping shrink tape over the Seilon. The mandrel, made of water-soluble salt, was molded by gelling the molten salt against the wall of a plastic mold. This provided a rigid mandrel that could be washed out with water.

*Astro Research Corporation, Santa Barbara, California.

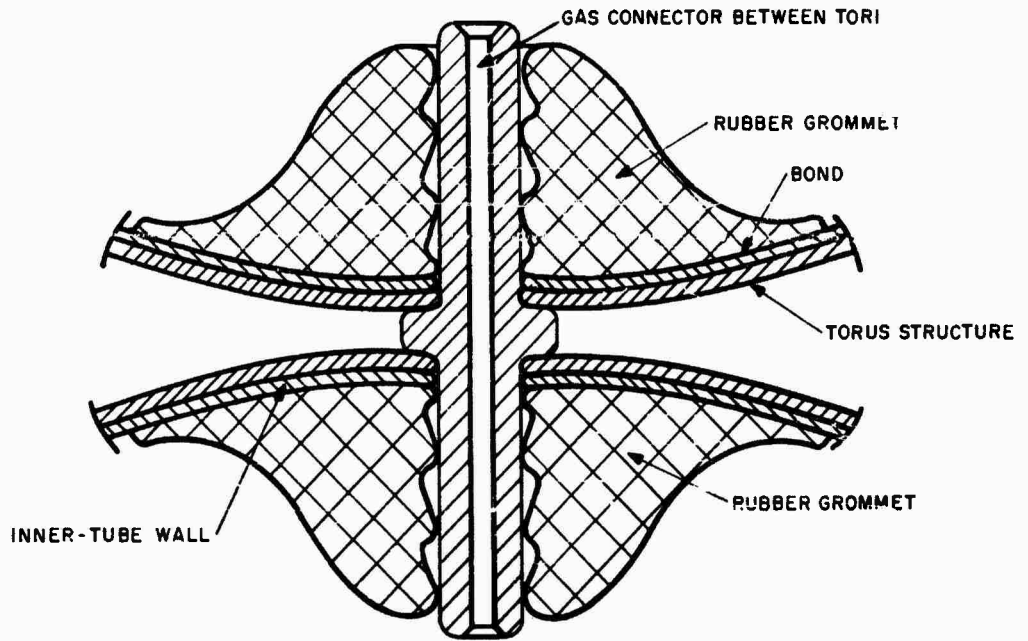


Fig. 5.6--Typical gas connection between adjacent tori (U)

(U)

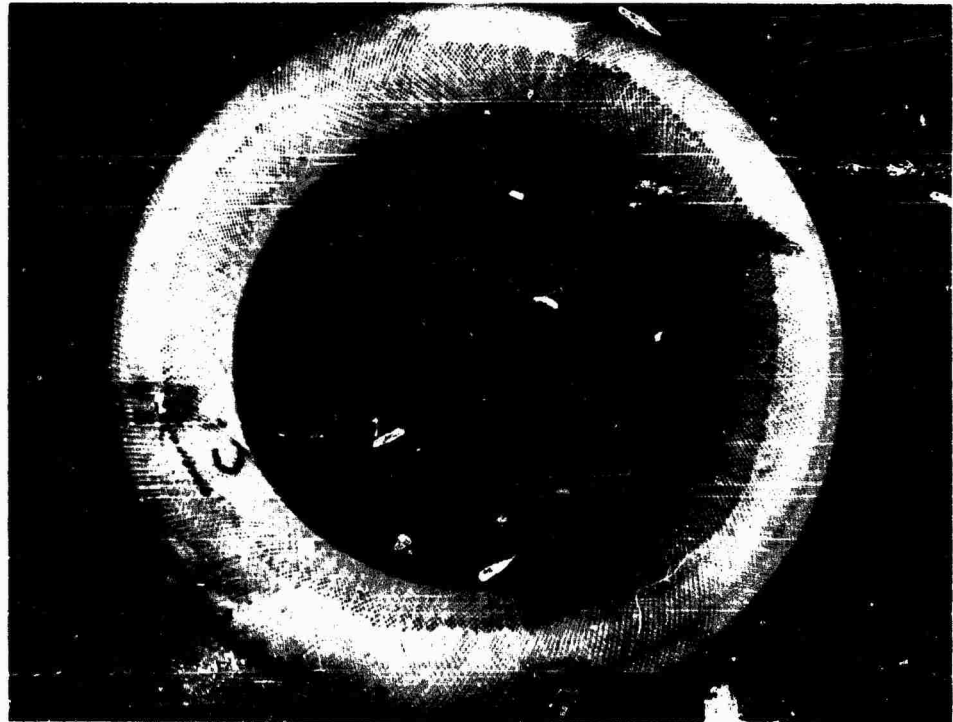


Fig. 5.7--Typical filament-wound torus structure (U)

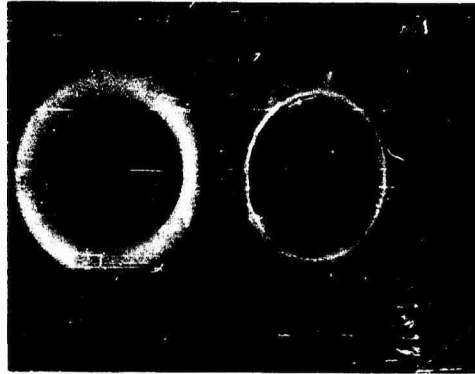
Figure 5.8 shows (a) the mold and a molded mandrel and (b) the molded mandrel and an inner tube. The salt mandrel can be washed out either before or after the installation of the structural filament. The mandrel was left inside the inner tube of the filament-wound torus to provide the rigid frame required by this technique. Provisions were made in the mandrel for locating the washout holes and for inflation or connecting-hole nipples. These were molded separately and installed under the Seilon tape during the wrapping operation. The inner tube was then checked for leaks.

5.3.2. Inflation Valve (U)

(C)(Gp-4) The torus inflation valve was used only for the single-torus system because the upper torus of all multistack systems was clamped to a rigid structure to which the inflation mechanism was attached. The valve had to be extremely light since it was attached directly to the torus wall and was subjected to very high accelerations (between 10,000 and 15,000 g).

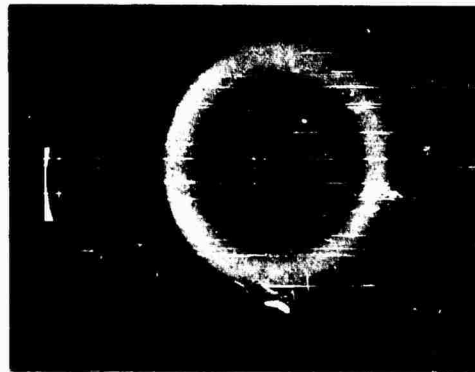
(U) At first, it was thought that the core of a bicycle inner-tube inflating valve could be used if it was installed inside a light-weight aluminum alloy body. The first two single tori tested with such a valve were found unsatisfactory. The first valve ripped from the torus wall, and after modification of the valve mounting to the torus wall to strengthen the attachment, it was found that the valve remained on the torus but the valve core was damaged by the shock and leaked.

(U) Rigid metallic valves were abandoned and replaced by a flexible rubber nipple. To inflate the torus, the nipple was punctured with an hypodermic needle and a light plug was then inserted in the puncture to prevent leakage. The plug was then locked in place. A shortcoming of this technique is that it is not possible to check the pressure inside the torus before or between testing. One must rely on the hardness of the torus wall for a qualitative check of leak tightness. But the risks of leakage at the valve were eliminated. Since the valve was only used for single-torus experiments, this solution was found to be acceptable.



(U)

(a) Salt mandrel and mold



(U)

(b) Salt mandrel and inner tube

Fig. 5.8--Inner-tube fabrication process (U)

5.3.3. Plate Clamping Bead (U)

(C)(Gp-4) This part of the torus attached to the pusher plate is the most critical since it is the first link between the plate and the upper structure and therefore is exposed to the full plate acceleration. Its shape, dimensions, and simplicity were dictated by the pusher-plate design, as explained in Section 4. A small, compact, rigid arrangement was conceptually designed as described in Ref. 6 and in Volume III of this report (see also Section 4). Although the details of the final design were unknown, it was decided to investigate the possibility of using resin as the locking structure for reasons of expediency. Resin was injected inside a small-diameter thin-wall inner tube which had been laced to the torus structure. The lacing process was done by looping the bead filaments over the torus structural filaments. This produced a weak spot at the point of contact between the two loops and also allowed a small relative motion of one loop with respect to the other, since the loops were not locked together. This was, of course, undesirable because of filament abrasion and wear that could result during the torus cycling. Unfortunately, if one does not use a bonding process with the filament-wound torus, there is no alternative for this type of attachment.

(C)(Gp-4) Another design was also investigated wherein the torus basic structure consisted of a knitted shell into which meridional filaments were interwoven during the knitting process. These filaments were twisted, as illustrated in Fig. 5.9, to form loops through which the locking ring was inserted to provide a continuous filament passing around the clamping bead and the torus and to eliminate the looping weak point and the risk of abrasion. It is conceivable that this scheme could also have been used with the resin-inflated inner-tube design.

5.3.4. Counterweight Attachment Design (U)

(U) Initially, it was assumed that the single-torus construction could have been qualified by overdriving it to simulate the loads at the attachment, since there was no large weight on the back of the torus to

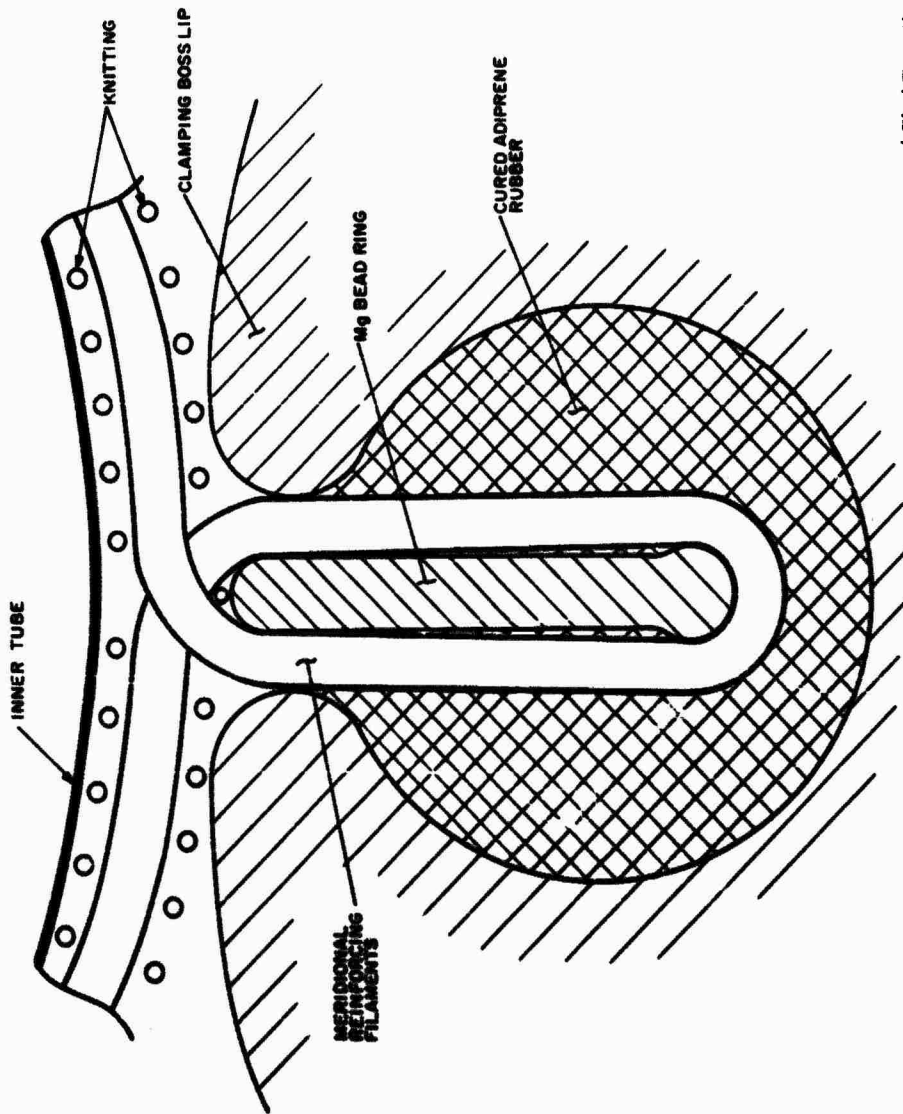


Fig. 5.9--Typical flat magnesium-bead-ring torus attachment (U)

(C) (Gp-4)

develop significant tension loads. Also, the attachment of a rigid but light structure to the single torus appeared difficult at first. But after several torus failures at 1.5 times the full normal impulse, it was realized that other phenomena were probably taking place that were caused by the unsymmetrical dynamic behavior of the torus wall and were creating unrealistic stresses at the torus attachment. In the meantime, the composite structure described in Section 5.2 had been adopted, making the attachment of a counterweight on the top of a single torus much easier. The mass of this counterweight was such that the torus had full energy storage capacity of the torus for the full-impulse load. This counterweight was rigid and simulated the adjacent torus reaction rather well.

(U) The ends of the filament loops interwoven with the knitted structure were laced around the counterweight and locked together, as illustrated in Fig. 5.10. The counterweight was made of magnesium alloy to obtain the maximum rigidity for a given weight. Provisions were made in the design for location of the inflation valve, washout holes, and accelerometer.

5.3.5. Torus Structure (U)

(U) Several types of filaments were investigated for the torus structure, the requirements of which were high strength-to-weight ratio, low elongation (for torus dimensional stability), ready availability, and amenability to being wound or knitted with standard equipment. Nylon was not satisfactory because of its stretch characteristics, so Dacron was chosen. Two comparable types of filaments are available, braided and twisted; both have been used.

(U) After inflation to 80 psig (normal operating pressure), the torus structure was impregnated with liquid Adiprene* dissolved in acetone and then cured to lock all the meshes and filament loops to prevent any shifting and to ensure that the torus shape be maintained. Furthermore,

* Adiprene, a du Pont trademark for polyurethane rubber compound.

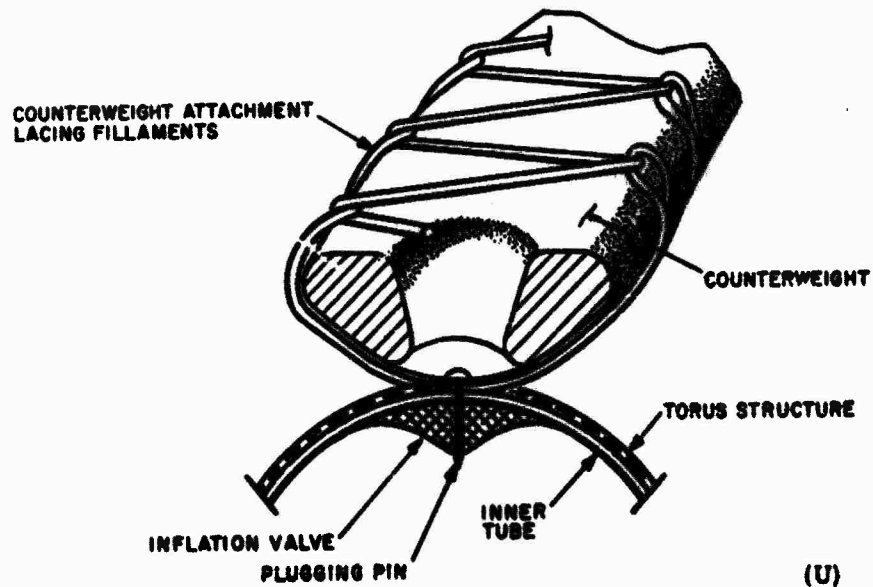


Fig. 5.10--Typical counterweight attachment to the single torus and inflation valve (U)

this method ensured that the torus inner tube and structure would not separate when the torus was deflated.

5.3.6. Torus Quality-control and Acceptance Test (U)

(U) It was determined at the start of this program that the torus structure should withstand a peak stress in excess of that developed during normal operation of the torus, which corresponds roughly to a pressure of about 250 psig in the torus neutral position. Therefore, the desired torus burst pressure had to be higher. A burst test conducted with a typical torus yielded a burst pressure of 450 psig, which was adequate and agreed well with the calculated data (400 psig).

(U) Each single torus was then subjected to the following control procedures:

1. The torus dimensions (major and cross-section diameters) were checked at 80 psig.
2. The torus gas tightness was checked with air at 80 psig for leak detection in water.
3. The torus structural integrity and tightness were checked with hydraulic pressure at 250 psig for 5 min.

This procedure proved to be satisfactory, except in one instance a leak developed at the inflating valve after an acceptance test.

5.4. DESCRIPTION OF EXPERIMENT (U)

(C)(Gp-4) All single tori were tested under similar conditions at the cable-stand facility. The torus was attached to a steel plate, as described above and in Section 4, and the plate was accelerated with sheet HE to the desired velocity. The nominal plate velocity increment was chosen to be around 130 ft/sec (see Vol. III of this report for the justification of this value). The steel-plate thickness was kept as small as possible to minimize the mass to be stopped during deceleration. A shield was bolted to the plate to protect the torus from damage. A sketch of the test assembly is presented in Fig. 5.11.

(C)(GP-4) The following combination of sheet HE and attenuator was used to obtain a velocity increment of 130 to 140 ft/sec:

Impulse	ΔV Obtained (ft/sec)	Sheet HE	Attenuator
Nominal	130 - 140	A-2	4 in. of 2-lb density
Partial	80 - 90	A-1	4 in. of 2-lb density
1.5 Full	180 - 190	A-3	4 in. of 2-lb density

The plate velocity increment was determined from Fastax camera film. The results obtained showed good consistency.

(U) The sheet HE was detonated at one point at the plate edge. In isolated instances, the A-1 sheet HE did not detonate completely, but all the A-2 and A-3 HE pulse units detonated satisfactorily. The last torus to be tested was instrumented with two accelerometers bolted to the counterweight ring after this torus had satisfactorily survived several repeated impulses.

5.5. EXPERIMENTAL RESULTS AND DATA (U)

(U) Nine single-torus systems were delivered by the subcontractor and eight of them were installed on plates and tested dynamically. One was found to be defective after the acceptance test but before its installation on a plate. The defective torus had a leaking valve which could not be adequately repaired.

(C)(Gp-4) Three types of attachments to the plate were tried: (1) resin-inflated clamping bead, (2) a flat magnesium ring bonded inside the plate groove, and (3) a circular magnesium ring locked to the plate with a clamping ring; and two combinations of torus-attachment loads were used: (1) a torus with no mass attached was overdriven to 1.5 times the full impulse and (2) a torus with a counterweight attached was driven to full impulse.

(U) In each case design modifications were intended to eliminate the assumed cause of the past failures. All single-torus systems were installed on a steel test plate as shown in Fig. 5.11.

(U) The test results are presented to correspond with the chronological order of the tests.

5.5.1. Single Torus with No Counterweight (U)

(C)(Gp-4) The first torus of this test series was filament wound and impregnated with Adiprene on the outside. The resin-inflated clamping bead failed because of a leak that developed in the bead inner-tube wall during the inflation process. The urethane rubber poured inside the plate groove to fill the void between lacing filaments had started curing when the failure occurred and the torus could not be pulled off the plate. It was decided to submit this torus to 1.5 times the full impulse to free the torus.

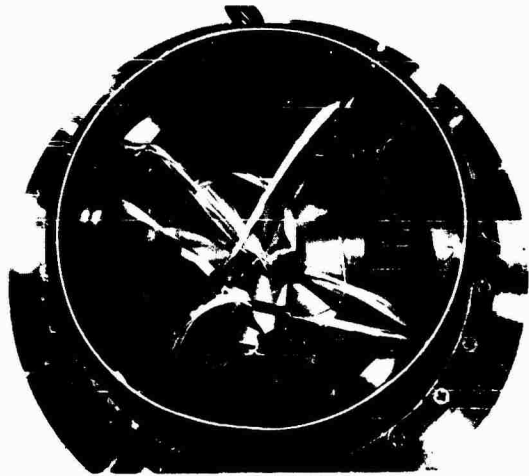
(C)(Gp-4) During this test, the inflation valve that was attached only to the inner-tube wall sheared from the wall and was found inside the torus. Several torus filaments were cut at the bead attachment and the torus was damaged beyond repair. Figure 5.12 shows the more important failures and Fig. 5.13 shows this torus installed on a control aluminum test rig.

(C)(Gp-4) The second torus tested was the first knitted structure. It was reinforced with wound filaments and was equipped with the same type of inflation valves as the first torus. For this test, the valve attachment to the torus wall had been reinforced to clamp on the torus filament structure in an attempt to avoid the type of failure previously encountered. Figure 5.14 presents photographs of this torus as it was being inspected before installation. When subjected to the first full impulse, this torus operated satisfactorily without structural failure, except that it deflated. The valve cores had been damaged and the valves leaked. After the valves were plugged, a small leak was then discovered in the inner tube, so the testing was discontinued.

(C)(Gp-4) The torus remained attached to the plate even though the resin inflation had failed. The resin inflation technique was thus abandoned for the time being. This torus is shown in Fig. 5.15.

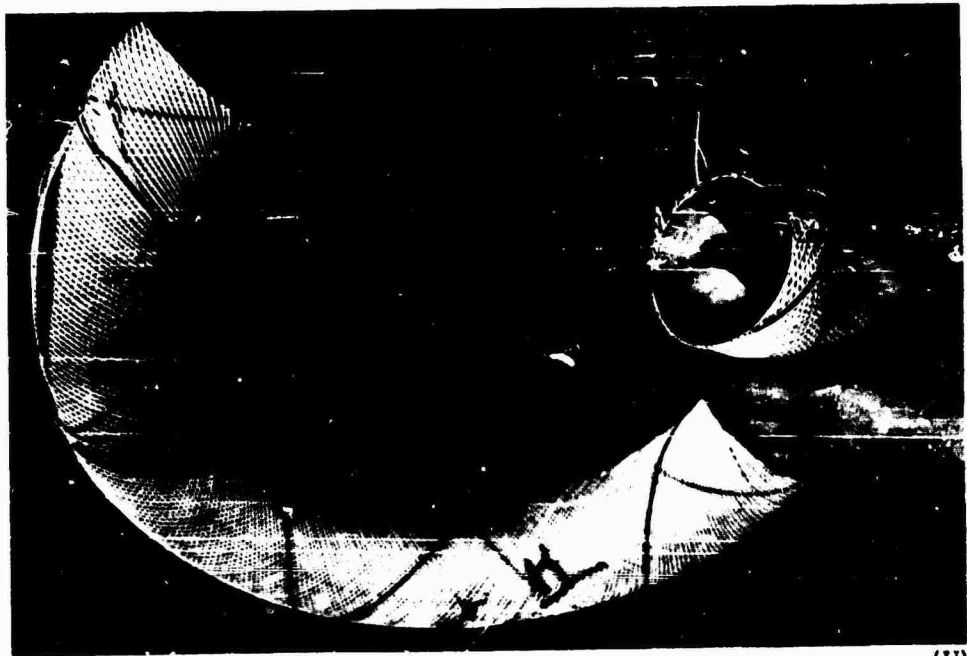
(C)(Gp-4) The third torus tested had a knitted structure that was reinforced externally with meridional filament winding. The clamping-bead scheme was an embedded flat magnesium ring laced to the torus inside the plate groove that was filled with Adiprene rubber. This torus had a nipple-type inflation valve. The torus remained attached to the plate by the rubber bond inside the plate groove after the test, so this concept seemed satisfactory. To minimize the weight, this torus was not impregnated with rubber.

(C)(Gp-4) This torus was exposed to a partial, a nominal, and a 1.5 full impulse. After the first exposure, there was no sign of failure, but after the second exposure, some of the meridional loops had slipped sideways, creating slight bulges. This slippage was due to the lack of filament



(U)

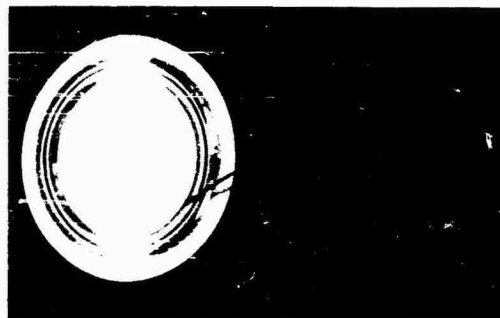
(a) Showing valves gone



(U)

(b) Showing inner-tube delamination

Fig. 5. 12--First torus (filament wound) failure (U)



(U)

(a) Torus before installation



(U)

(b) Installed on check rig



(U)

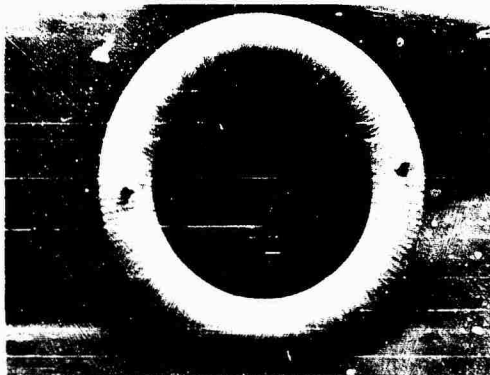
(c) Another view of torus
installed on check rig

Fig. 5.13--First torus (filament wound) for checking on control rig (U)



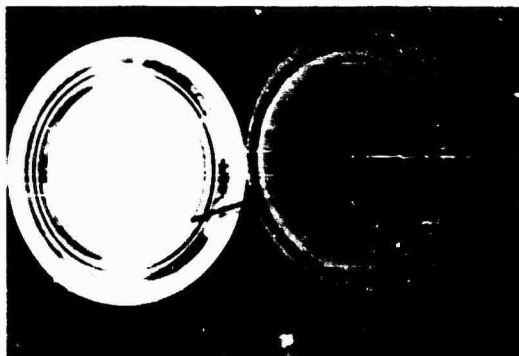
(a) Side view

(U)



(b) Top view

(U)



(c) Torus before installation on control rig

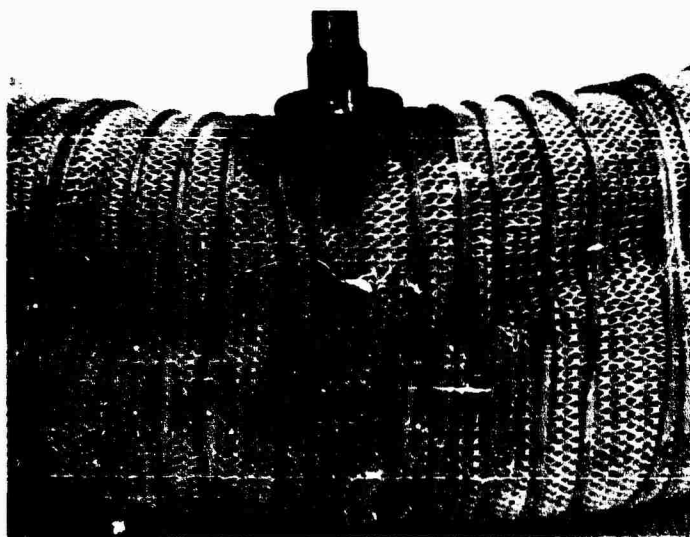
(U)

Fig. 5.14--Second torus (knitted structure) for checking on control rig (U)



(C) (Gp-4)

(a) Torus over-all aspect (deflated)



(C) (Gp-4)

(b) Detail of valve reinforcement

Fig. 5.15--Second torus after testing (U)

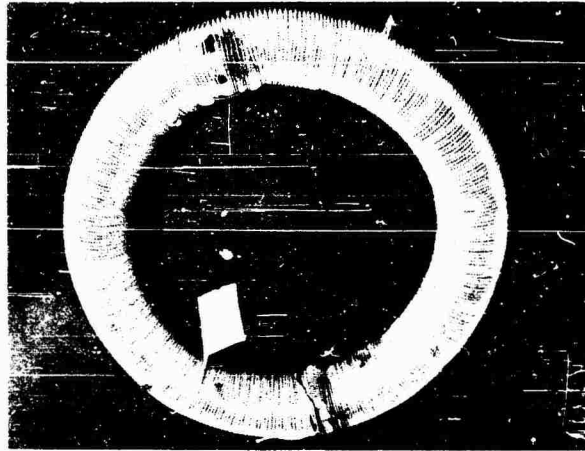
locking (no external impregnation). After the third exposure, the bulges grew in size and caused the rupture of some of the meridional filaments and of the knitting near the inflation valve. The meridional filaments again failed at the bead attachment. As evidenced in the case of the first torus, it seemed that the rupture might have been caused by a weakening of the filament due to local abrasion. This abrasion was probably the result of small relative motion of the filaments with respect to the clamping-bead lacing loops. Figure 5.16 shows the various torus failures.

(C)(Gp-4) The fourth torus was filament wound and equipped with a flat magnesium ring inside the clamping bead; the installation inside the plate groove was also satisfactory. This torus system did not show any signs of damage after one partial impulse followed by five full-impulse exposures, but when it was exposed to a 1.5 full impulse, it failed. About one-third of the torus had pulled loose from the plate and all the filaments were cut, causing the torus to rupture. There was no other sign of damage. Figure 5.17 presents photographs of the failure. Again, it appeared that the torus filament had probably been weakened by the bead lacing loops chafing the torus filaments. Although this cause was not an absolute certainty, there was enough evidence to direct the work toward a more realistic testing procedure, i.e., full impulse, but with a counterweight attached to the torus, and not lacing the clamping bead to the torus, if possible.

5.5.2. Single Torus with Counterweight (U)

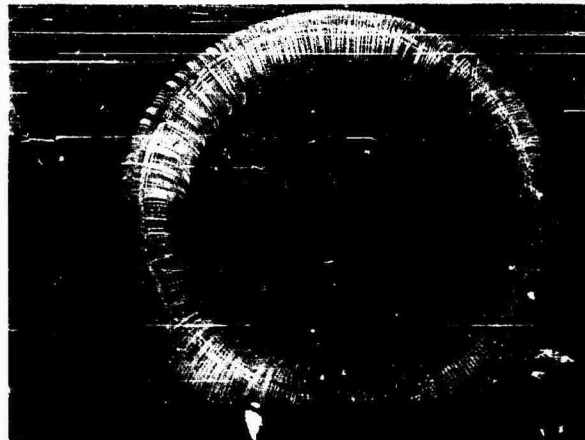
(C)(Gp-4) For this series of tests, a counterweight was attached to each torus and the torus was bonded to its test plate with a flat magnesium ring inserted inside the clamping bead. A typical cross section of such a single-torus system is presented in Fig. 5.18

(C)(Gp-4) In the testing of the first torus of this series, a last attempt was made to determine whether the filament-wound structure should be definitely abandoned (although it appeared to be the most efficient). But after two full-impulse exposures this torus also failed, in the very same



(a) Upper face

(C)(Gp-4)



(b) Bead side

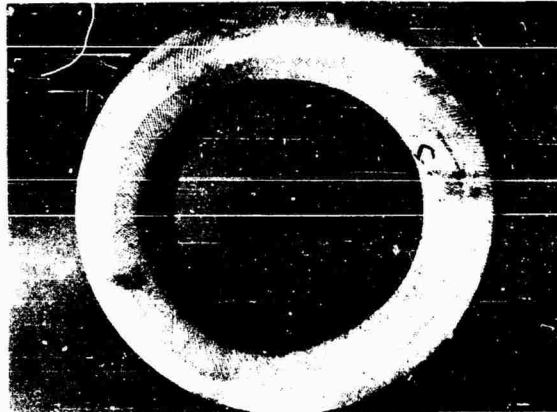
(C) (Gp-4)



(c) Detail of the
valve location

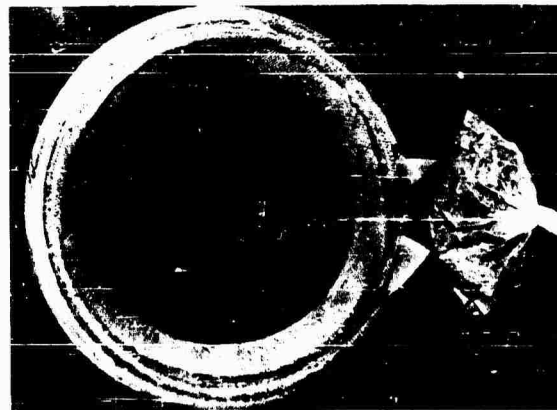
(C) (Gp-4)

Fig. 5.16--Third torus (knitted) failure (C) (Gp-4)



(a) Upper face

(C) (Gp-4)



(b) Bead side and debris found inside torus

(C) (Gp-4)



(c) Typical structure and inner-tube failure

(C) (Gp-4)

Fig. 5.17--Fourth torus (filament wound) failure (U)

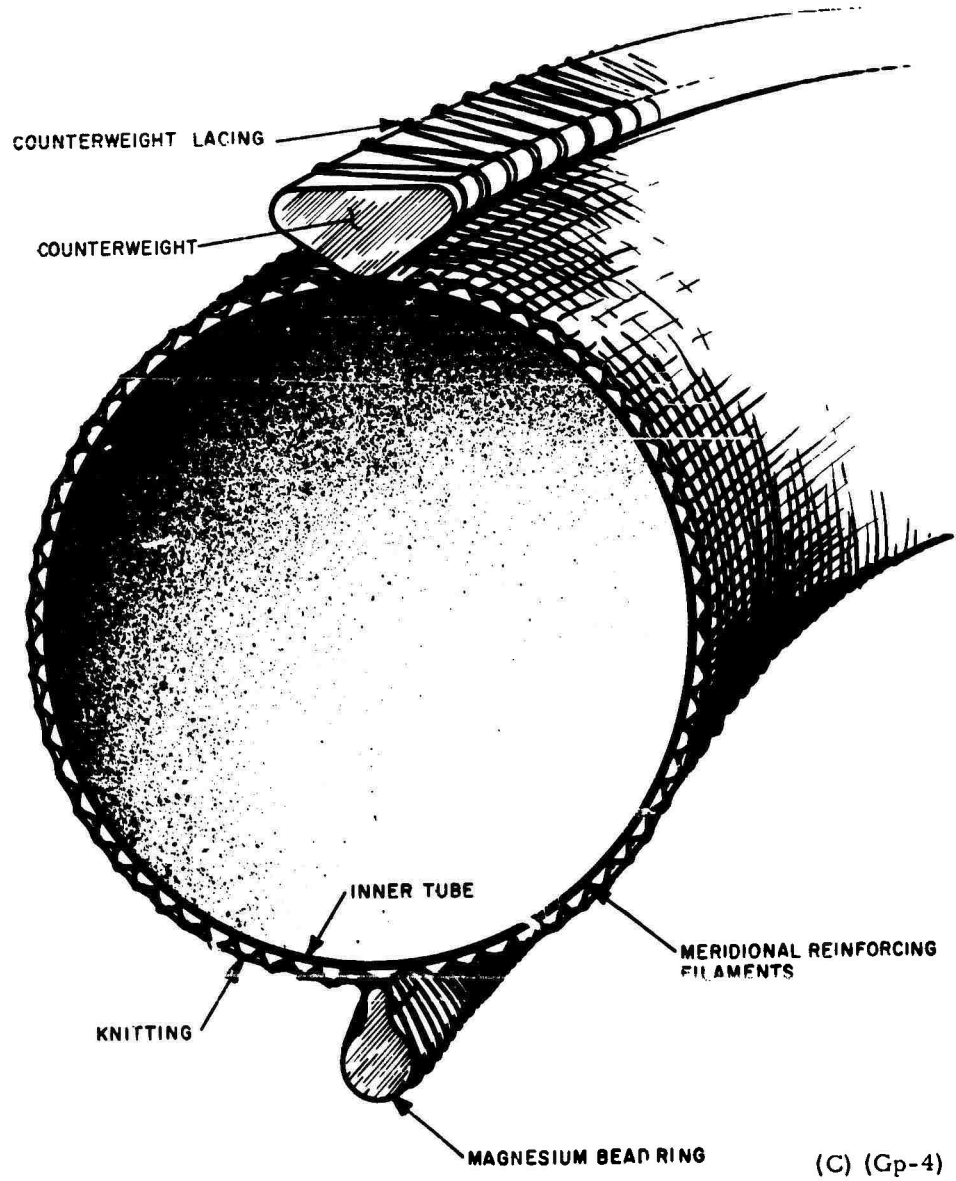


Fig. 5.18--Typical single-torus-system cross section (clamped torus)
(U)

way the previous system had failed. Nevertheless, the counterweight attachment, which was a lacing process, did not show any sign of damage even though it was subjected to high localized stresses. Again, the failure pointed to the possible abrasion problem. Figure 5.19 shows views of this failure.

(C)(Gp-4) The second torus of this series, as were all subsequent tori, was a knitted structure reinforced with interwoven meridional filaments. The interweaving was intended to avoid the failure described in Section 5.5.1. For reasons that were not quite clear, this torus failed after the first full-impulse exposure. The clamping-bead magnesium ring appeared to be defective and the torus was not well installed on the plate, which might have caused stress concentrations. A 5-in.-long strip of the bead had been pulled out of the groove, and this possibly caused the torus-structure rupture. Photographs of this failure are presented in Fig. 5.20.

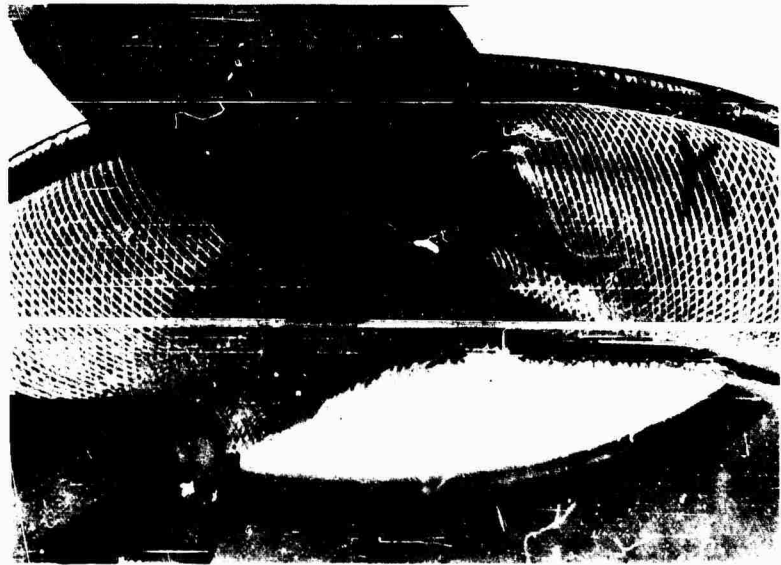
(C)(Gp-4) The quality control was more stringent and the manufacturing more careful for the third torus system. Forty percent more meridional filaments were used to strengthen the attachment to the clamping bead, resulting in a better quality item. However, the torus failed after two full-impulse exposures. Again, about two-thirds of the magnesium ring was pulled out of the groove, causing the torus wall to rupture. But this time, none of the meridional loop ruptured and only the knitted structure failed at the place where the flat magnesium ring had broken.

(C)(Gp-4) It became apparent that the bonding of the clamping ring inside the plate groove could not be adequately controlled with the existing design. Failure of this bond was directly causing subsequent torus failure. Figure 5.21 illustrates this torus failure. Figure 5.22 shows the plate-clamping boss with part of the torus attachment bead locked in the groove after the torus was cut loose from the plate.



(C) (Gp-4)

(a) Torus mounted on plate



(C) (Gp-4)

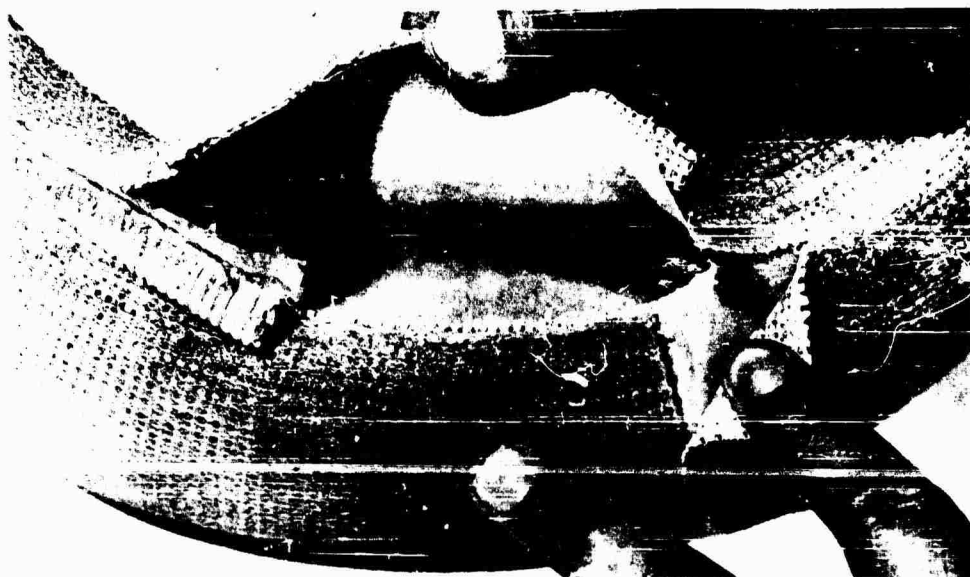
(b) Typical structural failure

Fig. 5.19--Failure of first torus (filament wound) with counterweight (U)



(C) (Gp-4)

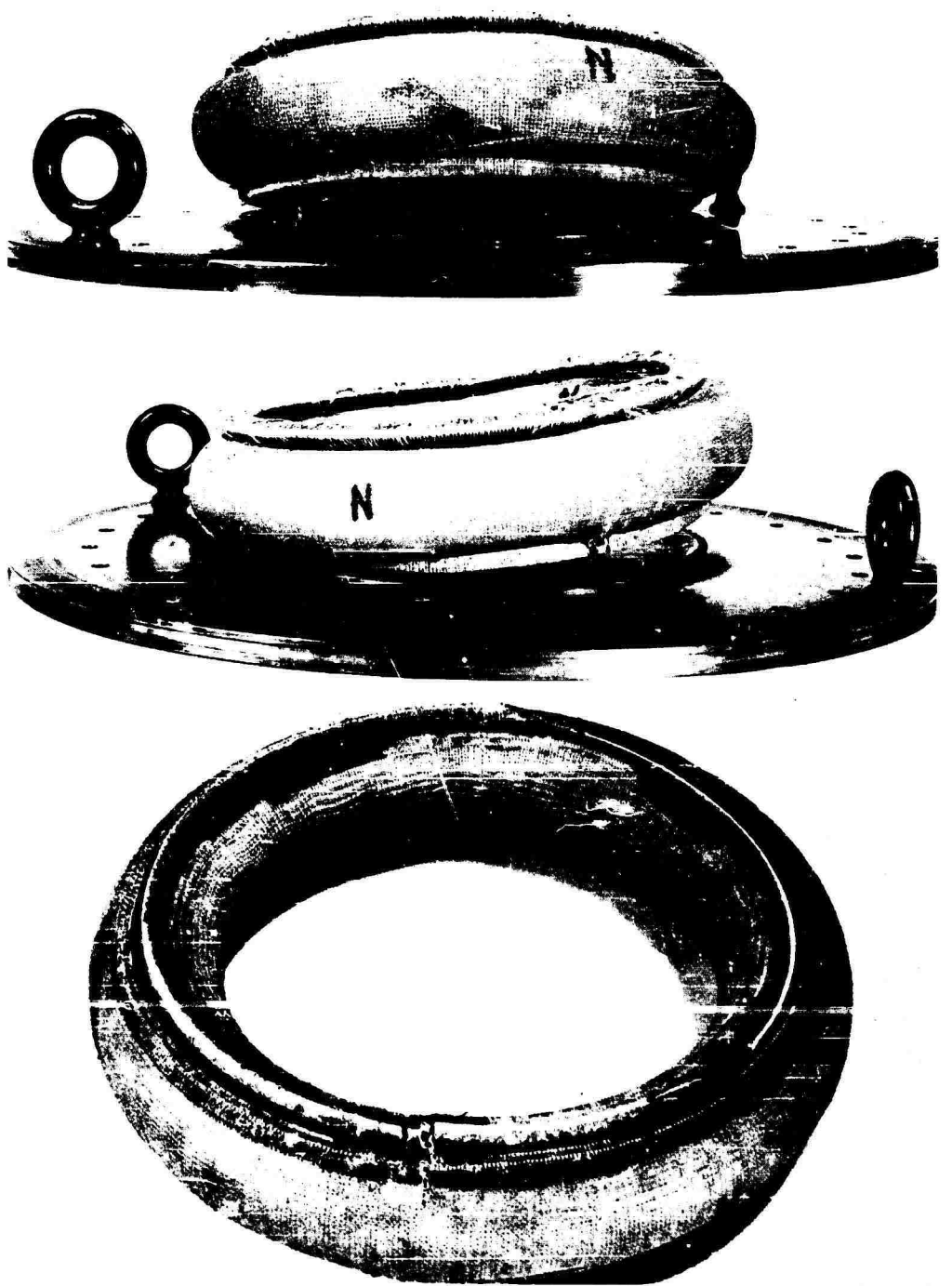
(a) Torus on plate



(C) (Gp-4)

(b) Typical failure at bead attachment

Fig. 5. 20--Failure of second torus (knitted structure) with counterweight (U)



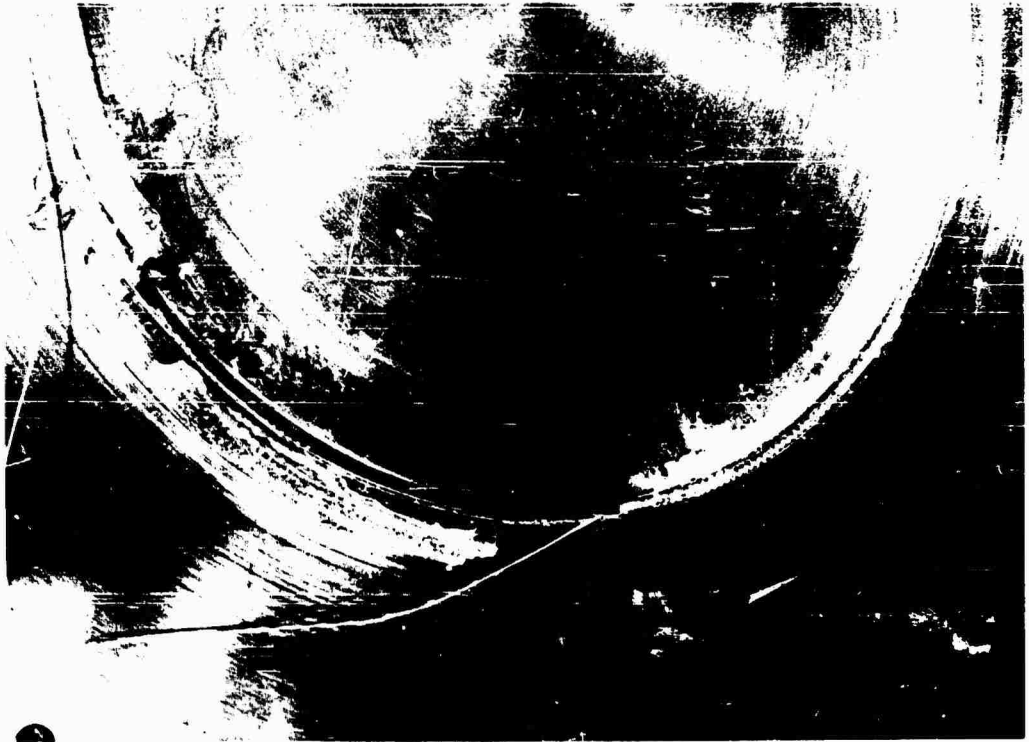
(C)(Gp-4)

Fig. 5.21a--Failure of third torus (knitted structure) showing the torus on the plate after testing, bead failure, over-all failure (U)



(C)(Gp-4)

Fig. 5.21b--Failure of third torus (knitted structure)
showing inside and outside failures (U)



(C) (Gp-4)

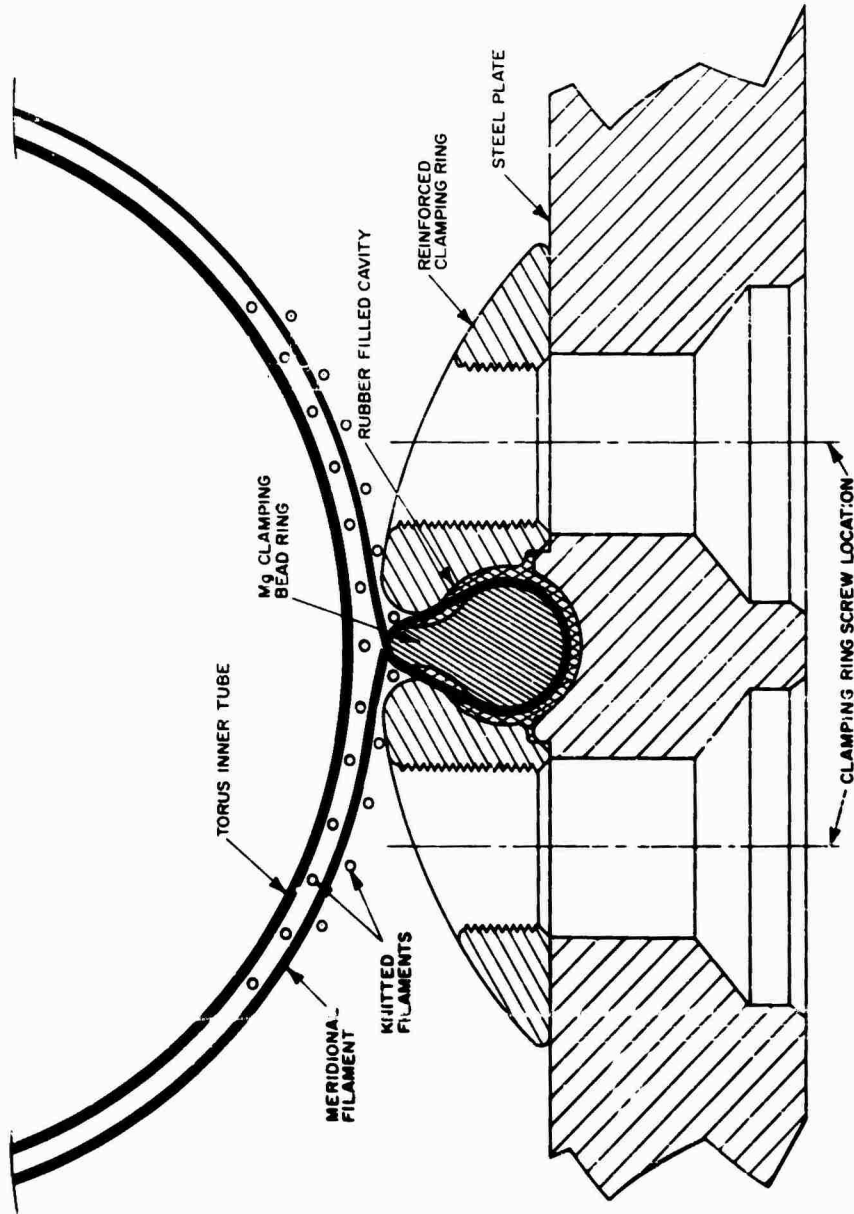
Fig. 5.22--Typical torus failure at the attachment to the plate (plate side)(U)

5.5.3. Plate-clamped Single-torus System (U)

(C)(Gp-4) Considering all the failures described above, it is clear that the torus attachment to the plate presents a critical design problem. Although the resin-inflating scheme was, and still is, attractive, it appeared that the development of a satisfactory bead inner tube would require a larger effort than possible in the program of current limited scope. Therefore, a decision was made to concentrate only on the torus structural problem by making sure that the bead attachment could not fail. It was thus decided to employ separate clamping rings that would positively hold the bead. A solid, round magnesium ring was used, as illustrated in Fig. 5.23; Fig. 5.24 shows the plate-clamped single-torus system prior to assembly on the plate.

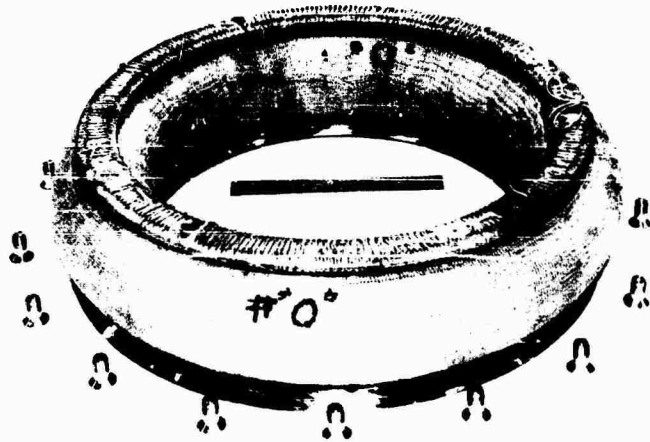
(U) This torus was exposed to twenty-two full impulses without failure. Figure 5.25 show the torus after completion of all testing.

(U) Two accelerometers were installed on the counterweight (see Fig. 5.26) after the fifth full impulse when it became apparent that the test specimen was satisfactory. After the accelerometers were attached, two partial impulses and two full impulses were imparted to the plate. Acceleration of the counterweight was recorded versus time. The first instrumented partial-impulse test was not completely successful because part of the A-1 HE did not detonate; this caused the plate to spin and produced an erratic signal from the accelerometers. Also the signal amplitudes were too low, corresponding to a below-normal plate velocity. A second A-1 shot was successful. The leads of one accelerometer ruptured during the first compression cycle of the two A-2 shots, so only one signal was available for the full-impulse shots. Some typical signals are given in Figs. 5.27 through 5.30. The acceleration peaks recorded during the second A-1 and the two A-2 shots are given as a function of time elapsed from the HE detonation in Tables 5.1 and 5.2. The traces in Fig. 5.31 show the signal decay versus time.



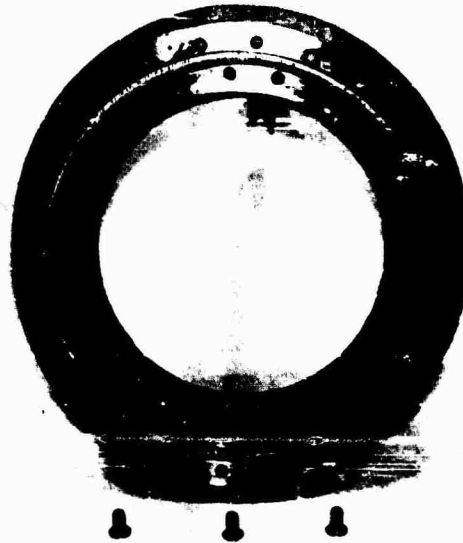
(C) (Gp-4)

Fig. 5.23--Typical clamped torus attachment (1)



(C) (Gp-4)

(a) Torus with clamping rings installed



(C) (Gp-4)

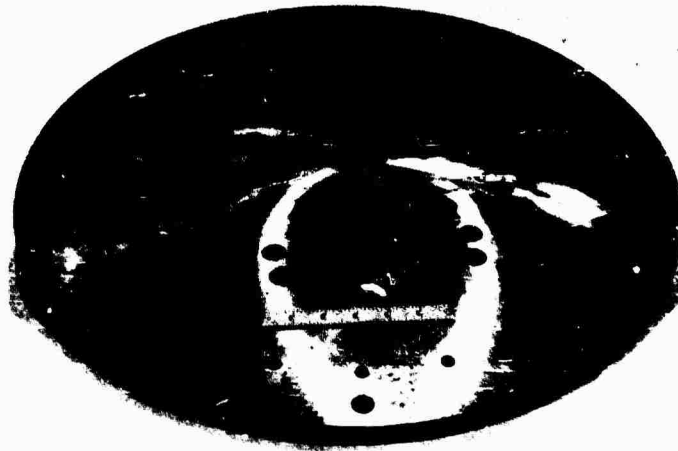
(b) Back view of torus with clamping ring

Fig. 5.24--Plate-clamped single torus before test (U)



(C) (Gp-4)

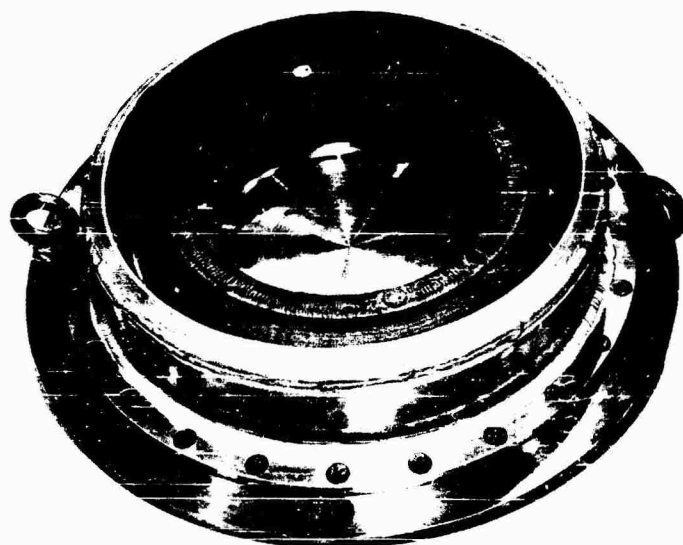
(c) Torus installed on plate



(C) (Gp 4)

(D) Back face of plate

Fig. 5.24 continued--Plate-clamped single torus before test (U)



(C) (Gp-4)

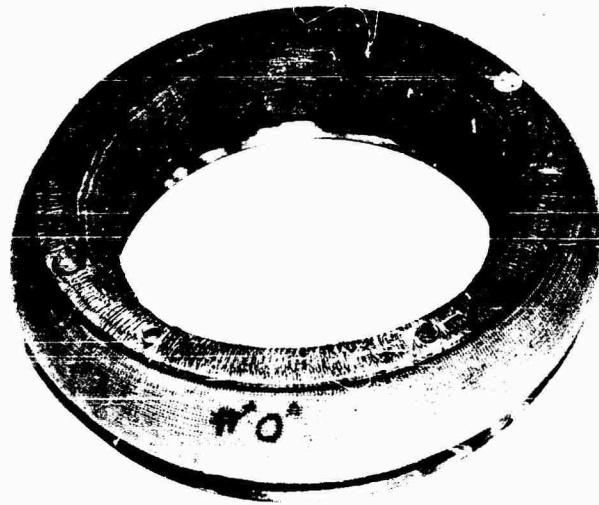
(a) Installed on plate with shield



(C) (Gp-4)

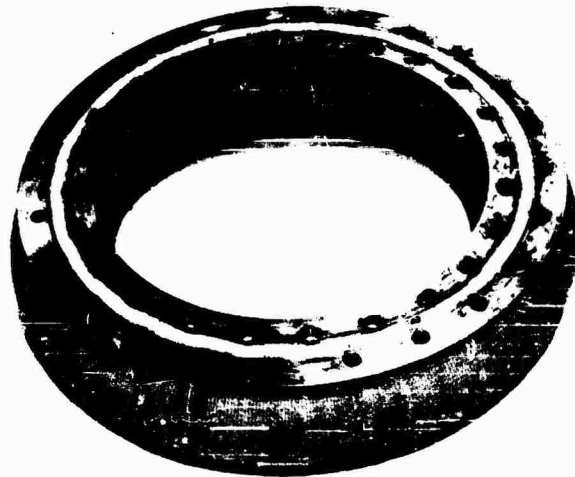
(b) Shield removed

Fig. 5.25--Clamped single torus after testing (U)



(C) (Gp-4)

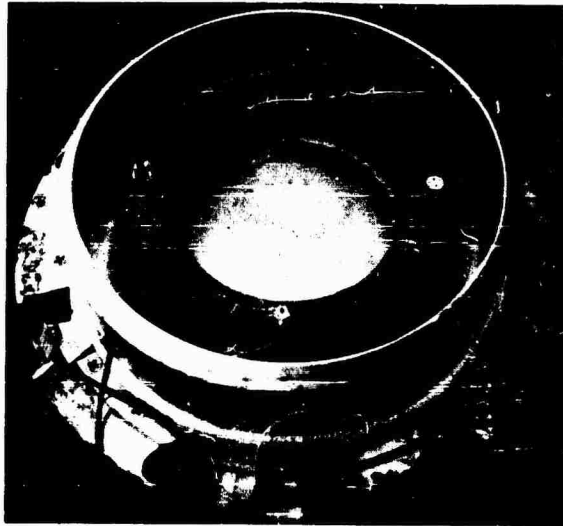
(c) Torus removed from the plate



(C) (Gp-4)

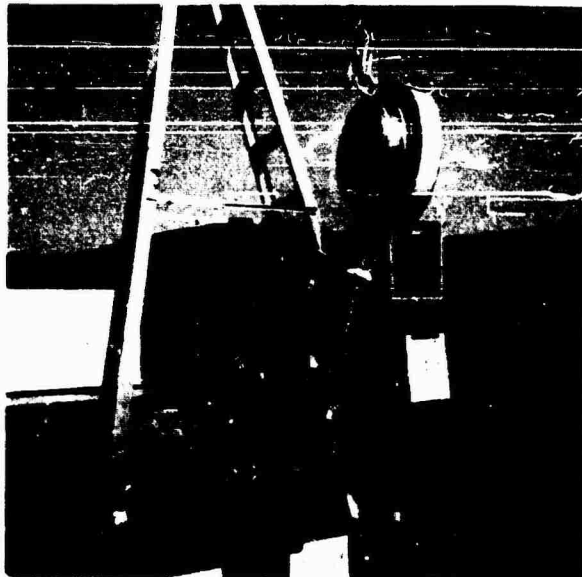
(d) Torus removed from the plate (bottom view showing clamping rings)

Fig. 5.25 continued--Clamped single torus after testing (U)



(C) (Gp-4)

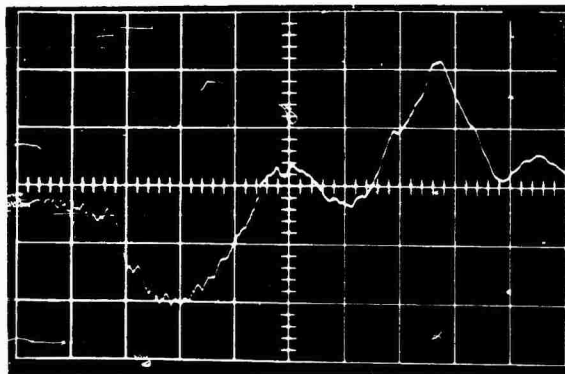
(a) Torus with accelerometers installed on counterweight



(C) (Gp-4)

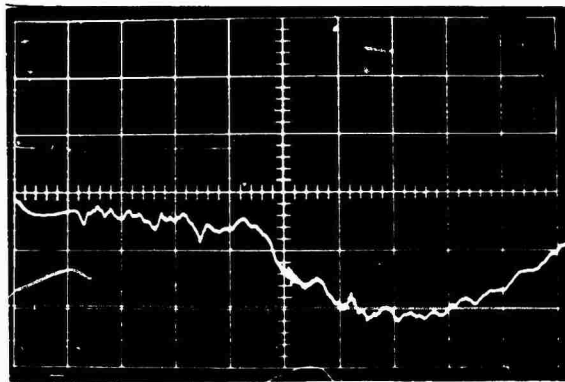
(b) Torus and plate installed before shot (note slack accelerometer leads)

Fig. 5.26--Single-torus instrumented test (U)



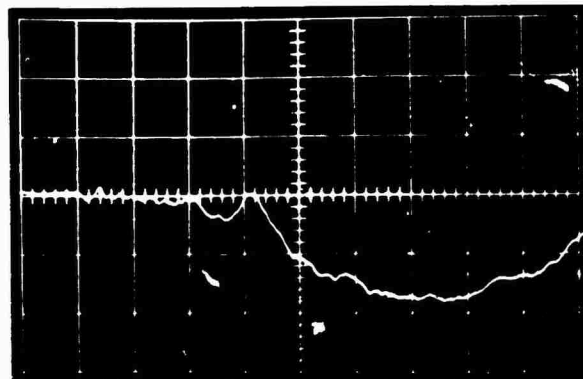
(a) 2220 accelerometer
(3000 g/cm, 0.5 msec/cm)

(C) (Gp-4)



(b) 2220 accelerometer
(3000 g/cm, 0.2 msec/cm)

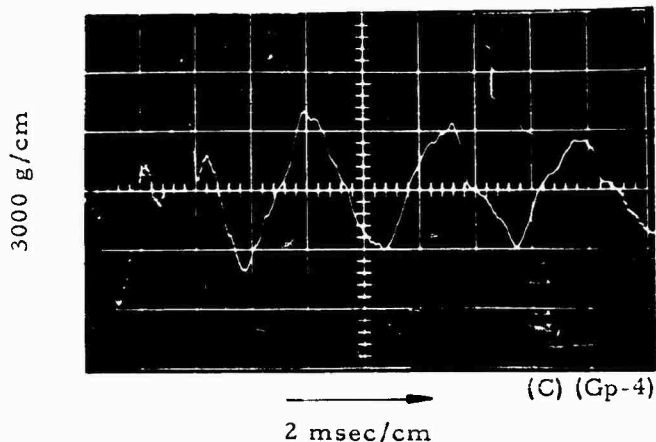
(C) (Gp-4)



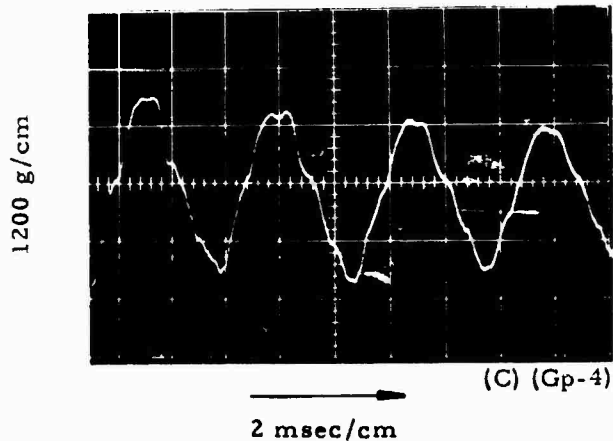
(c) 2275 accelerometer
(2500 g/cm, 0.2 msec/cm)

(C) (Gp-4)

Fig. 5.27--Accelerometer signals from second A-1 shot using different accelerometers (U)

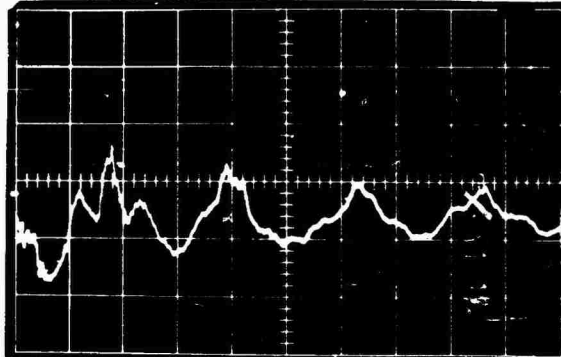


(a) First 20 msec



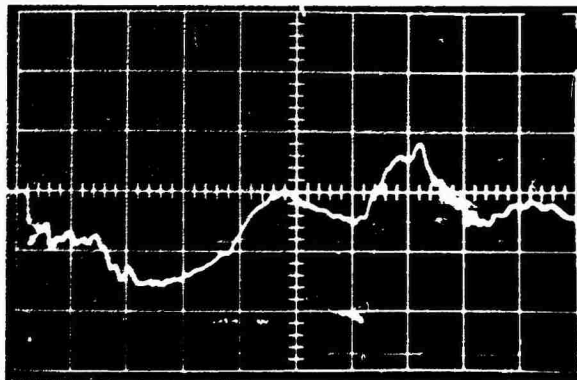
(b) 20 to 40 msec

Fig. 5.28--Typical accelerometer signals from second A-1 shot (U)



(C) (Gp-4)

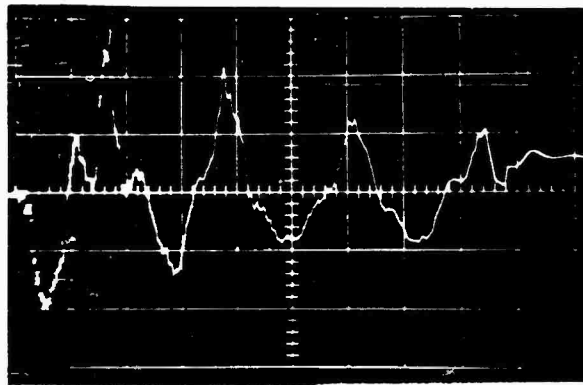
2 msec/cm



(C) (Gp-4)

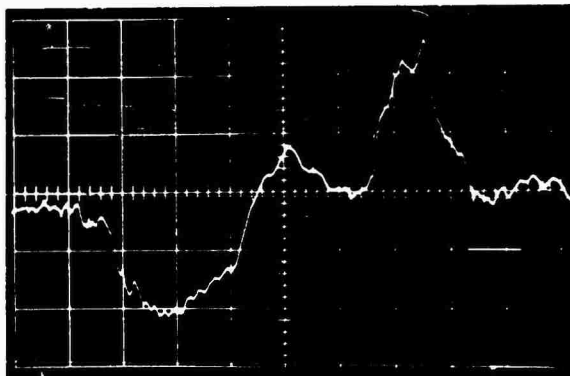
0.5 msec/cm

Fig. 5.29--2220 accelerometer signals (12,000 g/cm) from first A-2 shot (U)



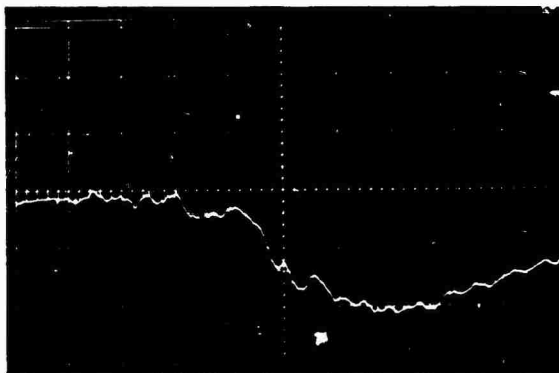
2 msec/cm

(C) (Gp-4)



0.5 msec/cm

(C) (Gp-4)



0.2 msec/cm

(C) (Gp-4)

Fig. 5.30--2220 accelerometer signals (6,000 g/cm) from second A-2 shot (U)

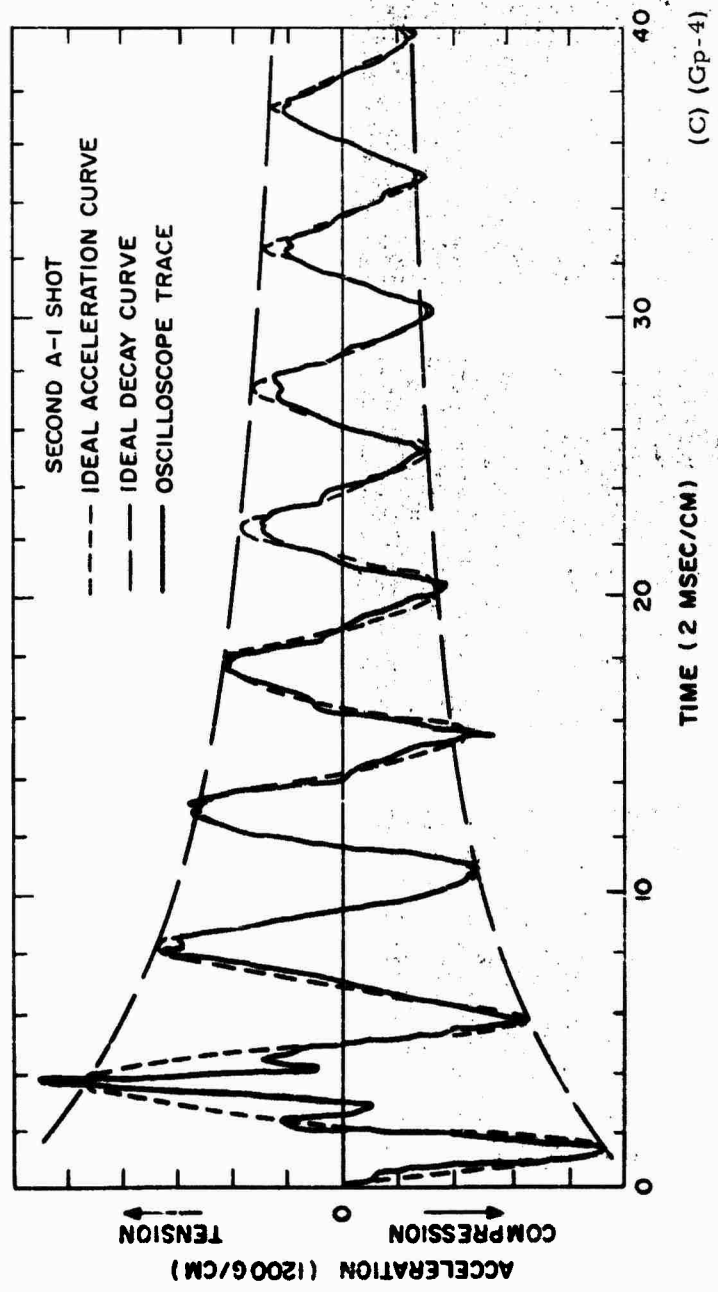


Fig. 5.31--Typical acceleration imposed on counterweight (U)

Table 5.1

ACCELERATION MEASUREMENT TEST RESULTS (A-1) (U)
(Acceleration peaks, g)

Time Elapsed from HE Detonation (msec)	2220 Accelerometer	2275 Accelerometer
1 - 1.2	+ 6,000	+ 4,500
3.5 - 3.6	- 6,600	- 6,000
5.8	+ 4,200	+ 4,000
8.0 - 8.4	- 3,800	- 4,250
10.8	+ 3,000	+ 3,500
13.2 - 13.3	- 3,500	- 4,000
15.5 - 15.6	+ 3,000	+ 3,500
17.6 - 18.0	- 2,400	- 3,750
20.2	+ 2,100	
22.4	- 1,700	
25.2	+ 1,900	
27.4 - 27.8	- 1,440	- 2,100
30.2	+ 2,040	+ 2,200
32.2 - 32.4	- 1,200	- 1,500
34.8	+ 1,800	
37.0	- 1,080	

(C)(Gp-4)

Table 5.2

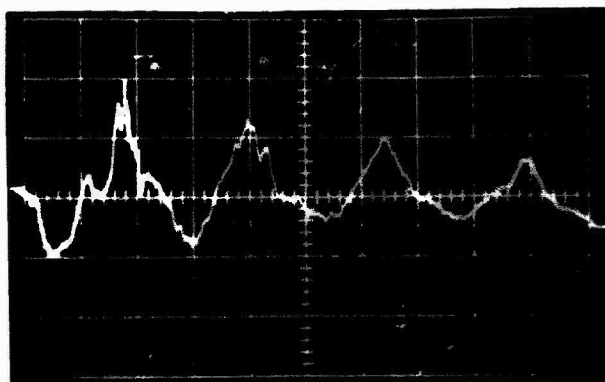
ACCELERATION MEASUREMENT TEST RESULTS (A-2) (U)
(Acceleration peaks, g)

Time Elapsed from HE Detonation (msec)	2220 Accelerometer	
	First shot	Second shot
1 - 1.2	+ 13,200	+ 12,000
3.5 - 3.6	- 14,400	- 16,800
5.8	+ 8,200	+ 8,400
7.6 - 7.8	- 10,600	- 12,800
9.0	+ 6,000	+ 5,000
12.2 - 12.5	- 7,000	- 7,200
14.4 - 14.5	+ 4,800	+ 4,800
16.8 - 17.3	- 6,800	- 6,400
19.4	+ 3,600	

(C)(Gp-4)

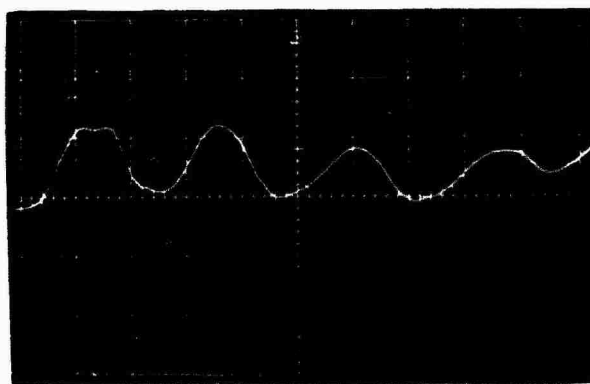
(U) A final full impulse (the twenty-second shot) was delivered to the torus with the small accelerometer (Type 2220) mounted on the counterweight ring. This time the acceleration signal was integrated to obtain the counterweight velocity versus time. A second integration gave the displacement versus time. The oscilloscope traces are shown in Figs. 5.32 and 5.33.

(C)(Gp-4) The first integration smoothed out the acceleration curve and the second integration yielded a very smooth curve. The integral below the first velocity cycle was appreciably higher than that under the following cycles. This means that the rate of damping of the torus-wall wave was very high during the first counterweight oscillation cycle and that a considerable amount of the energy trapped in these waves was dissipated at an early time.



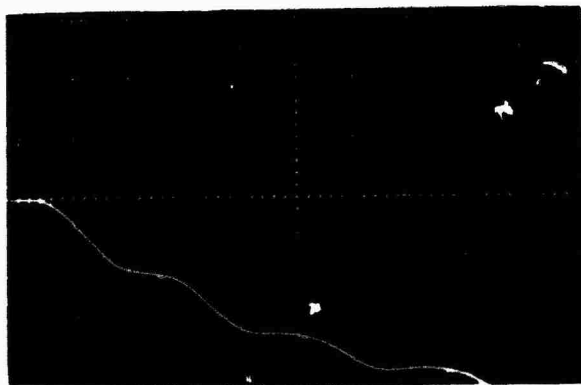
(a) Acceleration
(5000⁰ g/cm)

(C) (Gp-4)



(b) Velocity
(200 ft/sec/cm)

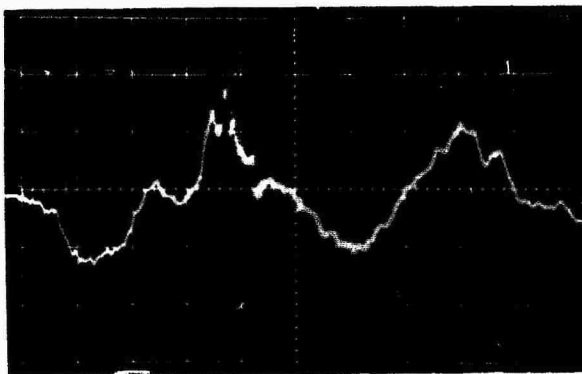
(C) (Gp-4)



(c) Displacement
(6.73 in/cm)

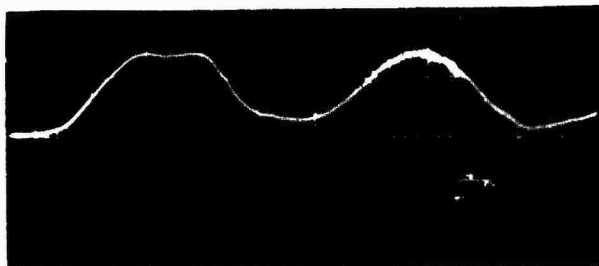
(C) (Gp-4)

Fig. 5.32--Counterweight acceleration, velocity and displacement from A-2 shot (2 msec/cm) (U)



(C) (Gp-4)

(a) Acceleration (5000 g/cm)



(C) (Gp-4)

(b) Velocity (200 ft/sec/cm)

Fig. 5.33. - Counterweight acceleration and velocity from A-2 shot (1 msec/cm) (U)

(C)(Gp-4) The results of Table 5.1 are somewhat surprising since the negative accelerations (torus tension) were larger in absolute value than the positive accelerations (torus compression) during the first 20 msec. After 30 msec, the phenomenon was reversed, the negative accelerations were smaller (in absolute value) than the positive accelerations. This reversal is illogical, because the force developed in tension by the torus is always larger than that developed in compression for the same amount of energy storage. A close examination of the oscilloscope traces in Fig. 5.27 revealed that the acceleration peaks resulted somewhat from the influence of the torus-wall wave traveling back and forth between the plate and the counterweight. The time taken by these waves to travel from the plate and back did not coincide with the counterweight oscillation period. These two phenomena were apparently out of phase and the "overshoot" peaks in tension (seen at the beginning of the trace) appeared at the peak of the compression cycle and thus canceled out the tension acceleration peak that normally would be present.

(C)(Gp-4) This observation means that the acceleration peaks obtained from these tests are very different from those which would be obtained with a much lighter torus and also that the torus-wall waves do not damp out as rapidly as one would expect since their effects are still quite evident, even after several cycles of the counterweight.

5.6. CORRELATION OF TEST RESULTS WITH PREDICTED RESULTS (U)

(U) Since it is difficult to mount sophisticated instrumentation on a single-torus dynamic test setup, little recorded time-resolved data were obtained during the test program. Nevertheless, an attempt was made to correlate the test results with some rough estimates of the system frequency, wave velocity along the torus wall, amount of torus flattening against the clamping boss, and counterweight travel with respect to the plate.

(C)(Gp-4) As foreseen, the torus clamping rings loosened after each impulse and the screws had to be retorqued. It was anticipated that the screws would deform plastically but would not rupture. ⁽¹⁾ This is exactly what happened, but all screws withstood the twenty-two impulse exposures without fracture. Figure 5.34 presents views of some of these screws after disassembly to show the amount of screw punching effect caused by the impulses. The photograph of an unused screw is also shown for comparison.

5.6.1. Wave Velocity along the Torus Wall (U)

(C)(Gp-4) The deformation wave created by the flattening of the torus against the plate reaches the counterweight with a delay that is caused by the time it takes for that wave to travel around the torus wall, resulting in the perturbations shown on the oscilloscope traces, at least during the first cycle. The time delay can be estimated within ± 10 percent. The results are given in Table 5.3. The delay due to the attenuator and the pressure-pulse duration is roughly 0.2 msec, which is relatively small compared to the delay caused by the torus-wall mass.

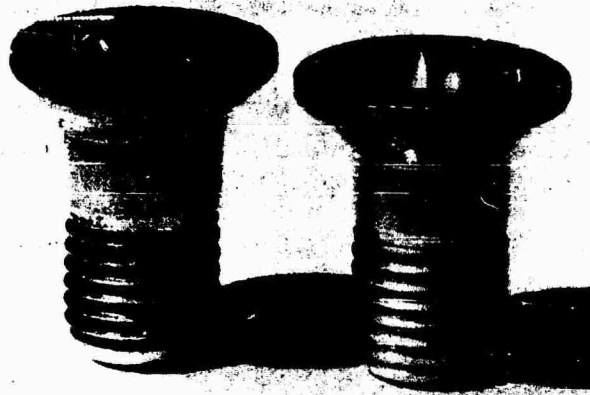
Table 5.3

ACCELEROMETER SIGNAL DELAY
(in milliseconds)

Delay	Partial Impulse (A-1)	Full Impulse (A-2)
Due to attenuator	~ 0.20	0.15 to 0.20
Due to torus wall	0.55 to 0.60	0.55 to 0.60

(C)(Gp-4)

(C)(Gp-4) For the torus-wall weight (0.0033 lb/in.^2) and the pressure inside the torus (80 psig), the average transversal wave velocity, V_w , is roughly 300 ft/sec. This wave must travel about 4 in. before it reaches the counterweight. (The signal transmitted through the air inside or around the torus arrives sooner but is of low amplitude.) This would indicate an expected delay of 1.2 msec, which is appreciably longer than the delay



(C) (Gp-4)

(a) Used screw and new screw



(C) (Gp-4)

(b) Used screw (screw grip still clean)



(C) (Gp-4)

(c) Used screw (screw covered with soot)

Fig. 5.34--Typical clamping ring screw damage (after 22 shots) (U)

given in Table 5.3. During 1 msec, the plate travels about 1.5 in. and the torus has time to be compressed to a point where the pressure inside the torus has appreciably increased, increasing the wall hoop tension and therefore the transverse wave velocity. Also, the unrestrained length of wall is less than $\pi d/2$, since the torus is flattened against both the plate and the counterweight ring. These two corrections to the calculations could account for the observed factor of 2 discrepancy.

(C)(Gp-4) As determined from the oscilloscope traces of Fig. 5.27, the torus-wall wave traveled twice the torus-wall length in about 1.3 to 1.4 msec. This indicated that the wave must have traveled at a speed of about 500 ft/sec at the point of maximum elongation (tension) of the torus and that tension was about three times larger than it would be in the neutral position. Therefore, the wave velocity should have been $\sqrt{3}$ times higher. This checks with the experimental figure ($300 \times \sqrt{3} = 520$ ft/sec). Assuming an average wave velocity of 400 ft/sec, the frequency of this wave effect was between 2.5 to 3 times higher than that of the counterweight oscillation. This explains why the wave effect superimposed upon the counterweight reaction shifts in phase, as clearly illustrated in Fig. 5.28.

5.6.2. System Frequency (U)

(C)(Gp-4) Since the torus system is a nonlinear spring, the frequency of oscillation of a mass attached to it depends on the oscillation amplitude. Since the torus becomes stiffer for large amplitudes, the frequency decreases slightly when the amplitude increases, as indicated in Tables 5.1 and 5.2. The system frequency is thus approximately 200 cps.

(C)(Gp-4) The total mass of the counterweight ring is ~ 1.0 lb. The calculated equivalent stiffness of the toroidal spring is roughly 60,000 to 80,000 lb/ft. Neglecting the torus mass (~ 1.0 lb), a frequency of 230 cps is obtained. But, actually, part of the torus mass should be added to that of the counterweight ring, which would decrease the calculated frequency to a value closer to that measured.

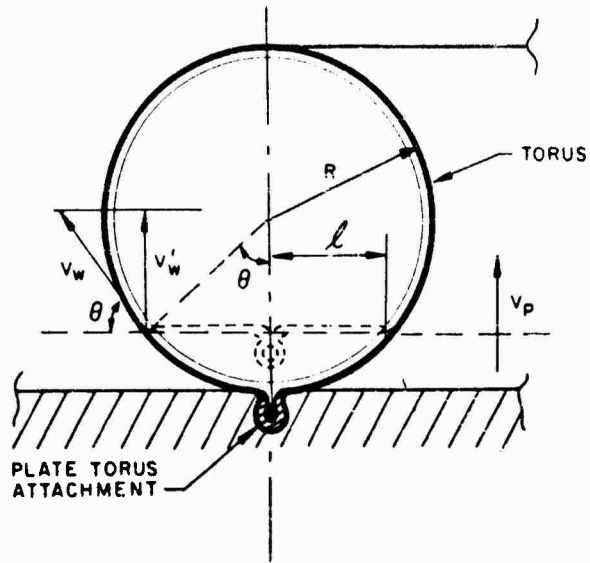
5.6.3. Torus Flattening Against the Plate (U)

(C)(Gp-4) It was possible to determine in two instances the amount of torus flattening against the plate during the first torus compression cycle with no counterweight ring attached. This was done with the first two tori, which were lighter than the last torus tested. In this case the torus weights were 0.62 lb and 0.58 lb, respectively. For a plate velocity increment, V_p , of about 190 ft/sec, the torus contact marks on the plate extended an average of 1.00 in. between the outside and inside bosses in the first torus (wound structure) and 1.10 in. in the second torus (knitted reinforced structure). Although the first torus was slightly heavier, it flattened less than the second torus, which is not consistent. The actual transverse wave velocity along the torus wall must have been close to 330 ft/sec. Referring to Fig. 5.35, one can calculate the angle θ so that $\sin \theta = 190/330$ or ~ 0.58 . Then $\theta = 35.5^\circ$. The half-chord length, l , for such an angle and a diameter of 2.5 in. is $\sim 3/4$ in. This value is appreciably less than the measured value of 1 in., which would indicate that the transverse wave velocity was less than calculated or that the torus flattens more than theoretically expected.

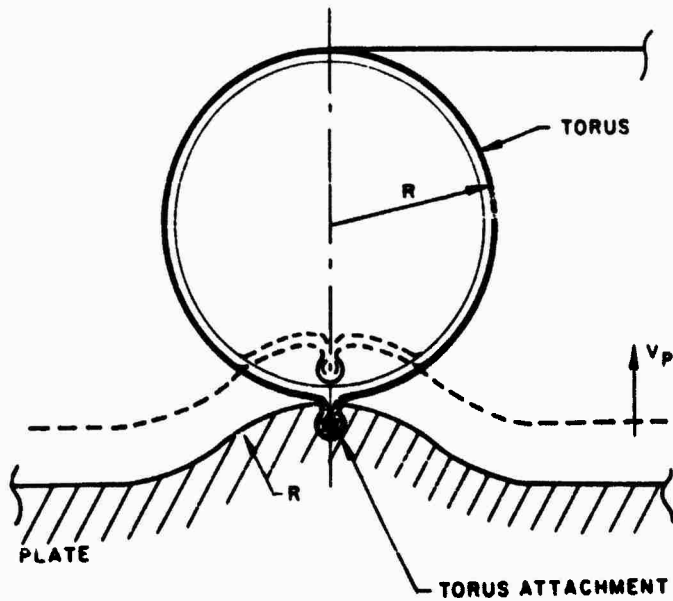
5.6.4. Torus Reaction (U)

(C)(Gp-4) A typical torus force characteristic is given in Fig. 5.36 for the torus size investigated. This force versus displacement curve was derived by assuming that the torus wall does not stretch or shrink when subjected to variable stresses. It was also assumed that the torus flattens between two planes in compression. This was not the case at all, since the test torus was compressed between two circular-shaped surfaces, i.e., the plate clamping boss and the counterweight ring. These two discrepancies led to a softer spring in compression, probably similar to the curve shown as a dashed line.

(C)(Gp-4) For the full impulse, the acceleration peaks, as calculated, should have been +7,000 g in compression and -10,000 g in tension. This does not take into account the overshoot caused by the torus-wall waves as



TYPICAL FLAT CLAMPING GROOVE



TYPICAL IDEALLY SHAPED CLAMPING BOSS

(C) (Gp-4)

Fig. 5. 35--Typical clamping boss shape for torus attachment (U)

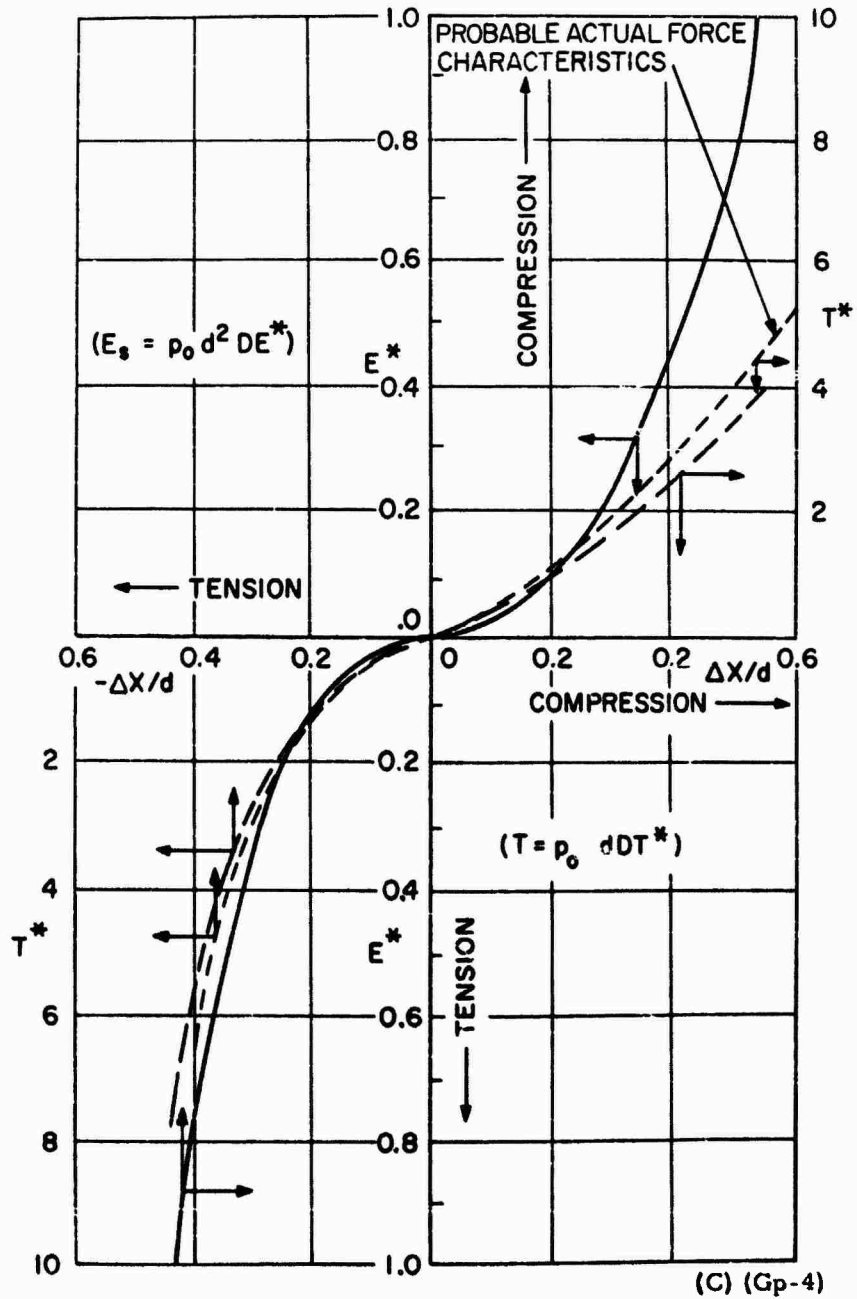


Fig. 5.36--Torus gas spring characteristics (U)

shown in Fig. 5.31. For the partial impulse case, the calculated acceleration peaks are +4,000 g and -5,300 g in compression and tension, respectively. Although these numbers are slightly lower than expected, they agree fairly well with the results given in Tables 5.1 and 5.2.

5.6.5. Torus Travel and Energy-storage Capacity (U)

(C)(Gp-4) The calculated stored energy for the single-torus system was about 260 lb-ft, corresponding to a flattening of about 45 percent of the torus cross-section diameter if the torus is compressed between two rigid planes. In the actual case, the flattening ($\Delta X/D$) could have extended to 50 percent, but in tension the counterweight travel could not have been much more than 35 percent according to the curves given in Fig. 5.36.

(C)(Gp-4) Data reduction of the oscilloscope traces shown in Figs. 5.32 and 5.33 yield acceleration peak values similar to those presented in Table 5.3. From a (measured) plate velocity increment of 130 to 140 ft/sec, the counterweight travel is 1.30 to 1.35 in. in compression and ~1.0 in. in tension. These experimental quantities are only slightly higher than those calculated above (52 percent versus 50 percent and 40 percent versus 35 percent)

(C)(Gp-4) Also, the torus pressure must have been slightly lower because the torus wall appeared softer than originally, which would explain why longer travels than expected were obtained. This is corroborated by the shape of the acceleration traces (more pointed for the tension stroke) if one compares them with those of Figs. 5.29 and 5.30, for instance.

(U) Thus, the agreement between analytical and experimental results is very good and perhaps better than expected for both energy storage capacity of the torus and the counterweight travel.

5.6.6. Counterweight Oscillation Damping (U)

(C)(Gp-4) As shown in Fig. 5.31, an attempt was made to idealize the counterweight oscillations to correct for the influence of the dynamic effects of the torus-wall wave. The ideal curve of acceleration versus time is shown as a dotted line in Fig. 5.31. If one assumes that the system behaved as a linear spring, the curve of displacement of the counterweight

with respect to the torus attachment plate is similar to the acceleration curve, and the damping of the counterweight oscillations can be represented by the dashed line showing the logarithmic decay of the oscillations. It is straightforward to calculate the amplitude ratio between two adjacent peaks and to compute the system damping. The average amplitude ratio per cycle for the first three cycles is about 1.274 and for the first five cycles is about 1.24. The logarithmic decrements are then 0.2413 and 0.2151, respectively. The logarithmic decrement is

$$n\tau = \frac{2n}{p} \times \frac{2}{\sqrt{1 - n^2/p^2}} \quad (5.1)$$

where

$$n = \frac{cg}{2W}, \quad p^2 = \frac{kg}{W}, \quad \text{and } \tau = \text{period (sec)},$$

in which W = weight of the sprung mass (lb),

$$g = 32.2 \text{ ft/sec}^2,$$

c = damping coefficient,

k = spring stiffness (lb/ft)

Equation (5.1) allows the calculation of n and p , since τ is known (4.8 msec), deriving

$$n \cong 45 \text{ for the first five cycles,}$$

$$n \cong 50 \text{ for the first three cycles.}$$

(C)(Gp-4) Assuming that part (about 25 to 30 percent) of the torus wall moves with the sprung mass, one gets $p^2 \cong 1.70 \times 10^6$ for both cases.

Knowing W (1 lb + 0.30 lb), one can calculate and obtain $k \cong 68,700$ lb/ft.

This value is half-way between the calculated (estimated) values given in Section 5.6.2, thus showing excellent agreement.

(C)(Gp-4) The calculated value of c varies between 2.8 and 3.15 for the first five and three cycles, respectively, indicating that more damping is present at the beginning of the oscillations. This is reasonable since the torus-wall waves are highly damped during the first two oscillations of the counterweight, as illustrated in Figs. 5.27 and 5.30.

(C)(Gp-4) In comparing these results with those obtained with a three-torus stack tested three years ago,⁽⁷⁾ it appears that the present system is more highly damped. The logarithmic decrement was 0.17 for the earlier (three-torus stack) system. Again, this is easy to account for since the mass ratio between the present torus system and the counterweight was roughly unity (1.0) (indicating a heavy spring), whereas it was about 0.5 for the plate-torus combination described in Ref. 7.

(C)(Gp-4) From the calculated results in Ref. 9, one sees that the energy trapped in the torus-wall waves is proportionally larger for the present system, and because of the high rate of damping of the waves, this leads to higher damping of the sprung mass oscillations at the beginning of the cycling. Once the waves have nearly damped out (after the third cycle), the logarithmic decrement decreases to about 0.14 to 0.15, very similar to that obtained during the early three-torus-system dynamic tests.

(C)(Gp-4) These experiments have therefore broadly confirmed the toroidal-system calculations performed four years ago and the results of the test agree well with what was predicted for the specific test specimens.

5.7 CONCLUSIONS AND RECOMMENDATIONS (U)

(C)(Gp-4) During this year's program, not all the objectives set forth in Section 5.1 were reached. The primary objective would probably have been entirely achieved if the resin inflation system had been successful. Solutions to the bead inner-tube problem are apparent and represent a purely technological problem solvable with existing materials and techniques but requiring an effort beyond the scope of the current study. It is confidently felt that this could be achieved concurrent with a three-torus-system test, so that at the end of these two programs, a complete multitorus stacked system could be fabricated for testing on the shock-absorber test facility.

(C)(Gp-4) The type of torus construction used for the last single torus is compatible with the manufacturing of a multitorus stack and is adaptable to full-size toroidal shock absorbers, although special equipment would be required. It has been proven that the current designs employing light

structure can withstand repeated and severe shock loads. The last torus test item was heavier than originally specified but could certainly be built lighter after an adequate development program has been conducted. Therefore, for full-size systems, it can be proposed, with a fair amount of conservatism, that up to 500 lb-ft can be stored per pound of toroidal gas spring.

(C)(Gp-4) This would result in shock absorbers even better than what has been assumed for the 10-m-engine optimized design.⁽⁶⁾ Moreover, there is little doubt now that the upper tori, which are not exposed to severe shock environment, could be built even lighter. It should be emphasized that these results were attained after a very modest amount of effort with readily available materials and techniques. Structurally speaking, these results are quite encouraging. Even after twenty-two exposures and over a period of several weeks, the final test item maintained its pressure to the point where no additional inflation was needed. This indicates good gas tightness and a very rugged inner-tube construction.

(C)(Gp-4) The good agreement of the test results with the calculated data confirms the validity of many earlier assumptions for the torus-system design analysis. The only large discrepancy is the amount of observed torus flattening against the plate; this might have been caused by the clamping-boss punching effect, which could be reduced by flattening the boss in later designs.

(C)(Gp-4) Based on the results obtained to date, it is recommended that

1. The clamping-bead problem be further investigated as a high-priority task,
2. The possibility of attaching the clamping bead to a filament-wound torus for further weight reduction should be explored,
3. The construction of a three-torus system for dynamic testing be pursued, and

4. The construction and testing of a 4 by 7 torus shock-absorber system be considered.

Such a program would provide sufficient information to prove that a complete torus system could be built and that it would operate as predicted and would also provide valuable data applicable to the following:

1. The torus column stability (barreling, buckling),
2. The torus lateral response (restoring side force and moment),
3. The damping of the pressure wave along the torus stack, and
4. The damping properties of the torus in the lateral displacement mode.

6. FUTURE EXPERIMENTAL ENGINEERING PROGRAM (U)

(U) The test results obtained during this current program indicate that the design solutions proposed so far are sound. Furthermore, they have highlighted the subsequent effort required to obtain more definitive answers to the remaining basic questions. Positive results have been obtained in general, but there have also been some negative counterparts.

(U) Cracks developed in some of the USS T1 steel plates and did not in others. The type of impulse given to these plates was slightly different but not enough to explain the discrepancies in the results. Also, it is not known accurately what these differences were and which type of impulse loading is the most realistic.

(C)(Gp-4) In other cases, only partial answers have been obtained. For instance, structural design of a single torus system has been proven but an adequate attachment to the plate has not been developed. Therefore, work should be continued in many areas to clarify the obscure points, to conform earlier results, and to find solutions to problems still unsolved. Because of experience over the past year, it is clear as to the orientation of this further work. The following outlines the various problem areas and recommends a method of approach.

6.1 PULSE-GENERATION DEVELOPMENT (U)

(C)(Gp-4) The development of a system for producing pulses pertinent to ORION using sheet HE has advanced to the point where it can be shown that this simulation technique can approximate the pressure-time history of the calculated operational impulse for small vehicles. This technique of pulse generation has been utilized primarily to provide forcing

functions within certain prespecified ranges. Many ranges have been covered so that scaling relations are apparent. However, for the development of ORION pusher and pusher-shock-absorber systems, there is a requirement for pulse simulation wherein the impulse distribution is a continuum through a factor of ten. The impulse distribution is dependent on the pusher radius.

(U) For the development of a complete HE pulse unit to simulate the dynamic loading of the nuclear pulse system, a two-phase program is recommended.

(U) First, the orderly development of HE units to generate uniform (in area) pulses. This is a continuation of past work with emphasis on a systematic variation of one parameter at a time to show its influence on over-all system performance. By thus varying the important parameters, one should be in a position to select the appropriate materials and configurations to produce any impulse within a specified range. This would then provide the basis for the second phase -- the development of a specific radially varying impulse generator or pulse unit. The phase-one development can be continuously exploited to provide experimental forcing functions for tests on segments of the pusher and pusher-shock-absorber systems.

(U) Second, the actual development of the detail material techniques required to develop an HE pulse unit which, upon detonation, will generate a specific pulse that simulates a nuclear-produced pressure pulse in time and radial dependence.

6.2 PLATE RESPONSE (U)

(U) Additional work should be pursued to correlate the response of plates to mismatched impulses and to off-centered impulses with analytical investigation schemes such as BMM or with semianalytical approaches in the case of off-centered impulses. No code is available at the present time to tackle such problems. Scaled plate models should be

used to obtain data that could be extrapolated to a full-size pusher plate to obtain information on questions not amenable to direct analyses.

(U) The influence of material flaws on the fatigue properties of plates should be investigated. Both flawless plates and identical plates with flaws detected prior to testing should be tested under identical conditions until some conclusive results are obtained. The same type of work should be conducted for welds and integral attachments. A large number of repeated exposures will be required, ultimately up to several thousand, before any valid conclusions can be drawn on the qualification of candidate materials from which full-scale test pusher plates may be constructed.

6.3. THREE-TORUS SYSTEM (U)

(U) The point has been reached where a three-torus system can be built to investigate the torus interconnection and the attachment to the upper structure. The plate clamping scheme described in Section 5.5 allows the testing and development of a three-torus system even though the resin clamping system might, as yet, not be operating.

(U) This work could furnish the basic design information required to build the 4 by 7 torus system to reach the objectives outlined in Section 5.1.

6.4. TORUS-PLATE ATTACHMENT (U)

(U) At the same time that the three-torus system is being developed, the resin-inflated bead attachment should also be developed so that the 4 by 7 torus system might be designed. In the event the resin inflation scheme does not operate satisfactorily, alternative solutions would be sought to eliminate the bolting of clamping rings. The following steps are recommended:

1. Establish that this shock-absorber concept is satisfactory, that the energy storage is adequate for the hardware weights involved, and that the design is adequate for multiple full-impulse loading so that hardware may be qualified for integrated over-all shock-absorber testing.

2. Determine the dynamic effect of the compression-tension waves traveling along the torus walls (acceleration overshoot peaks and frequency) and the rate of damping.
3. Determine the amount of damping inherent to such a system and the method of introducing artificial damping.
4. Investigate the buckling and barreling behavior of such a system under dynamic loading.
5. Check the lateral stiffness of such a system with the use of off-centered charges.

6.5 TORUS-STACK-SYSTEM STATIC INVESTIGATION (U)

(U) In parallel with the dynamic testing of torus systems, a static loading test program should be conducted to determine

1. The longitudinal and lateral stiffness of a torus stack, constructed in accordance with the design chosen for this proposed program.
2. The correlation between the results from these tests and the analytical studies made over the last two years, as well as with the dynamic test results.
3. The conditions leading to undesirable behavior of a torus stack in compression (such as buckling or barreling) and their correlation with the results obtained during the dynamic tests.

7. CONCLUSIONS (U)

(U) In most cases the primary objectives set forth at the beginning of this program have been reached. As is typical of all experimental research, the results obtained did not always coincide with the expectations and the course of action had to be altered and the thinking changed. This explains why not all secondary objectives have been reached.

(U) Worthwhile results have been obtained which have furnished the information needed for a better definition of subsequent development research and efforts required to develop the propulsion system to an operational status.

7.1. PULSE-GENERATION DEVELOPMENT (U)

(C)(Gp-4) It is now possible to generate pressure pulses which simulate the ORION impulses under certain conditions. The peak pressures which are expected to be limited to approximately 100,000 psi for presently available materials can be readily attained. For the 10-m-engine pulse, the duration of the pressure is somewhat longer than that reliably obtained from HE simulation.

(C)(Gp-4) Dynamic loading of segments of the 10-m pusher can be accomplished at full size under full stress conditions except for the thickest section at the center of the pusher. Impulse per unit area has been repeatedly simulated to values of approximately 0.7 times that required at the center of the 10-m pusher. Extension to values equal to and beyond the requirements at the center of the 10-m pusher can be attained by properly up-scaling the HE pulse unit. Sufficient experience is available to give good direction to this process.

(U) For the experimental investigation of certain problem areas, scaled pusher-thickness tests are preferred. Also, full-scale attachments can be tested on plates of thickness less than that of the center thickness of the pusher for the 10-m engine. These tests have been made under full stress conditions. For future tests of thicker plate sections and of tapered plates, extension of existing pulse simulation techniques is required.

7.2 PLATE RESPONSE (U)

(U) Plate-response experimental studies have produced sufficient positive results to support the following conclusions:

1. Existing materials can be economically fabricated into suitable shapes that will withstand many shock loadings and will permit the attainment of very high performance ORION operation.
2. Welding of one candidate test specimen proved to be unsatisfactory in the one welded test plate. However, the weld itself did not fail, and the failure of the parent metal was very similar to the failure of a similar specimen (attachment plate 1) which was weld free. Both failures may have been initiated from material flaws. Similar weld-free specimens similarly loaded showed no failures. Quality control of material production will be a very important factor in ORION pusher-plate development.
3. Correlation of experimental results and computer calculations has been achieved in a preliminary way. Experimental techniques appear extendable so that the understanding of the effects of off-center pusher loading can be obtained.

7.3. PLATE-ATTACHMENT RESPONSE (U)

(U) The integral clamping-boss design does not seem to cause unacceptable stress concentrations. The shape of the boss

internal groove appears to sustain only very minor dimensional changes after a number of exposures, which should point out gross conceptual discrepancies.

(U) The failures observed in some samples are difficult to explain. To eliminate any doubt, a thorough material quality control should be exercised before any test sample of this kind is submitted to endurance testing. Also, it might be advisable to subject the plate to nondestructive investigations periodically before the end of a test series and before a destructive-type structural investigation is carried out. Various techniques, such as X-ray, ultrasonic, magnetic, and fluorescent dyes, are available for such structural integrity checks. This would allow the detection of the start of a failure and also the recording of its subsequent history.

(U) The influence of small flaws in the parent material which are the origin of fractures should also be investigated.

7.4. TORUS RESPONSE (U)

(U) A satisfactory torus structural design and inner-tube system have been developed. The energy storage capacity per unit torus system weight has been determined and appears compatible with the assumptions made for the engine design. The additional work required to produce a full toroidal shock-absorber system is now quite straightforward.

(U) The design and analytical study results obtained during the past four years have been verified with enough accuracy to warrant high confidence in the performance predictions of the whole toroidal shock-absorber system. It should be pointed out that the experimental tests were carried out with materials currently available and that the improvements in materials expected during the next several years should allow even better performance.

REFERENCES

1. (Unclassified title) Technical Summary Report, Nuclear Pulse Propulsion Project (ORION), Vol. IV--Experimental Structural Response, Report TDR-RTD-63-3006, Air Force Contract AF29(601)-2207. (Secret/RD report)
2. (Unclassified title) Nowak, M. J., BAMM--A Fortran IBM-7090 Code for the Calculation of Bending and Membrane Motion, General Atomic, Informal Report GAMD-3432, August 28, 1962. (Secret report)
3. Hoffman, A. J., and S. N. Mills, Jr., Air Blast Measurements About Explosive Charges at Side-on and Normal Incidence, Ballistic Research Laboratories. Report BRL-988, July 1956 (DDC No. AD114880), Sec. II.
4. Blackstock, A. W., H. R. Kratz, and M. E. Feency, "Piezoelectric Gauges for Measuring Rapidly Varying Pressure up to Seven Kilobars," Rev. Sci. Instr., Vol. 35, 1964, p. 105.
5. Cerni, R. H., and L. E. Foster, Instrumentation for Engineering Measurements, John Wiley and Sons, Inc., pp. 83-87.
6. (Unclassified title) Technical Summary Report, Nuclear Pulse Propulsion Project (ORION), Vol. I. Reference Vehicle Design, Report TDR-RTD-63-3006, Air Force Contract AF29(601)-2207. (Secret/RD report)
7. (Unclassified title) David, C. V., Toroidal Shock Absorber Scale Model Testing, General Atomic, Informal Report GAMD-2554, Air Force Contract AF29(601)-2207, October, 1961. (Secret report)
8. Schuerch, H. U., R. Burggraf, and A. C. Kyser, A Theory and Applications of Filamentary Structures, NASA TN D-1692, December 1962.
9. David, C. V., Minimum Energy Loss in a Two-mass Spring System, General Atomic, Informal Report GAMD-2331, Air Force Contract AF29(601)-2207, June 14, 1961. (Unclassified report)

DISTRIBUTION

Cy no.

HEADQUARTERS USAF

Hq USAF, Wash, DC 20330

- 1 (AFORQ)
- 2 (AFTAC)
- 3-4 (AFRSTG, Lt Col Burke)
- 5 Office of the Undersecretary of the Air Force, ATTN: Maj L. A. Skantze, Deputy Executive Officer, Rm 4E886, The Pentagon, Wash, DC 20301
- 6 USAF Dep, The Inspector General (AFIDI), Norton AFB, Calif 92409
- 7 USAF Directorate of Nuclear Safety (AFINS), Kirtland AFB, NM 87117

MAJOR AIR COMMANDS

AFSC, Andrews AFB, Wash, DC 20331

- 8 (SCT)
- 9 (SCLT)
- 10 (SCGP, Maj Welch)
- 11 TAC (DORQ-M), Langley AFB, Va 23365
- 12 SAC (DPLBS, Maj Mixson), Offutt AFB, Nebr 68113
- 13 ADC (ADLPD), Ent AFB, Colo 80912
- 14 ATC (S-W), Randolph AFB, Tex 78148
- 15 AUL, Maxwell AFB, Ala 36112
- 16 USAFIT, Wright-Patterson AFB, Ohio 45433
- 17 USAFA, Colo 80840

AFSC ORGANIZATIONS

- 18 FTD (TDBTL), Wright-Patterson AFB, Ohio 45433
- FTD, Bolling AFB, Wash, DC 20332
- 19 (RTTP, Maj Mott-Smith)
- 20 (RTGS)
- 21 AF Msl Dev Cen (RRRT), Holloman AFB, NM 88330
- 22 SSD (SSTAE, Maj Builta), Los Angeles AFS, AFUPO, Los Angeles, Calif 90045
- 23 AFRPL (PRRA, Mr. J. B. Mullen), Edwards AFB, Calif 93523

KIRTLAND AFB ORGANIZATIONS

- 24 AFSWC (SWEH), Kirtland AFB, NM 87117
- 25 ADC (ADSWO), Special Weapons Office, Kirtland AFB, NM 87117

DISTRIBUTION (cont'd)

Cy no.

AFWL, Kirtland AFB, NM 87117

26-35

(WLIL)

36

(WLAX)

37-38

(WLDA-3, Maj Berga)

39

(WLR)

40

(WLREH)

41

(WLRM)

42

(WLRP)

43

(WLX, Col Beckham)

44

SAC Res Rep (SACLO), AFSWC, Kirtland AFB, NM 87117

OTHER AIR FORCE AGENCIES

Director, USAF Project RAND, via: Air Force Liaison Office, The RAND Corporation, 1700 Main Street, Santa Monica, Calif 90406

45

(RAND Physics Div)

46

(RAND Library)

47

1st Missile Div (OA), Vandenberg AFB, Calif 93437

48

Hq OAR, ATTN: Dr. Wm. J. Price, Bldg T-D, Wash, DC 20333

ARMY ACTIVITIES

49

Redstone Scientific Information Center, US Army Missile Command, Chief, Document Section, Redstone Arsenal, Ala 35899

NAVY ACTIVITIES

50

Commanding Officer, Naval Weapons Training Center, Pacific, ATTN: Director, Weapons Employment and Planning Dept, Naval Air Station, North Island, San Diego 35, Calif

51

Commander, Naval Ordnance Laboratory, ATTN: Dr. Rudlin, White Oak, Silver Spring, Md 20910

52

Commanding Officer, US Naval Weapons Evaluation Facility (NWEF, Code 404), Kirtland AFB, NM 87117

OTHER DOD ACTIVITIES

Director, Defense Atomic Support Agency, Wash, DC 20301

53

(Document Library Branch)

54

(Dr. T. B. Taylor)

55

Commander, Field Command, Defense Atomic Support Agency (FCAG3, Special Weapons Publication Distribution), Sandia Base, NM 87115

56

Director, Weapon Systems Evaluation Group, Rm 1D847, The Pentagon, Wash, DC 20301

DISTRIBUTION (cont'd)

Cy no.

57 Director, Advanced Research Projects Agency, Department of Defense,
The Pentagon, Wash, DC 20301
Office of Director of Defense Research and Engineering, The Pentagon,
Wash, DC 20330

58 (SA(S), Lt Col Lew Allen, Jr.)

59 (Dr. Chalmers Sherwin)

60-79 DDC (TIAAS), Cameron Station, Alexandria, Va 22314

AEC ACTIVITIES

80 US Atomic Energy Commission (Headquarters Library, Reports Section),
Mail Station G-017, Wash, DC 20545

81 Sandia Corporation (Information Distribution Division), Box 5800,
Sandia Base, NM 87115

82-83 Chief, Division of Technical Information Extension, US Atomic
Energy Commission, Box 62, Oak Ridge, Tenn 37831

84-85 University of California Lawrence Radiation Laboratory, ATTN:
Director's Office, Technical Information Division), P. O. Box 808,
Livermore, Calif 94551
Director, Los Alamos Scientific Laboratory, P. O. Box 1663, Los
Alamos, NM 87554

86-87 (Helen Redman, Report Library)

88 (T-Div, Dr. Stanislaw Ulam)

OTHER

89 Central Intelligence Agency (OSI/N), 2430 E StreetNW, Wash, DC 20505

90 Manned Spacecraft Center (NASA), ATTN: Chief, Technical Information
Division, Houston 1, Tex

91 Arms Control and Disarmament Agency, Chief, Reference Research
Bureau, Wash 25, DC

92-93 Marshall Space Flight Center (NASA), ATTN: R-P&VE-AN, Mr. J. C.
Whiton, Huntsville, Ala

94 Administrator, NASA, 400 Maryland Ave SW, Wash 25, DC

95 Lewis Research Center (NASA), ATTN: Dr. J. C. Evvard, 21000
Brookpark Rd, Cleveland 35, Ohio

96 Goddard Space Flight Center (NASA), ATTN: Dr. R. Jastrow, 8719
Colesville Rd, Silver Spring, Md

97 AEC-NASA Space Nuclear Propulsion Office, ATTN: Mr. Harold B.
Finger, Mgr, Wash 25, DC

98 Ames Research Center (NASA), ATTN: Tech Library, Moffett Field,
Calif

DISTRIBUTION (cont'd)

Cy no.

99-123 General Atomic Division, General Dynamics Corporation, ATTN: Chief,
Technical Information Services, P. O. Box 1111, San Diego, Calif
92112 Contract AF 29(601)-6214

124 Official Record Copy (Maj Berga, WLDA-3)

DOCUMENT CONTROL DATA - R&D		
<i>(Security classification of title, body of abstract and indexing annotation must be entered when the overall report is classified)</i>		
1. ORIGINATING ACTIVITY (Corporate author) General Atomic Division, General Dynamics Corp. San Diego, Calif		2a. REPORT SECURITY CLASSIFICATION CONFIDENTIAL
		2b. GROUP IV
3. REPORT TITLE (U) NUCLEAR PULSE PROPULSION PROJECT (PROJECT ORION), VOL IV, (U) ENGINEERING EXPERIMENTAL TESTS		
4. DESCRIPTIVE NOTES (Type of report and inclusive dates) Technical Summary Report; July 1963-September 1964		
5. AUTHOR(S) (Last name, first name, initial) General Atomic Division, General Dynamics Corp.		
6. REPORT DATE January 1965	7a. TOTAL NO. OF PAGES 156	7b. NO. OF REFS 9
8a. CONTRACT OR GRANT NO. AF 29(601)-6214		8b. ORIGINATOR'S REPORT NUMBER(S) WL TDR-64-93, Vol IV
a. PROJECT NO. 3775		8c. OTHER REPORT NO(S) (Any other numbers that may be assigned this report) GA-7386
c. Task No. 377501		
d.		
10. AVAILABILITY/LIMITATION NOTICES Qualified users may obtain copies of this report from DDC.		
11. SUPPLEMENTARY NOTES		12. SPONSORING MILITARY ACTIVITY AFWL (WLDA-3) Kirtland AFB, NM 87117
13. ABSTRACT (U) Segments of an ORION pusher plate and scaled primary shock absorbers with scaled pusher-shock-absorber attachments have been repeatedly shocked up to full stress conditions with high explosives (HE). The results of these response measurements and post-test inspections are presented along with the results of HE-pulse-generator development tests. In addition, a comparison of the results of a computer program and an experimental test of plate flexural stresses is presented. The primary importance of these results is the indication that ORION components can be developed to function in the manner prescribed by design studies and than nonnuclear pulse systems for the development and life-testing on the ground of full-size ORION vehicles are practical.		

14. KEY WORDS	LINK A		LINK B		LINK C	
	ROLE	WT	ROLE	WT	ROLE	WT
Project ORION Nuclear Pulse Propulsion Pusher Plate Shock Absorbers and attachments Dynamic Mechanical response High explosive experiments Electronic instrumentation						

INSTRUCTIONS

1. **ORIGINATING ACTIVITY:** Enter the name and address of the contractor, subcontractor, grants, Department of Defense activity or other organization (corporate author) issuing the report.

2a. **REPORT SECURITY CLASSIFICATION:** Enter the overall security classification of the report. Indicate whether "Restricted Data" is included. Marking is to be in accordance with appropriate security regulations.

2b. **GROUP:** Automatic downgrading is specified in DoD Directive 5200.10 and Armed Forces Industrial Manual. Enter the group number. Also, when applicable, show that optional markings have been used for Group 3 and Group 4 as authorized.

3. **REPORT TITLE:** Enter the complete report title in all capital letters. Titles in all cases should be unclassified. If a meaningful title cannot be selected without classification, show title classification in all capitals in parentheses immediately following the title.

4. **DESCRIPTIVE NOTES:** If appropriate, enter the type of report, e.g., interim, progress, summary, annual, or final. Give the inclusive dates when a specific reporting period is covered.

5. **AUTHOR(S):** Enter the name(s) of author(s) as shown on or in the report. Enter last name, first name, middle initial. If military, show rank and branch of service. The name of the principal author is an absolute minimum requirement.

6. **REPORT DATE:** Enter the date of the report as day, month, year, or month, year. If more than one date appears on the report, use date of publication.

7a. **TOTAL NUMBER OF PAGES:** The total page count should follow normal pagination procedures, i.e., enter the number of pages containing information.

7b. **NUMBER OF REFERENCES:** Enter the total number of references cited in the report.

8a. **CONTRACT OR GRANT NUMBER:** If appropriate, enter the applicable number of the contract or grant under which the report was written.

8b, 8c, & 8d. **PROJECT NUMBER:** Enter the appropriate military department identification, such as project number, subproject number, system numbers, task number, etc.

9a. **ORIGINATOR'S REPORT NUMBER(S):** Enter the official report number by which the document will be identified and controlled by the originating activity. This number must be unique to this report.

9b. **OTHER REPORT NUMBER(S):** If the report has been assigned any other report numbers (either by the originator or by the sponsor), also enter this number(s).

10. **AVAILABILITY/LIMITATION NOTICE:** Enter any limitations on further dissemination of the report, other than those

imposed by security classification, using standard statements such as:

- (1) "Qualified requesters may obtain copies of this report from DDC."
- (2) "Foreign announcement and dissemination of this report by DDC is not authorized."
- (3) "U. S. Government agencies may obtain copies of this report directly from DDC. Other qualified DDC users shall request through _____"
- (4) "U. S. military agencies may obtain copies of this report directly from DDC. Other qualified users shall request through _____"
- (5) "All distribution of this report is controlled. Qualified DDC users shall request through _____"

If the report has been furnished to the Office of Technical Services, Department of Commerce, for sale to the public, indicate this fact and enter the price, if known.

11. **SUPPLEMENTARY NOTES:** Use for additional explanatory notes.

12. **SPONSORING MILITARY ACTIVITY:** Enter the name of the departmental project office or laboratory sponsoring (paying for) the research and development. Include address.

13. **ABSTRACT:** Enter an abstract giving a brief and factual summary of the document indicative of the report, even though it may also appear elsewhere in the body of the technical report. If additional space is required, a continuation sheet shall be attached.

It is highly desirable that the abstract of classified reports be unclassified. Each paragraph of the abstract shall contain an indication of the military security classification of the information in the paragraph, represented as follows: (S), (C), (R), (T).

There is no limitation on the length of the abstract. However, the suggested length is from 150 to 255 words.

14. **KEY WORDS:** Key words are technically meaningful terms or short phrases that characterize a report and that may be used as index entries for cataloging the report. Key words must be selected so that no security classification, such as identification, such as equipment model designation, trade name, military project code name, geographic location, may be used as key words but will be followed by an indicator of technical content. The assignment of links, rules, and weights is optional.